Low Complexity Channel Estimation for OFDM based Satellite Systems

Mo Zhu

Submitted for the Degree of
Doctor of Philosophy
from the
University of Surrey

Centre for Communication Systems Research
Faculty of Engineering and Physical Sciences
University of Surrey
Guildford, Surrey, GU2 7XH, UK

February 2011

Abstract

The demand for high data rate and high user mobility has driven modern wireless communications into a new era, in which advanced technologies are developed to facilitate the fulfilment of such demands, as well as to guarantee the quality of service of transmissions under adverse channel conditions. OFDM has become a popular choice for wideband high data rate communication systems due to its strength in mitigating frequency selective fading as well as inter-symbol interference. However, OFDM operation faces a number of challenges, such as high channel estimation complexity and sensitivity to Doppler shift. In this thesis, we investigate channel estimation techniques for OFDM systems, especially with a view to the optimisation of estimation accuracy at low complexity, so as to maximise the practicability and minimise the cost of user terminals.

Firstly, we investigate channel estimation techniques for an OFDM based satellite mobile broadcast system DVB-SH. The main difficulty DVB-SH faces is its large frame size that drastically increases the channel estimation complexity. We have proposed an optimised estimation scheme that has much lower complexity, whilst minimising performance degradation.

Secondly, we investigate the impact of severe inter-carrier interference caused by large Doppler shift. Inter-carrier interference damages the orthogonality between subcarriers and leads to performance degradation. In order to optimise the existing interference cancellation techniques, we have proposed an adaptive cancellation scheme that achieves a significant performance improvement over existing technique whilst the computational complexity is maintained at the same level.

Finally, we consider channel estimation in the time-domain in the presence of synchronisation errors. We have proposed a low-complexity time-domain scheme that compensates performance degradation due to synchronisation errors. The proposed scheme achieves near-ideal accuracy at low speed while it can be widely applicable to many existing systems.

Keywords: channel estimation, OFDM, adaptive, low complexity
E-mail: mo.zhu@surrey.ac.uk
WWW: www.ee.surrey.ac.uk/ccsr

Acknowledgements

I wish to express my most sincere gratitude to my supervisors Professor Barry Evans, Dr Adegbenga Awoseyila and Dr Christos Kasparis. They have shared with me their knowledge, experience and vision which have helped me tremendously during my PhD study. Your support and guidance have been extremely important throughout the years. I would also like to express my appreciation to European SatNEx project for the financial support during my study.

I am fortunate to know and work with some of the finest academics and most talented students in CCSR, who were kind to give me their friendship and support. I also wish to thank all my friends who have helped and encouraged me during my study.

My deepest love and gratitude goes to my family, who always stand beside me, giving me endless love and encouragement, as well as financial support. Without my family I would never have had the chance to come to England to do my MSc and PhD. My family are my most precious and important treasure.

Contents

List of Figures

List of Tables

Acronyms

2D	Two dimensional
3G	3rd Generation
3GPP	3rd Generation Partnership Project
4G	4th Generation
APSK	Asymmetric Phase-Shift Keying
AWGN	Additive White Gaussian Noise
BER	Bit Error Rate
BPSK	Binary Phase-Shift Keying
CDF	Cumulative Distribution Function
CDMA	Code Division Multiplexing Access
CFR	Channel Frequency Response
CIR	Channel Impulse Response
CP	Cyclic Prefix
DAB	Digital Audio Broadcasting
DDCE	Decision-Directed Channel Estimation
DFT	Discrete Fourier Transform
DVB	Digital Video Broadcasting
DVB-H	DVB Handheld
DVB-SH	DVB Satellite to Handheld
DVB-T	DVB Terrestrial
ESA	European Space Agency
ETSI	European Telecommunications Standard Institution
FD	Frequency Domain
FDMA	Frequency Division Multiplexing Access
FEC	Forward Error Control
FFT	Fast Fourier Transform
FIR	Finite Impulse Response
ICI	Inter-carrier Interference
IFFT	Inverse Fast Fourier Transform
IMR	Intermediate Module Repeater
ISI	Inter-symbol Interference
LOS	Line of Sight
LS	Least Squares
LTE	Long Term Evolution
ML	Maximum Likelihood
MMSE	Minimum Mean Square Error
MSE	Mean Square Error
MSS	Most Significant Samples

NLOS	Non Line of Sight
OFDM	Orthogonal Frequency Division Multiplexing
OPT	Operator-Perturbation Technique
PAPR	Peak to Average Power Ratio
PDF	Probability Density Function
PDP	Power Delay Profile
PIC	Parallel Interference Cancellation
PN	Pseudorandom Number
PRBS	Pseudorandom Binary Sequence
QAM	Quadrature Amplitude Modulation
QPSK	Quadrature Phase-Shift Keying
QoS	Quality of Service
RMS	Root Mean Square
RSC	Recursive Systematic Convolution
SC-FDMA	Single Carrier FDMA
SIC	Serial Interference Cancellation
SIR	Signal to Interference Ratio
SNR	Signal to Noise Ratio
SoF	Start of Frame
TD	Time Domain
TDM	Time Division Multiplexing
TPS	Transmission Parameter Signalling
WiFi	Wireless Fidelity (for WLAN)
WiMAX	Worldwide Interoperability for Microwave Access

1. Introduction

1.1. OFDM based Wireless Communication Systems

Modern wireless communications is no longer simply about making and receiving phone calls, but it involves much more interesting functions thanks to the integration of IP-based wireless access networks. Nowadays, a handheld device can provide to the users a wide range of services from internet surfing to online video streaming. Most of these services require data access and some of them demand rather high bit-rate connection. These demands have driven up the need for larger bandwidth and since high-speed transportation was made available in recent years, receivers that can work under high mobility are also desirable. Subsequently, the development of wireless communication technologies has focused on enabling wider radio spectrum transmission without compromising power efficiency as well as optimising the spectral efficiency by using advanced modulation techniques. However, the mobile radio channel becoming wideband raises issues, one of which is that the wideband channel will consequently become highly frequency selective, which causes the whole spectrum to suffer from uncorrelated fading. This affect is undesirable as it degrades the quality of the reception.

These issues have driven research into the multi-carrier domain, where orthogonal frequency division multiplexing (OFDM) has emerged as one of the most popular techniques in recent years for high data-rate transmission. OFDM tackles the issue of frequency selectivity by dividing up the wideband channel into orthogonal narrowband subcarriers, thus ensuring each subcarrier will only be subject to frequency flat fading. As a result channel estimation and equalization can be performed with relatively low complexity. On

the other hand, the spectra of subcarriers overlap since they are orthogonal to each other, hence the occupied bandwidth is halved and spectral efficiency increased.

For these reasons, OFDM has been widely used in both terrestrial and satellite communication services. In terrestrial systems OFDM has become the transmission choice due to its multipath mitigation advantages whilst in satellite systems it suffers from the drawback of its high peak to average power ratio (PAPR). High PAPR is a direct result of multiple subcarriers and results in poor quality of service (QoS) in a non-linear channel. Signals with higher PAPR are more vulnerable to non-linear satellite amplification distortion, and this will drive up the cost of satellite systems, which are particularly sensitive to this distortion and require more advanced linear amplifiers. In terrestrial systems like the most recent LTE standard, OFDM is only used for downlinks while for uplinks less affected single-carrier FDMA (SC-FDMA) is used.

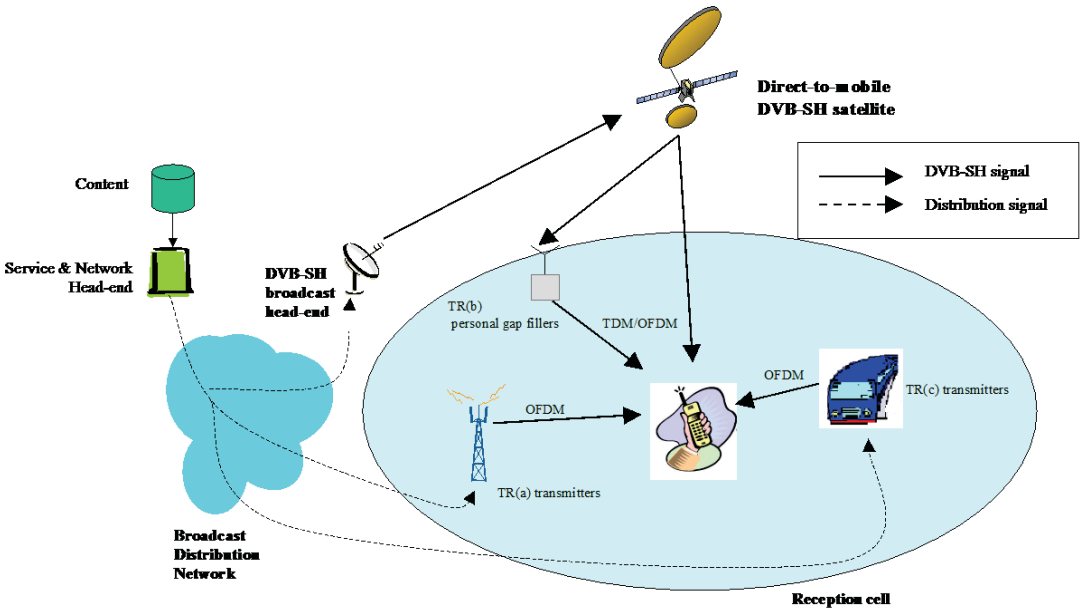

Figure 1.1: DVB-SH architecture

The applications of OFDM includes some of the most well-known standards today such as DAB [1], DVB-T [2], DVB-H [3], DVB-SH [4], WiFi [5] and WiMAX [6], as well as forthcoming fourth generation mobile communication standard 3GPP LTE [7]. The architecture of a new satellite broadcast standard DVB-SH, which we will discuss further in the thesis, is shown in Figure 1.1.

1.2. Channel Estimation Issues in OFDM Systems

Channel estimation is a vital component of any receiver design as it directly affects the receiver performance as well as the manufacturing cost of the receiver. The greatest challenge in OFDM based channel estimation is the trade-off between performance and complexity. Advanced channel estimation techniques achieve good accuracy at the price of high complexity. They often involve complex operations such as matrix inversion and require additional information such as SNR or time/frequency correlation of the subcarriers. These will nonetheless increase the implementation complexity and cost which will potentially be passed on to consumers. In this case, low complexity methods are advantageous since simpler implementation leads to lower terminal costs. However, they usually achieve degraded performance of a few dB compared to advanced methods, which will also drive up the cost as additional power is required for transmission to compensate the loss, hence a capacity reduction. Therefore, channel estimation design for OFDM systems has to account for a number of factors and a solution can only be reached based on the trade-off between such factors under specific circumstances.

Another challenge in OFDM channel estimation is the impact of mobility. Increasing demand for high data-rate service delivery at high speed has emerged in recent years, due to the

development of new technologies and markets for handheld and in-vehicle devices and the popularity of high-speed passenger transportation such as high-speed trains. However, in order to guarantee the symbol duration in OFDM systems and to ensure sufficient length of cyclic prefix (CP), subcarrier bandwidth becomes smaller and is vulnerable to Doppler shift, caused by high velocity. As a result, orthogonality between subcarriers is damaged and the common assumption that fading within a symbol is flat is invalidated. A number of techniques have been introduced to tackle this effect, known as inter-carrier interference (ICI). However they are not optimised in terms of both performance and complexity. Therefore an optimised algorithm is required to address the degradation caused by ICI.

OFDM systems are also vulnerable to synchronisation errors, although moderate tolerance is achieved via the use of the CP. It is known that ideal synchronisation is not practical in real systems due to the fast varying nature of wireless and mobile propagation channels, and that the synchronisation error can be compensated by means of the CP provided that it is within the ISI-free region. However, synchronisation error outside of the ISI-free region will still cause degraded performance. For frequency-domain channel estimation processing it is reflected as a mismatch of the FFT window where an error term is applied to each subcarrier in addition to the AWGN, while in the time-domain processing, synchronisation errors lead to the missing of channel taps due to the shift of the estimation window. Performance degradation is observed in both domains so that a channel estimation scheme that considers this scenario and compensates such degradation is highly desirable.

1.3. Structure of the Thesis

This thesis consists of six chapters, which are organised as follows:

Chapter 1 gives a brief introduction to the research work and the problem. This includes the reason for focusing on OFDM based systems as well as the challenges of channel estimation in OFDM systems plus the achievements contained in the thesis.

Chapter 2 presents the background OFDM theory key to this thesis. This includes a review of the wireless fading channels, and a thorough review of the conventional techniques used in OFDM channel estimation.

Chapter 3 presents DVB-SH, a satellite mobile broadcasting standard using OFDM. Channel estimation in DVB-SH faces complexity issues due to its large FFT size. In this chapter a comparison study is carried out in order to find an optimised channel estimation scheme for DVB-SH.

Chapter 4 considers inter-carrier interference in OFDM systems caused by high velocities. A number of techniques have been reviewed for estimating and cancelling such interference. An adaptive cancellation technique is subsequently proposed to improve the cancellation performance. The proposed method achieves improved performance in terms of BER over conventional methods while the complexity has been maintained at a similar level.

Chapter 5 considers time-domain channel estimation in the presence of synchronisation error. A number of time-domain techniques have been reviewed under the assumption of perfect synchronisation. However severe performance degradation is observed due to synchronisation mismatch. We have proposed a low-complexity time-domain scheme to compensate this degradation via a CIR optimisation mechanism. In addition, we have proposed two approaches for estimating the delay spread, which is a vital parameter in the

synchronisation and estimation scheme. The proposed scheme is supported by simulation results which show that near-ideal accuracy can be achieved for quasi-static channels whilst the complexity is much lower than other novel techniques.

Chapter 6 concludes the thesis by presenting a summary of the research work within the thesis and suggesting some future research avenues.

1.4. Novel Achievements

The major achievements in this thesis can be summarised as follows:

- A combined MMSE and FFT based technique is proposed as the optimised channel estimation scheme for DVB-SH systems. The DVB-SH system defines an OFDM symbol consisting of very large number of subcarriers, which leads to very high computational complexity for advanced channel estimation techniques such as MMSE. The proposed method reduces the complexity of MMSE by at least 50% while the performance degradation is very limited (0.1-0.3dB). This reduction of complexity facilitates the implementation of the proposed method into practical DVB-SH systems.
- A technique is proposed for adaptive inter-carrier interference cancellation. The proposed technique uses the channel SIR information to adaptively allocate the off-diagonal elements in forming the sparse matrix for the process of PIC. The proposed technique enables a well balanced interference cancellation on all subcarriers, and thus reduces the risk of performance degradation caused by a few particularly weak subcarriers. The complexity of the proposed technique is maintained at a similar

level to that of PIC and simulation results show that improved cancellation performance in terms of BER is achieved in all cases.

- A channel estimation scheme is proposed for training symbol based time-domain processing. The proposed scheme takes synchronisation error into account and uses an optimisation mechanism to compensate such error. It can be easily integrated with existing synchronisation techniques. The proposed scheme achieves similar performance, in terms of BER, as MMSE while the complexity is much lower. The proposed method can be easily implemented in systems such as WiFi and WiMAX where training symbols are already used and spectral efficiency can be achieved by avoiding the use of scattered pilots in these systems.
- Two techniques are proposed for delay spread estimation in this thesis. These techniques are based on the channel estimates obtained from the time-domain estimation scheme. Both methods involve threshold setting, where one method is implemented via the CIR estimates after the optimisation mechanism whilst the other one via the estimates before the optimisation. Near ideal accuracy is achieved from the estimation which can be fed back to the time-domain channel estimation scheme to further reduce the overall complexity.

1.5. List of Publications

- M. Zhu, A. Awoseyila, B.G. Evans, "*Low Complexity Time-Domain Channel and Delay Spread Estimation for OFDM Systems*", IEEE Transactions on Consumer Electronics, vol. 56, no. 4, pp.2170-77, November 2010
- M. Zhu, A. Awoseyila, B.G. Evans, "*Low Complexity Time-Domain Channel Estimation for OFDM Systems*", IET Electronics Letters, vol. 47, no. 1, pp.60-62, January 2011

- M. Zhu, A. Awoseyila, B.G. Evans, "*Low complexity time-domain channel estimation for OFDM using training symbols*", The 5th Advanced Satellite Multimedia Systems Conference , Cagliari, September 2010
- M. Zhu, C. Kasparis, A. Awoseyila, B.G. Evans, "*Adaptive Inter-carrier Interference Cancellation Techniques for OFDM Systems*", 27th International Communications Satellite Systems Conference, Edinburgh, June 2009
- M. Zhu, C. Kasparis, B.G. Evans, "*A Comparison Study of Channel Estimation Techniques in OFDM Based DVB-SH System*", 26th International Communications Satellite Systems Conference, San Diego, June 2008

2. Channel Estimation for OFDM Systems

2.1. Introduction

In wireless mobile communications, signals are transmitted through a wireless fading channel which can have complicated impact on the signal. The behaviour of fading channels is characterised by several factors including geographical environment, propagation distance, additive noise and the mobility of the receiver/transmitter. As a result, both amplitude and phase of the received signal is distorted by such channels, which cause reception errors at the receiver. The aim of channel estimation at the receiver is to restore the received signal to its original state by means of approximating the attenuation and compensating the phase distortions accordingly. Channel estimation is an indispensible component of a digital receiver because accurate channel estimation will significantly reduce error levels and improve the system performance.

OFDM has become a popular modulation technique for wideband signals in recent years due to its superiority in combating inter-symbol interference (ISI) and facilitation of low complexity frequency-domain equalization over conventional single-carrier systems. An OFDM symbol usually comprises of data subcarriers, pilot subcarriers (or training symbol) and null subcarriers as used in standards such as DVB-T [2], DVB-H [3] and DVB-SH [4]. Pilot subcarriers are used for synchronisation and channel estimation while null subcarriers as frequency guard bands. Given the frame structure of OFDM symbols, channel estimation for OFDM systems can be divided into two stages: Pilot estimation and interpolation. A simplified block diagram of an OFDM receiver is shown in Figure 2.1.

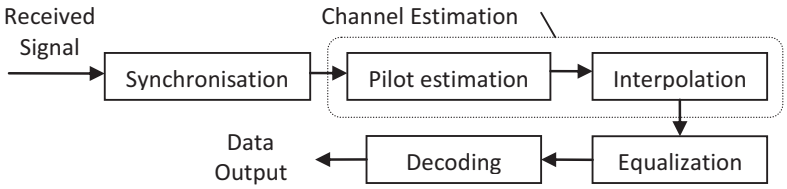

Figure 2.1: Block diagram of a simplified OFDM receiver

In this chapter, the background theory of channel estimation for OFDM systems is introduced. First we review the characteristics and statistical models for wireless fading channels, which include different components that will cause signal distortion such as multipath, additive noise and inter-carrier interference. This is followed by a review of conventional channel estimation for OFDM, such as Minimum Mean Square Error (MMSE) and Least Squares (LS), with a brief introduction to interpolation techniques.

2.2. The Wireless Fading Channel

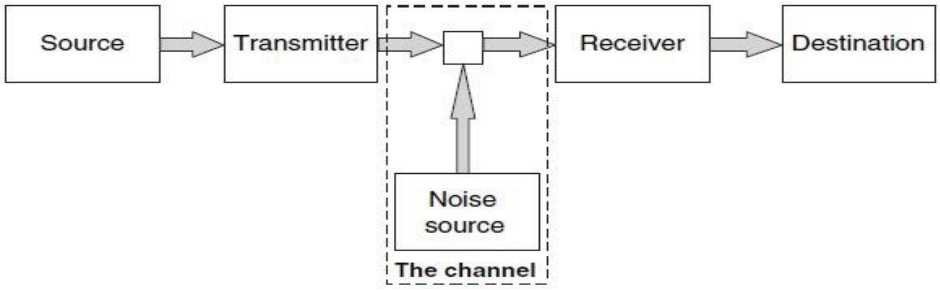

Figure 2.2: Schematic diagram of a general communication system

Figure 2.2 illustrates the structure of a general communication system as described by Claude Shannon in 1948 [**8**]. An information source generates information and sends to a destination using a transmitter. The information is sent over the channel during which it is modified and distorted by noise in a random manner. The receiver receives and processes the distorted information and then delivers it to the destination. All communication systems follow this structure no matter whether wireless or wired, therefore a receiver needs to be

designed to be able to recover the modified information with as few errors as possible. In this sub-section we focus on the characteristics and the causes of various sources of noise in the wireless channel.

2.2.1. Basic Propagation Model

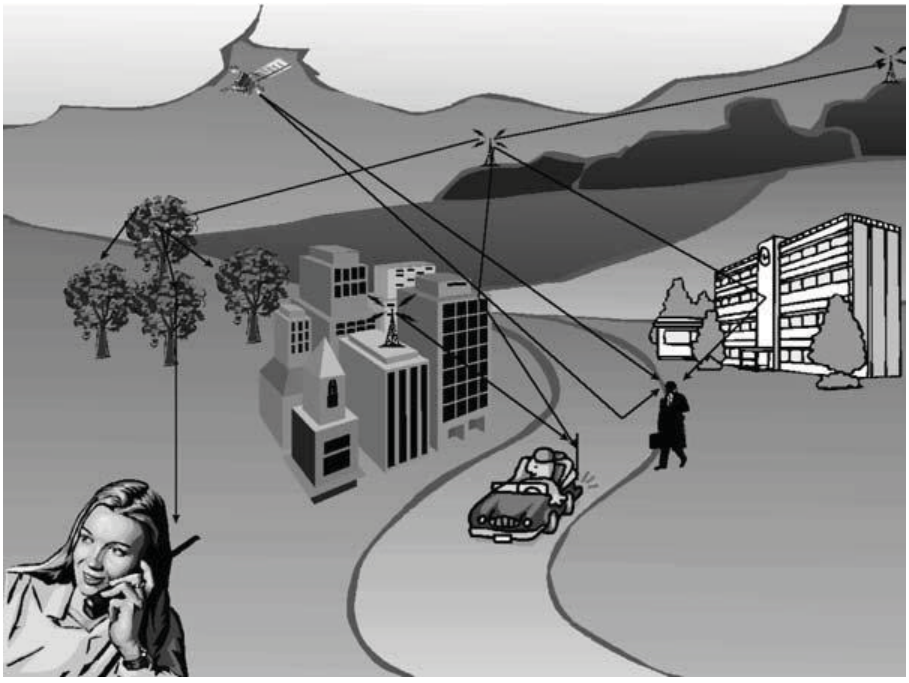

Figure 2.3: The wireless propagation landscape [9]

Figure 2.3 is a conceptual illustration of a combined satellite and terrestrial wireless communications system, within which propagation paths are established between source transmitters (satellites and base stations) and destination receivers via different routes [10]. Some paths are established via direct propagation, while others may be formed as the result of reflection from walls and surfaces, diffraction from edges of buildings or scattering from trees. Each path will suffer from noise during the transmission and various noise components will have a cumulative effect on the signal. In general, the noise sources can be

categorized into two kinds: multiplicative and additive. Given the input signal to the channel, the simplest representation of output signal can be written as:

$$y = ax + w, \tag{2.1}$$

where x is the input signal, y is the output signal, a is the collective multiplicative noise and w is the additive noise. Multiplicative noise is mainly caused by propagation effects due to the geographical environment, such as reflection, diffraction and scattering. Multiplicative noise can be further categorized into large-scale fading, shadowing and small-scale fading, while additive noise mainly arises due to the receiver itself, but may also be caused by external sources such as atmospheric effects [11].

2.2.2. Additive White Gaussian Noise

The simplest wireless channel model is referred to as the Additive White Gaussian Noise, commonly known as AWGN. Unlike other multiplicative noise and interference sources discussed previously, AWGN is – as its name suggests – an additive noise. Although the AWGN channel can be applicable to some line of sight (LOS) satellite communications environments, it is also widely used in modern radio systems as a reference background noise channel. The only impairment of AWGN channel is a linear addition of white noise to the received signal, where the white noise has a constant spectral density and power amplitude following zero-mean Gaussian distribution. In communications, the AWGN noise level is not always shown as the variance, but more often represented in terms of the Signal to Noise Ratio (SNR) in decibels and can be written as:

$$SNR_{dB} = 20\log\frac{\sigma_s}{\sigma_n}, \quad (2.2)$$

where σ_s is the root mean square (RMS) amplitude of the signal and σ_n is the RMS amplitude of the noise. Equation (2.2) indicates that the relative level of AWGN decreases when the value of SNR increases, and vice versa. SNR is an important measurement in wireless communications as it is usually used to compare the system performance of new techniques. For the same level of error rate, any techniques requiring lower SNR could lead to a cost reduction in practical implementation.

2.2.3. Path Loss and Shadowing

Path loss describes the level of power degradation of the received signal over a relatively long distance, usually ranging from a few hundred meters to a few kilometres, where the rate of fading is slow. It results from a propagation scenario where the transmitting and receiving antennas share a line of sight path where the impact of reflection and diffraction caused by obstacles is often negligible. Path loss gives an indication of the overall loss of power due to distance during the course of transmission so therefore path loss is only dependent on the distance separating the transmitting and receiving antennas as well as the transmission frequency. Path loss changes gradually and can be mathematically described by:

$$L_F = (\frac{4\pi rf}{c})^2, \quad (2.3)$$

where f is the transmission frequency in Hertz, r is the distance in metres, c is the speed of light. It can be re-written in terms of decibels (dB), as:

$$L_{F(dB)} = 32.4 + 20\log(r) + 20\log(f), \quad (2.4)$$

Therefore from (2.4) it can be estimated that path loss will increase by 6dB for each doubling in either frequency or distance [9]. Figure 2.4 shows how path loss increases with distance for a fixed frequency of 1 Gigahertz.

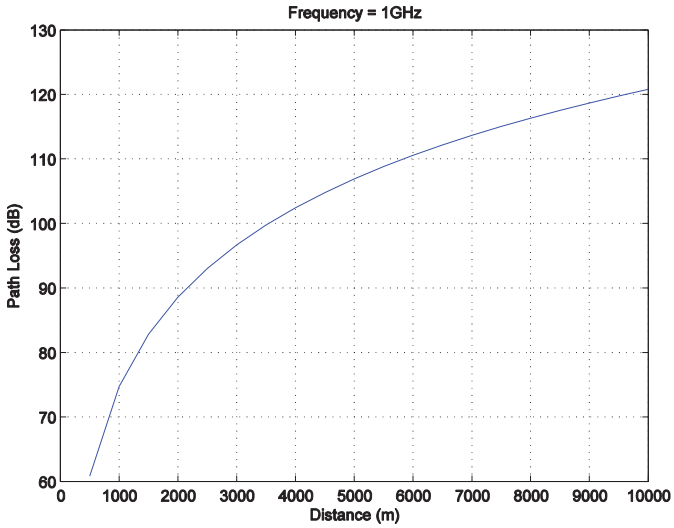

Figure 2.4: Path loss

Path loss only depends on distance and frequency, which suggests that signals at different locations will suffer from the same level of fading given that their respective distances to a transmitter are constant. However, even in a large-scale propagation environment, obstacles such as hills, buildings or trees will cause changes to the characteristics of the transmission path, thus leading to unpredicted variations in the path loss. This phenomenon is called shadowing which is in particular introduced to explain the signal attenuation due to the environment surrounding the transmitter/receiver. Shadowing is random, and it happens at a faster time-scale compared to path loss, but slower compared to small-scale

fading. In [12] and [13] it is verified that the rate of shadowing follows a Gaussian distribution with a standard deviation known as the location variability, given as:

$$p(L_S) = \frac{1}{\sigma_L \sqrt{2\pi}} e^{-\frac{L_S^2}{2\sigma_L^2}}, \tag{2.5}$$

where L_S is the shadowing loss and σ_L is the location variability. Figure 2.5 shows a typical variation of shadowing occurring in a mobile system [9].

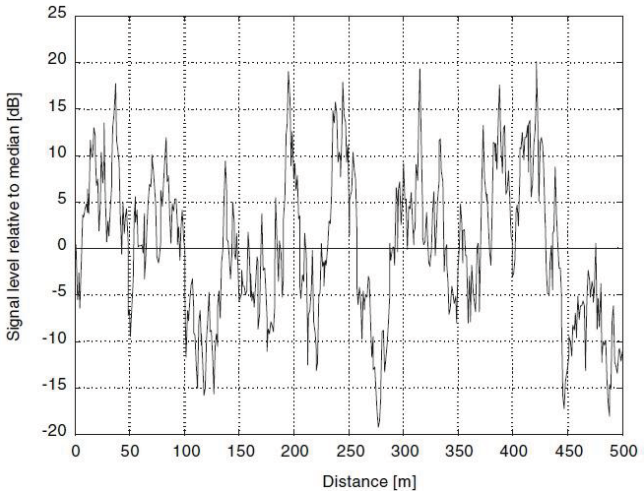

Figure 2.5: Typical variation of shadowing

2.2.4. Small-Scale Fading

Small-scale fading (also known as multipath) is the significant variations in the received signal after path loss and shadowing as the receiver moves over a relatively small-scale distance, usually within meters. As mentioned earlier, propagation between a pair of transmitter and receiver can be formed via various routes through reflection and diffraction, wherein each of them will have different rates of fading and transmission time due to the path differences. Multipath fading is caused by the arrival of a number of individual paths

with different delays, phases and magnitudes. Multipath is the most complicated fading process in wireless channels and it is only possible to estimate its characteristics by statistical means.

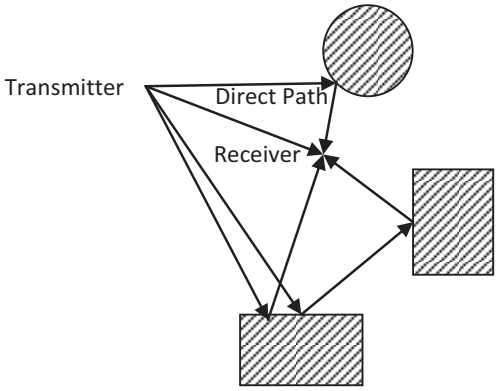

Figure 2.6: Multipath propagation

Figure 2.6 shows a simple multipath scenario [9], where there are four paths from the transmitter to the receiver, one of which is a direct path while the other three have either been reflected once or twice by different objects. Due to the complex nature of multipath fading it is neither accurate nor practical to predict its behaviour using only one statistical model. In fact, several models have been established to facilitate the analysis of different aspects of the fading so that the overall fading can be built on a combination of a few of these models. Fast fading can be further subdivided into different types. If there is energy in the received direct path, plus additional energy in incoherent received paths, this is characterised by Rician fading statistics where the Rician K factor is the ratio of the received energy in both paths (usually designated as the K factor – e.g. in a mobile satellite scenario it is between 5-12dB). On the other hand if there is no energy in the direct path, the statistical distribution becomes Rayleigh. Fast fadings can also be divided by their relative bandwidths, namely narrowband and wideband. Narrowband and wideband are defined using coherence

bandwidth, which is an indication of the separation of frequency after which two signals will experience uncorrelated fading [14]. If the bandwidth of signal is smaller than coherence bandwidth, the fading affects all frequencies in the modulated signal equally, and it is called a narrowband fading. In contrast, if the bandwidth of signal is larger than coherence bandwidth, the modulated signal will experience uncorrelated fading over its frequency, and this effect is called wideband fading.

2.2.4.1. Narrowband Fast Fading

Narrowband fast fading happens when a number of waves arrive at the receiver at almost the same time, and therefore their individual phases and magnitudes will have constructive or destructive effect on the received signal. Narrowband fast fading is also known as frequency-flat fading, which suggests that this effect will equally affect any frequency. In wireless communications, narrowband fast fading includes a few well established statistical models such as Rayleigh and Rician fading channels. In a practical multipath scenario, there may exist tens or even hundreds of paths between the transmitter and receiver due to all sorts of scatters, some of them will arrive at essentially the same time, while others may suffer delays in the order of bits or symbols. Rayleigh and Rician fading consider the former scenario.

2.2.4.2. Rayleigh and Rician Fading Channel

Rayleigh fading channel is a statistical model used to describe the propagation mechanism as shown in Figure 2.7, where there is no dominating direct Line-of-sight (LOS) path between the transmitter and receiver.

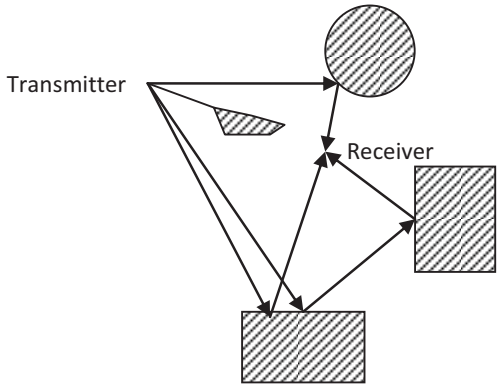

Figure 2.7: Non-line-of-sight propagation

According to central limit theorem, if enough samples are available, independent random variables approach closely to a normal distribution. In the propagation scenario in Figure 2.7, the real and imaginary parts of the complex magnitude of multipath signals can be considered as two uncorrelated normal distributed variables, since they meet the requirements of the central limit theorem, so therefore the sum of these two variables will follow a Rayleigh distribution. The probability distribution function (PDF) for Rayleigh distribution is given as:

$$P(x) = \frac{x}{\sigma^2} e^{\frac{-x^2}{2\sigma^2}}, \tag{2.6}$$

where σ is the standard deviation of either the real or imaginary parts of x.

Contrary to Rayleigh fading, Rician fading considers a propagation scenario where there is a dominant direct line-of-sight (LOS) path, as shown in Figure 2.6. As a result, the LOS path will provide a constant power component to the received signal, while the other scattered waves will have a random contribution based on a Rayleigh distribution. The Rician k-factor

is used to indicate the strength of the LOS path compared to other random parts and it is usually given in decibel as:

$$K_{dB} = 10 \times \log(\frac{s^2}{2\sigma^2}), \quad (2.7)$$

where s is the real constant power of the LOS path and σ is the variance of the real or imaginary component of the random parts. The PDF of Rician fading can thus be written as:

$$P(x) = \frac{x}{\sigma^2} e^{\frac{-x^2}{2\sigma^2}} e^{-k} I_0\left[\frac{x\sqrt{2K}}{\sigma}\right], \quad (2.8)$$

where I_0 is the modified Bessel function of the first kind and zeroth-order. It should be noted that Rayleigh fading is a special case of Rician fading, in which the k-factor becomes 0.

2.2.4.3. Doppler Shift and Doppler Spectrum

The previous sections do not consider mobility but if velocity exists between transmitter and receiver we have to consider Doppler shift. Doppler shift is the frequency shift of the signal caused by the relative movement of the receiver to the transmitter, proposed by Christian Doppler in 1842 and named after him. A practical example of Doppler shift being the siren of an approaching car, where the frequency of the siren sound increases significantly as the car moves towards the listening person, and decreases as the car passes and drives further away. The rate of frequency shift, under the condition that the relative mobility between transmitter and receiver is slow compared to the velocity of the radio wave (i.e. speed of light for wireless communications), can be mathematically represented as:

$$f_d = f_c \frac{v}{c} \cos a \,, \tag{2.9}$$

where f_c is the centre frequency, v is the relative speed between receiver and transmitter, c is the speed of light and a is the angle or arrival. The maximum Doppler shift occurs when the angle of arrival becomes 0, derived from (2.9) as:

$$f_m = f_c \frac{v}{c}, \tag{2.10}$$

Doppler shift on a single radio wave will not cause large interference to the received signal as the receiver can easily compensate for such shift. However, in a multipath scenario, when many waves arrive with different shifts, the sum of these shifts will have an impact on the received signal whose phase changes continuously, and thus also changes the signal amplitude. This phenomenon can be described as a U-shaped Doppler spectrum, which is used to determine the rate of the broadening and power fading caused by Doppler shift. The mathematical representation of Doppler spectrum under a Rayleigh fading can be written as [**15**]:

$$S(f_d) = \frac{1}{\pi f_m \sqrt{1 - (\frac{f_d}{f_m})^2}} \,, \tag{2.11}$$

The Doppler spectrum of a Rayleigh fading channel with maximum Doppler shift at 100Hz is shown in Figure 2.8.

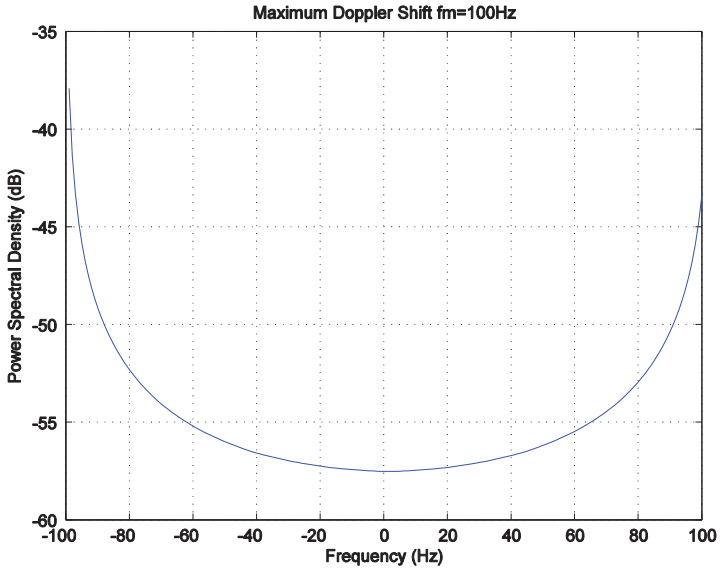

Figure 2.8: Classic Doppler spectrum

2.2.4.4. Wideband Fast Fading

Wideband fast fading in a multipath scenario explores the channel behaviour when different waves arrive at the receiver with relatively large time differences (usually measured in the order of bit duration). In wideband fast fading channels, the received signal will be a linear summation of a number of copies of itself, each subject to a different delay and amplitude distortion. As a result, the received signal will not only be distorted in phase and amplitude, but also be extended by the length of the maximum path delay.

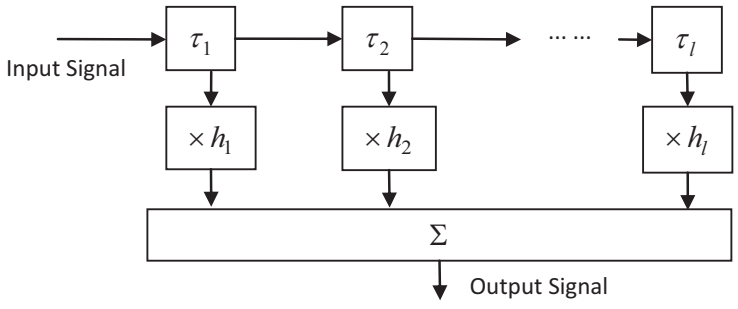

Figure 2.9: A classic wideband multipath channel model

Figure 2.9 shows a classic model of this type of fading, which is called the tapped-delay-line model. In the illustration, τ_l and h_l are the delay and phase/amplitude distortion of the l th tap respectively.

Degradation occurring due to wideband fast fading is called inter-symbol interference. In modern communications, data transmission is usually packet based, where data is divided into packets and each packet will experience coding and interleaving separately. ISI, having extended a portion of the packet into its adjacent packets, will cause great difficulty for decoding these adjacent packets at the receiver and thus lead to performance degradation. The wideband fast fading channel is usually characterized by a power delay profile (PDP), which specifies the delays and power losses of each path, as well as the K-factor if any of the paths is subject to Rician fading. Table 2.1 shows an example PDP measured by the EU project MAESTRO, this profile is suitable for satellite communications in an outdoor urban propagation environment with 3 terrestrial repeaters.

Tap	Delay (ns)	Relative Power (dB)	K-factor (dB)
1	0	-24.3	7
2	1692.7	-0.3	-inf
3	1757.8	-13.2	-inf
4	2278.6	0	-inf
5	2343.7	-5.3	-inf
6	2408.8	-2.1	-inf
7	3190.0	-5.6	-inf
8	8203.0	-7.3	-inf
9	8268.1	-10.9	-inf
10	8788.9	-14.1	-inf

Table 2.1: Power delay profile of MAESTRO profile 5

The PDP of a wideband channel is useful in specifying some important parameters such as delay spread and RMS delay. Delay spread is the maximum delay occurring as a result of the wideband multipath channel, which is a vital parameter for OFDM systems to combat ISI.

RMS delay on the other hand is an indicator of the dispersion of the channel and is important in calculating the correlation function in some techniques such as MMSE. RMS delay can be defined in (2.12):

$$\tau_{RMS} = \sqrt{[\sum_{i=1}^{l} P_i \tau_i^2 / P_{total}] - \tau_0^2}\ , \tag{2.12}$$

where P_i is the amplitude for each path and τ_0 is the mean delay defined as:

$$\tau_0 = \sum_{i=1}^{l} P_i \tau_i / P_{total}\ , \tag{2.13}$$

2.2.5. Summary

As stated in preceding sections, in modern wireless communications, any signal passes through a wireless channel will be disturbed by various types of fading, where the received signal is a collective result of noise and interference. In fact, if the impact of different fading can be categorized in a step by step manner, the signal will firstly suffer from path loss, which will fade the signal power to a predictable level. Then shadowing will randomly fade the resulting signal, although the difference of shadowing will depend on environmental parameters, fading rate will not be significant when the receiver's location only changes slightly. Multipath fading will take place, within which many multipath waves (e.g. 100's) can be sub-grouped into a few taps (e.g. 7), each with distinguishable delays. Each sub-group of waves will cause Rayleigh or Rician fading respectively depending on the absence or presence of the direct LOS, and the collection of taps will result in the extension of the signal and ultimately causing ISI. Finally, AWGN will be added at the receiver as the

background noise. Therefore, the simple continuous time representation of a wideband wireless fading channel in (2.1) can be expanded as:

$$y(t) = \sum_{i=1}^{l} L_P \times L_S \times h_i \times x(t - \tau_i) + w, \quad (2.14)$$

where L_P and L_S are the fading caused by path loss and shadowing as defined earlier, h_i is the fading of the ith tap. Conventionally, since path loss and shadowing change less dramatically, it can be considered as part of h_i, therefore re-writing the above equation as:

$$y(t) = \sum_{i=1}^{l} h_i x(t - \tau_i) + w, \quad (2.15)$$

It should be noted that (2.15) applies to any wideband fading channel models in use today.

2.3. Channel Estimation Techniques for OFDM Systems

2.3.1. Introduction

In wireless communications, channel estimation is an integral part of the receiver design. An accurate and low-complexity channel estimator will improve the system performance and efficiency. Channel estimation is essential in most wireless receivers although a few approaches have been made to avoid channel estimation. One of these is differential modulation, which however suffers from restriction to lower data rates and 3-4dB SNR degradation [**16**,**17**]. Another attempt was to try to use the base station to perform the channel estimation and transmit the pre-distorted signal to wireless receivers. This scheme, however does not achieve good accuracy in fast varying channels [18]. Therefore channel estimation is needed for high data rate systems.

The major challenge in OFDM channel estimation is to achieve best accuracy and least complexity, where varies methods have been studied and discussed over the years. Another challenge is to tolerate potential timing synchronisation errors. Through the use of CP some tolerance against synchronisation mismatch can be achieved as long as the synchronised start of frame (SoF) is within the ISI-free region, hence guarantying a full duplicate of the frame can be obtained. However, for synchronisation errors outside the ISI-free region, severe performance degradation is observed and there is no existing method to address this issue. Therefore it is important and necessary to consider this potential source of degradation during the channel estimation process.

Channel estimation has a long history in single carrier communication systems, where the channel impulse response (CIR) is treated as a time-varying FIR filter and needs to be estimated at the receiver [19]. However, the unique properties of OFDM have recently brought potentials for new channel estimation techniques for multi-carrier systems. Channel estimation for OFDM systems has been a very popular research topic during the past decade and several techniques have been developed. Usually, channel estimation techniques for OFDM can be grouped into two main categories: blind and non-blind. Blind channel estimation techniques rely purely on the wireless channel statistics and do not require any prior knowledge of the transmitted data [20]. Therefore blind channel estimation requires a large number of data samples and thus a large processing delay will occur. Moreover, in fast fading channels blind channel estimation will suffer severe performance degradation [21]. Despite these drawbacks, the main advantage of blind estimation is the high spectral efficiency, where all subcarriers can be used to transmit data content. Blind channel estimation is not popular in high data-rate systems nowadays

because the gain in spectral efficiency simply cannot compensate for the sacrifice on system performance due to the fast varying channels. On the other hand, non-blind channel estimation techniques use a portion of the data subcarriers as pilot tones, which are known to the receiver in order to facilitate the synchronisation and estimation process. Non-blind channel estimation loses spectral efficiency compared to blind but the estimation accuracy is much better thanks to the more up-to-date channel information provided by the pilot subcarriers. In this thesis, only non-blind channel estimation techniques will be investigated and blind estimation techniques are not considered.

In non-blind channel estimation techniques, two groups can be further formed: DDCE and data aided. Decision-directed channel estimation (DDCE) is one of the earliest methods of OFDM channel estimation and is a continuation from single-carrier systems where periodic training symbols are often incorporated with data. This scheme uses the estimates of previous symbols to decode the current symbol, thus the estimation accuracy is less reliable, given that outdated channel estimates are used for the current estimation especially when channels change rapidly between symbols [22,23].

Data-aided channel estimation is the mainstream estimation technique used today, as it does not lose too much spectral efficiency while achieving much better accuracy as compared to the blind estimation methods. Data-aided channel estimation cannot stand alone and must be accompanied by interpolation techniques since the pilot subcarriers are sparsely placed and cannot track all subcarriers at all time instants. A block diagram of the conventional pilot-assisted channel estimation process is shown in Figure 2.10, where dotted blocks are optional and only available in iterative estimation techniques. In the

following sub-sections, a brief introduction of OFDM basics will be presented followed by various channel estimation and interpolation techniques applied to data-aided estimation.

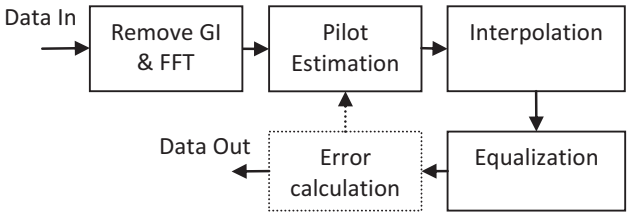

Figure 2.10: Channel estimation process

2.3.2. OFDM Basics

OFDM is a multiplexing scheme using a digital multi-carrier modulation method. The initiation of the idea to use a multi-carrier modulation method dates back to 1966 by Chang [24], but it was not until the mid 1980s, with the development of Fast Fourier Transform (FFT) techniques, that OFDM was finally able to be put into implementation. In 1985, Cimini proposed the use of OFDM for mobile communications [25]. Since then the research and development of OFDM has boomed, and it has become a major player in both wireless and wired systems, that use high bit rate and wide band services.

The concept of OFDM is to divide a wideband single-carrier signal into a number of narrowband subcarriers and transmit them simultaneously. The subcarriers are orthogonal so that they do not interfere with each other. The spectrum of each subcarrier overlaps and thus overall bandwidth can be saved. The major advantage of OFDM over conventional single carrier schemes is its ability to overcome ISI without using a complex equalizer. This is achieved by introducing a CP, which is used to duplicate a portion of an OFDM symbol at the tail and attach it to the front of each symbol. Therefore the time extension of the preceding

symbol cannot reach the current data symbol provided that the length of the CP is longer than the maximum channel multipath delay. At the receiver, ISI can be avoided by removing the CP, and since the CP itself is taken from the tail of the current symbol, its time extension into the current data symbol will not affect the orthogonality. A block diagram of an OFDM scheme is shown in Figure 2.11, and Figure 2.12 [26] shows a frequency-domain illustration for 6 subcarriers.

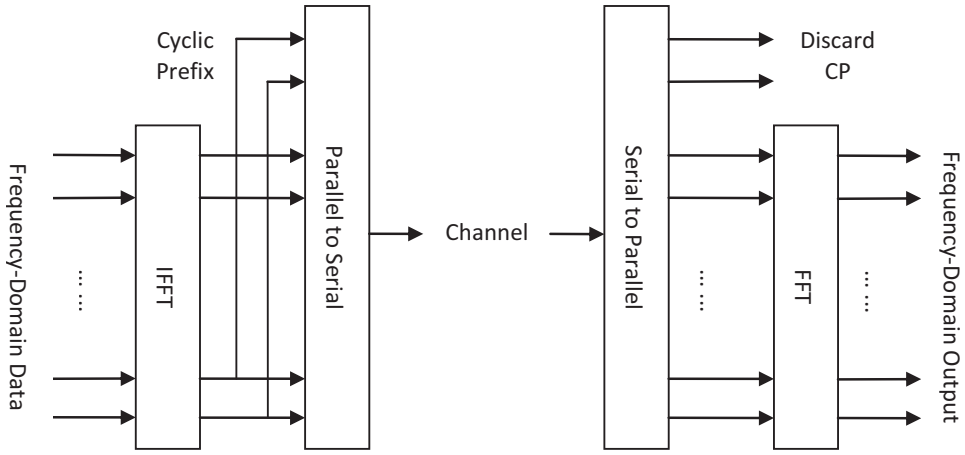

Figure 2.11: Block diagram of OFDM processing

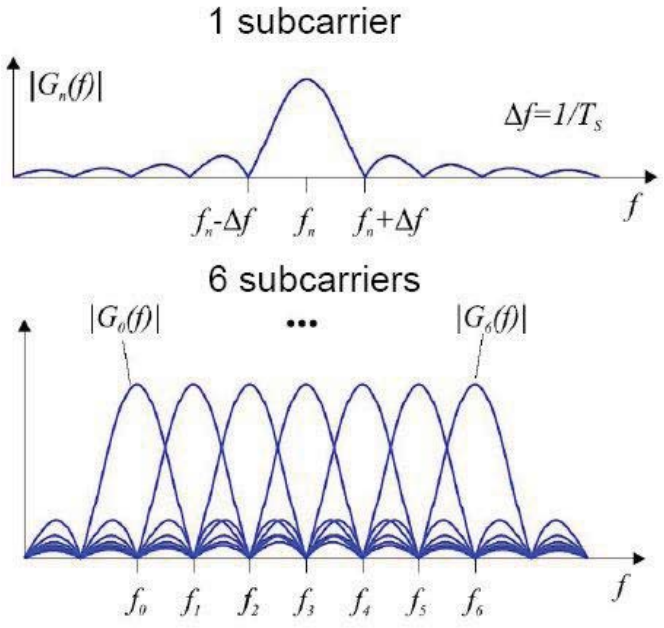

Figure 2.12: OFDM subcarriers in frequency-domain

The mathematical representation of the IFFT process can be written as:

$$x(k) = \frac{1}{\sqrt{N}} \sum_{n=0}^{N-1} X[n] e^{j2\pi k n/N}, 0 \le k \le N-1, \quad (2.16)$$

where N is the FFT size. $X[n]$ represents the data modulated on the n^{th} subcarrier while $x(k)$ represents the symbol samples after the IFFT processing. Equation (2.16) can usually be compressed as:

$$x = F^{-1}(X), \quad (2.17)$$

where F^{-1} is the IFFT process. Also the FFT process can be represented as:

$$X[n] = \sqrt{N} \sum_{k=0}^{N-1} x(k) e^{-j2\pi k n/N}, 0 \le n \le N-1, \quad (2.18)$$

or:

$$X = F(x), \quad (2.19)$$

where F is the FFT processing.

2.3.3. CIR and CFR

Channel Impulse Response (CIR) and Channel Frequency Response (CFR) are the complex responses reflecting the power attenuation caused by the fading channel and their determination is the ultimate aim of channel estimation. CIR is modelled over time and is equivalent in practice to the channel PDF. CFR on the other hand is modelled in the

frequency-domain. In OFDM systems CFR can be considered a vector of complex channel response for each subcarrier. One important property of CIR and CFR for the same channel is that they form a Fourier transform pair, which can be written as:

$$h(t) \xleftrightarrow{FFT/IFFT} H[n], \tag{2.20}$$

where $h(t)$ is CIR and $H[n]$ is CFR. This is illustrated in Figure 2.13 [27].

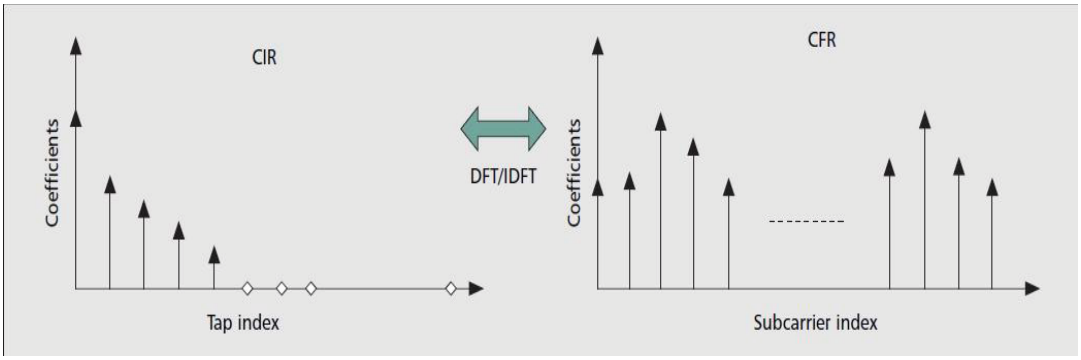

Figure 2.13: Relationship between CIR and CFR

2.3.4. Least Squares Estimation

Least Squares estimation is the simplest technique of channel estimation and is widely used by many more complex estimation techniques as an initial estimation. Considering a wideband multipath channel described in (2.15), the complex frequency-domain subcarriers after the CP and FFT removal process can be written as:

$$Y[n] = H[n]X[n] + W[n], \tag{2.21}$$

where $H[n]$ is the CFR and is a square matrix of size N, in which the diagonal positions are occupied by CFR and other components are 0. The LS estimation is then:

$$\hat{H}[n] = \frac{Y[n]}{X[n]} = H[n] + \frac{W[n]}{X[n]}, \tag{2.22}$$

It should be noted that simple LS estimations do not attempt to reduce the AWGN, therefore in practical systems its performance will be greatly affected by the noise level. As mentioned earlier, LS estimation is generally used for initial estimation of the pilot subcarriers, which will then be expanded into all subcarriers by interpolation.

2.3.5. Interpolation Techniques

Before going into the details of interpolation techniques, it is worthwhile to understand different pilot allocation schemes, which differ in functionality and will also affect the interpolation method. In general, three types of pilot allocation scheme exist: training symbol, continuous pilot and scattered pilot. Their respective illustrations are shown in Figure 2.14, where black boxes are subcarriers occupied by pilots while white ones by data.

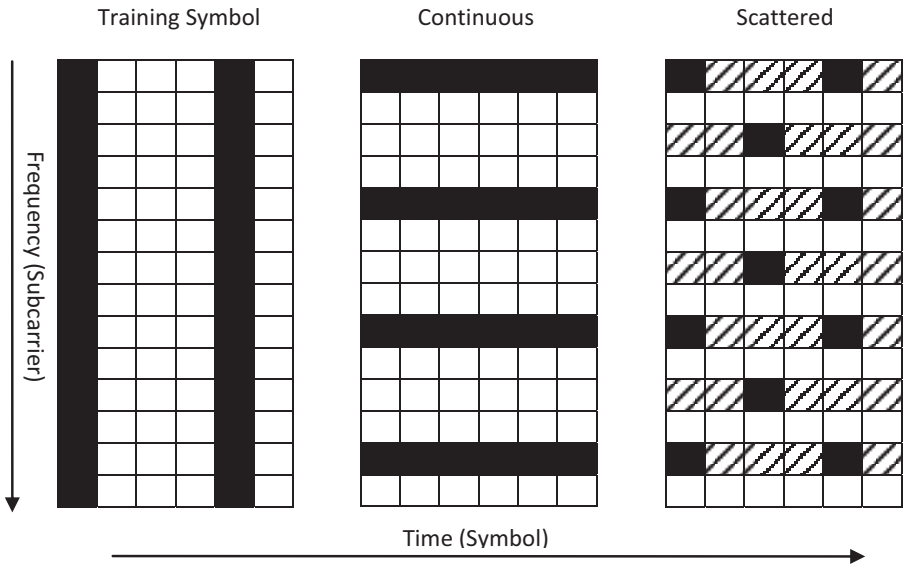

Figure 2.14: Pilot allocation schemes

For the ‘training symbol’ scheme pilot tones occupy all subcarriers within an OFDM symbol and repeat the scheme after a few symbols, leaving symbols in between entirely for data. Training symbols at the very start of a transmission are also known as preamble, and is usually used for synchronisation. LS estimation on a training symbol can easily estimate CFRs over the whole spectrum at an instant in time, and interpolation is one-dimensional over time. However, a training symbol scheme will not be able to accurately track the time variation between two training symbols, which can result in large errors due to inaccurate interpolation in fast varying channels. Therefore, the training symbol scheme is mostly used in systems where the time variation of channel is slow, such as WiFi [5] and Fixed WiMAX [6].

The ‘continuous pilots’ scheme on the other hand designates some subcarriers exclusively for the use of pilots, which are repeated in every symbol. Such pilot arrangements are able to track the time variations of the channel and one-dimensional interpolation is performed over frequency.

A trade-off of the above mentioned two schemes is called the ‘scattered pilots’ scheme. In this arrangement, a few subcarriers within a symbol are chosen as pilots but their position selection is changed for each symbol, making pilots a constant presence over both time and frequency. Two dimensional interpolation is thus associated with such scattered pilots, which are first done over time (shown as diagonally shaded in Figure 2.14), and then over frequency. Scattered pilots have been used in standards such as the DVB family.

In actual systems a combination of schemes may be used to strengthen the estimation performance, such as training symbol and scattered pilots in Fixed WiMAX, or continuous pilots plus scattered pilots in the DVB family.

2.3.5.1. Piecewise Constant Interpolation

Piecewise constant interpolation is one of two simple interpolation techniques, the other one being linear interpolation. The idea is to assign the value of CFR of one subcarrier at one time-instant, as in the scenario shown in Figure 2.14, to its nearest pilot subcarrier. Its performance in OFDM systems where only one or two dimensional interpolation is used is not comparable to that of linear interpolation. Therefore it is not popular in practice, however, in image interpolation and higher dimension interpolation, piecewise constant interpolation has gained much popularity due to its simplicity. Figure 2.15 illustrates the output of a piecewise constant interpolation process.

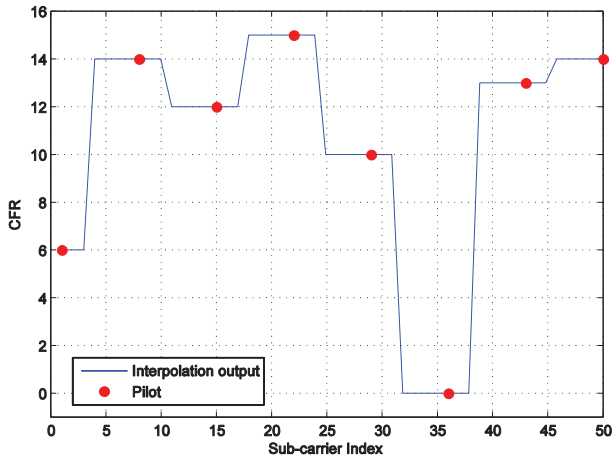

Figure 2.15: Piecewise constant interpolation

2.3.5.2. Linear Interpolation

Linear interpolation is an extremely popular technique for practical implementation, mainly due to its low complexity and reasonable accuracy compared to other simple techniques such as piecewise constant. Linear interpolation considers the variation of CFRs between two pilot subcarriers to be uniform, and therefore the output of interpolation will be a straight line. Linear interpolation between points is:

$$H = H_0 + (n - n_0)\frac{H_1 - H_0}{n_1 - n_0}, \tag{2.23}$$

where H_0, H_1 are the two pilot-subcarriers and H is the subcarrier to be interpolated, and n_0, n_1 and n are their corresponding subcarrier indices respectively. Figure 2.16 shows the output of a linear interpolator with the same pilots as in Figure 2.15.

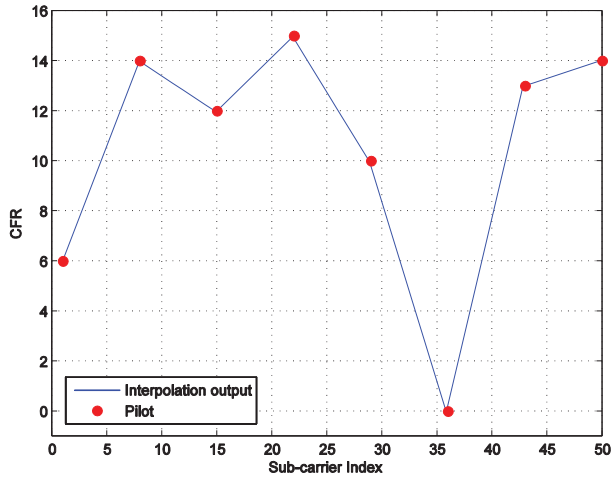

Figure 2.16: Linear interpolation

2.3.5.3. Higher Order Interpolation Techniques

The above mentioned first order interpolation techniques can provide acceptable performance in highly frequency selective channels [28,29,30]. Higher order interpolation techniques can achieve improved accuracy as smoother fittings can better approximate the wireless channels, which are smooth in both frequency and time domains [31]. However this improvement is achieved at the expense of higher computational complexity and in [31] it is also observed that when the channel variation is slow in both frequency and time domains higher order interpolation will have little impact on accuracy as the main interference source in such conditions is AWGN.

Higher order interpolation uses more than two pilot subcarriers while some may require more channel information. Common higher order interpolation methods include spline interpolation [**32**,**33**,**29**], Gaussian interpolation [**32**] and polynomial fitting [31,34,35,36,37]. The output of an example cubic spline interpolation is shown Figure 2.17.

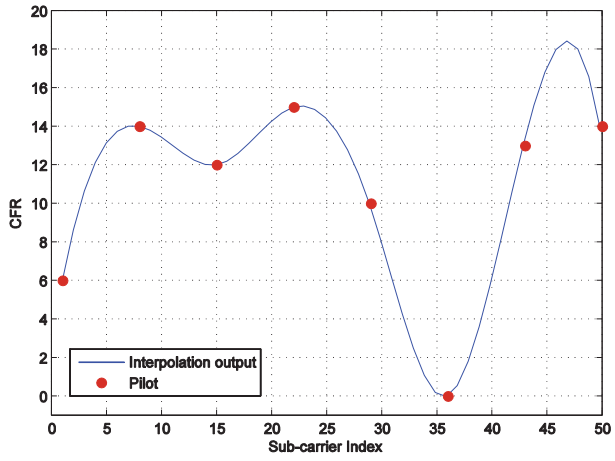

Figure 2.17: Cubic spline interpolation

2.3.6. Transform Domain Techniques

Transform domain techniques utilize FFT/IFFT to improve the accuracy over the LS estimation, as well as act as a frequency-domain interpolator [38,39]. Since this uses all pilot subcarriers to carry out the interpolation process, it performs better than other simple techniques [40]. A number of transform domain techniques have been studied over the years, including Fourier [22,41,42,43,44], Hadamard [45], Discrete Cosine [46,47], KLT [48] and 2D Fourier [49]. The common transform domain approach often involves transferring the signal into the time-domain and converting it back to the frequency domain with all estimated CFRs after reducing the noise level. Figure 2.18 illustrates the output of a Fourier Transform estimator.

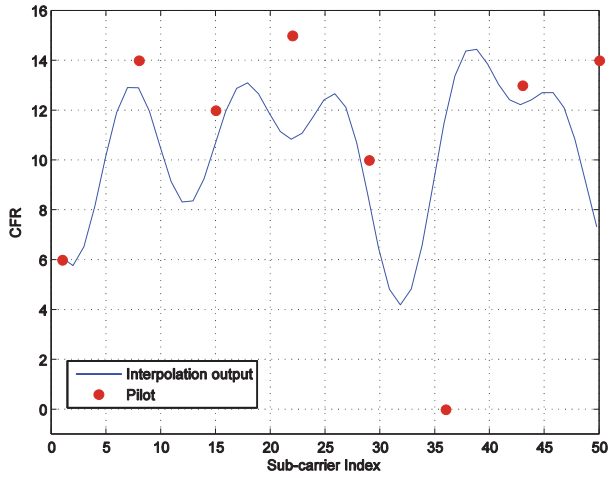

Figure 2.18: Transform domain estimation

The advantages of transform domain techniques can be highlighted by their improved estimation accuracy due to noise reduction as well as their capability to carry out frequency interpolation simultaneously. Although transform domain techniques are more complicated than simple interpolation techniques, they enjoy much lower complexity compared to other

advanced techniques such as MMSE. One possible drawback is that a large number of multipath taps is required by the interpolator in order to determine the number of significant values to remain. However this can be partially compensated by considering a channel length equal to that of the CP and is a common assumption in OFDM based systems.

2.3.7. MMSE Estimation

MMSE estimation is widely used in OFDM channel estimation in the presence of AWGN due to its ability to minimize the Mean Square Error (MSE) which is a common measurement of the estimation accuracy. MMSE can act as an estimator as well as an interpolator. It requires additional channel information such as channel correlation and SNR, thus resulting in a more complicated process and a much higher computational complexity compared to LS [**50**,**51**,**52**,**53**]. The MSE of the output of an estimator can be written as:

$$MSE = E\{\left|\hat{H} - H\right|^2\}, \tag{2.24}$$

where $\hat{H}$ denotes the estimated CFR. In order to derive the representation of MMSE which minimizes the MSE, the derivative of (2.24) is taken and the result is set to 0. After matrix processing, the output of a MMSE estimator is given as:

$$\hat{H}_{MMSE} = R_{yx}(R_{xx} + \frac{I}{SNR_{linear}})^{-1} H_{LS}, \tag{2.25}$$

where R_{yx} is the cross-covariance matrix of the pilot subcarriers and the subcarriers that the estimator is aiming to estimate, and R_{xx} is the auto-covariance matrix of the pilot subcarriers. I is an unitary matrix with size equal to the number of pilot subcarriers. It

should be noted that when the estimator does not interpolate the CFRs, the R_{yx} is replaced by R_{xx}. In [54] it is demonstrated that the calculation of R_{xx} or R_{yx} can be separated into frequency correlation and time correlation respectively, written as:

$$R_{yx} = r_f(\Delta k) \times r_t(\Delta t), \tag{2.26}$$

where $r_f(\Delta k)$ and $r_t(\Delta t)$ are the frequency and time correlations, wherein Δk and Δt are the distance and time differences between one pilot subcarrier and the subcarrier that is being interpolated. $r_f(\Delta k)$ is given as:

$$r_f(\Delta k) = \frac{1}{1 + j2\pi\tau_{rms}\Delta k / T}, \tag{2.27}$$

where $\frac{1}{T}$ is the subcarrier spacing, τ_{rms} is the channel RMS delay as defined in (2.12). $r_t(\Delta t)$ is based on the zero*th* order Bessel function of the first kind and is given as:

$$r_t(\Delta t) = J_0(2\pi f_D \Delta t T_s), \tag{2.28}$$

where f_D is the maximum Doppler shift and T_s is the OFDM symbol duration.

2.3.8. Maximum Likelihood Estimation

The maximum likelihood estimation (ML) is an estimator based on LS [55]. It is based on the assumption that the channel response (either frequency or impulse) is a deterministic but unknown vector [56]. In [57] a detailed comparison between ML and MMSE estimation is

given. In summary, ML enjoys a performance which is nearly equal to MMSE provided that the number of pilots is larger than the PDP length. In terms of complexity, ML is more straightforward and does not require additional channel information, while MMSE is more complex to implement in all scenarios. According to [57], the process of ML is given as:

$$\hat{H}_{ML}(n) = \sum_{m=0}^{N-1} H_{LS}(m) p_{ML}(n,m), \tag{2.29}$$

where $p_{ML}(n,m)$ is:

$$p_{ML}(n,m) = \sum_{k=0}^{L-1} \left[(B^H B)^{-1} B^H \right]_{k.m} e^{\frac{-j2\pi mk}{N}}, \tag{2.30}$$

with B being a $N \times L$ Fourier matrix, with entries

$$B_{n,k} = e^{\frac{-j2\pi kn}{N}}, \tag{2.31}$$

It should be noted that the weighting matrix $p_{ML}(n,m)$ can be pre-calculated and stored.

2.4. Conclusions

In this chapter, some fundamental topics in wireless mobile communications have been discussed. Firstly the characteristics of wireless fading channels have been reviewed, which includes large scale fading, narrowband and wideband fast fading, AWGN, and effects arising from Doppler shift. This review is concluded with a mathematical model of the received signal taking into account all the fading channel signals suffered during transmission. The second part of the chapter reviews common channel estimation

techniques for pilot based OFDM systems based on the channel model derived in the first part of the chapter. These techniques include initial estimates such as LS, advanced techniques such as MMSE, ML and transform domain techniques, as well as interpolation techniques such as linear interpolation. The literature review included in this chapter will serve as a background for the research described in succeeding chapters of the thesis.

3. Channel Estimation for DVB-SH

3.1. Introduction

DVB-SH is a Digital Video Broadcasting – Satellite services to Handheld standard, which is a physical layer standard aiming to provide digital video service from satellite to handheld devices. It is a member of the DVB standards family and a successor to DVB-H (Handheld). After the successful deployment of new generation high data rate networks and the rapid market growth for digital television, the DVB-SH standard was published in 2007 by ETSI (European Telecommunications Standards Institute) in order to maximize the natural advantage of satellite in broadcasting, due to its large coverage capability. DVB-SH uses satellite transmission combined with terrestrial repeaters to compensate the relatively small power gain at the receiver due to much smaller antenna size of handheld devices than those available to fixed terrestrial transmissions. In order to boost performance, state-of-art techniques are also adopted in the SH standard, which include 3GPP2 turbo coder, longer interleaver and new 1K transmission mode to support higher mobility.

Channel estimation for DVB-SH systems is challenging, mainly due to complexity issues. Unlike other OFDM systems such as fixed WiMAX where the FFT size is relatively small, the DVB-SH frame structure defines a minimum of 1024 subcarriers and a maximum 8192 subcarriers, which require huge amount of computing resource when carrying out operations such as matrix inversion. The greater number of subcarriers, on the other hand, leads to narrower carrier spacing, which decreases the system tolerance to Doppler shift, which could be as much as 20% of subcarrier bandwidth. This effect leads to severe inter-carrier interference and decreases system performance.

The structure of this chapter is organized as follows: the physical layer of DVB-SH is first reviewed, followed by a brief introduction of candidate channel estimation techniques suitable for the DVB-SH system. Complexity issues are then discussed supported by performance simulation results for Bit Error Rate (BER).

3.2. DVB-SH Physical Layer

DVB-SH specifies two operational modes: SH-A and SH-B. SH-A mode uses OFDM for both satellite and terrestrial links while SH-B mode uses TDM for the satellite link and OFDM for the terrestrial link. The use of TDM in mode SH-B is due to the high PAPR caused by FFT processing OFDM, which will lead to amplifier non-linearity distortion and reduction of satellite transmission efficiency. However due to the scope of this research work, only specifications relevant to SH-A mode will be addressed in this chapter.

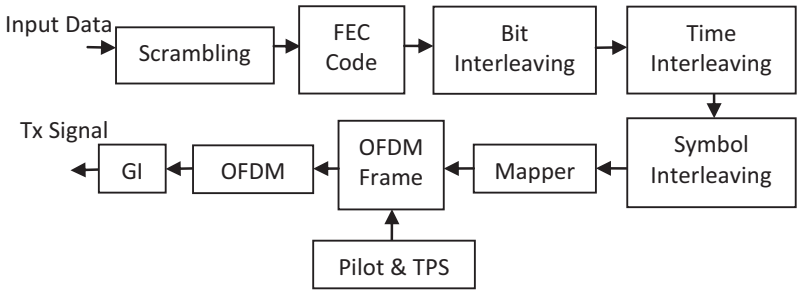

Figure 3.1: Block diagram of SH-A mode physical layer

The block diagram of the physical layer of a SH-A mode transmitter is shown in Figure 3.1. The input data is processed by a scrambler, followed by a Forward Error Control (FEC) encoder. The output of the encoder then goes through a serious of cascaded interleavers (bit, time and symbol). The mapper maps the signal into different constellations and the output is allocated into OFDM frames, at which stage the pilots and transmission parameter

signalling (TPS) are also inserted into the frame. Finally the signal is processed by OFDM modulation by means of IFFT and transmitted to air after Guard Interval (GI, which is equivalent to CP) is inserted.

3.2.1. Scrambling

In the physical layer, the output data is firstly processed by a scrambler, in order to randomize the data stream and avoid long sequences of '0's and '1's, which will cause reception difficulties. The scrambling process is carried out by a pseudorandom binary sequence (PRBS), which can be generated by a circular shift register. The implementation process of scrambling is shown in Figure 3.2 [4].

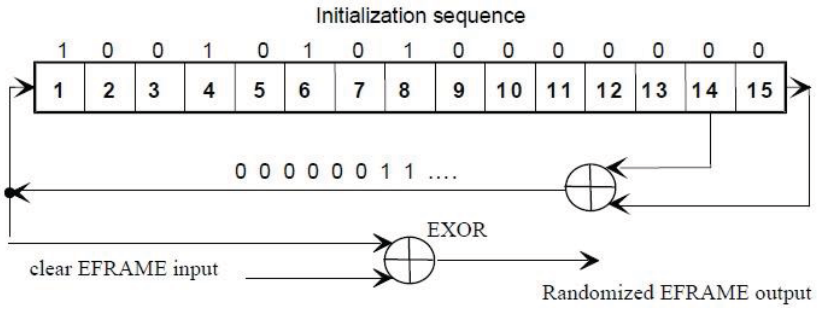

Figure 3.2: Process of data scrambling

3.2.2. FEC Encoding

Unlike its predecessor DVB-H, where concatenated convolutional code and Reed-Solomon code were used, DVB-SH adopts the state-of-art 3GPP2 turbo coding [58] as its FEC code scheme. The ETSI standard also adds some additional code rate on top of those already defined in the 3GPP2 standard to provide further flexibility. The turbo encoder is a block encoder based on a block size of 12282 bits and employs two parallel systematic recursive

convolutional encoders (RSC), with a turbo interleaver preceding the second. The process of encoding is shown in Figure 3.3 [4].

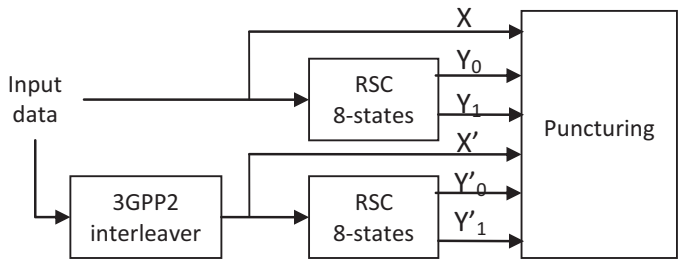

Figure 3.3: 3GPP2 turbo encoder

3.2.3. Interleaving

Three interleavers are used in DVB-SH, which are bit, time and symbol interleaving respectively. Bit interleaving is processed on a block basis, and uses address index permutation to calculate interleaved addresses for different code rates, i.e. to convert the data bit decimal index into binary data and permute the order according to defined algorithms and convert it back to decimal index. Bit interleaving also punctures the output data by 1.6% in order to facilitate the frame mapping. Time interleaving is the same as a convolutional interleaver, which is used to spread the data over time in order to avoid burst errors, which can cause severe disruption at the decoder. The length of the time interleaver in DVB-SH can range from about one hundred milliseconds to several seconds depending on the targeted service level and handheld terminal capabilities [59]. The symbol interleaver in DVB-SH is used to map data onto different subcarriers. Neighbouring data is also spread over the spectrum so as to avoid complete data loss due to severe interference over a limited bandwidth. The algorithm to calculate the address permutation is similar to that of bit interleaving.

3.2.4. Bit Mapping and Frame Structure

The DVB-SH bit mapping constellation consists of QPSK, 16QAM and hierarchical 16QAM as OFDM mode, with the exclusion of 64QAM as in DVB-H. In the TDM mode, QPSK, 8PSK and 16APSK are available.

DVB-SH offers a flexible frame structure and transmission parameters which closely follow the specifications for DVB-T and H. DVB-SH offers a new 1K mode to provide a solution for high Doppler shift scenarios, as well as a new 1.7MHz bandwidth only for the 1K mode to provide service in narrow bandwidth scenarios. The pilot allocation scheme follows that of DVB-H, where scattered and continuous pilots are combined. Table 3.1 shows the OFDM parameters for 8MHz channels and Figure 3.4 shows the pilot allocation scheme for DVB-SH.

Parameter	1K	2K	4K	8K
Total number of subcarrier	1024	2048	4096	8192
Data subcarrier	756	1512	3024	6048
Number of continuous subcarrier	25	45	89	177
Pilot and TPS subcarrier	97	193	385	769
Total useful subcarrier	853	1705	3409	6817
Null subcarrier	171	343	687	1375
Carrier spacing (Hz)	5580	2790	1395	698
Symbol duration without GI(μs)	179.2	358.4	716.8	1433.6
Available GI ratio	1/4, 1/8, 1/16, 1/32			

Table 3.1: OFDM parameters for 5MHz channels

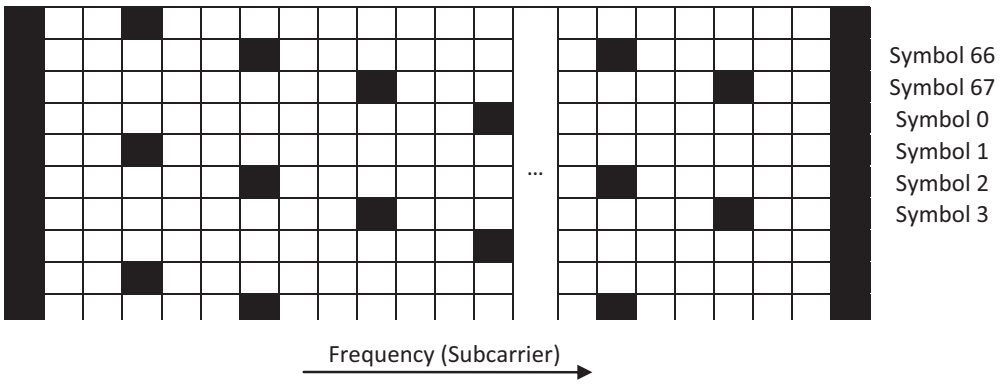

Figure 3.4: DVB-SH pilot allocation

3.3. Channel Estimation Techniques for DVB-SH

3.3.1. Signal Model

Before reviewing any existing techniques that might be suitable for DVB-SH, it is necessary to derive the mathematical representation of the received signal. Assuming perfect synchronisation and sampling precision, the complex time-domain samples of the received signal are as given in (2.15):

$$y[n] = \sum_{l=0}^{L-1} h_l x[n - D_l] + w, \tag{3.1}$$

where D_l is the delay of l th sample tap. After CP removal and FFT processing, the resultant frequency-domain signal is given as:

$$Y = HX + W, \tag{3.2}$$

where H is the CFR matrix. H is diagonal provided that the channel remains constant during the symbol duration, otherwise it will be a dense matrix with non-zero off-diagonal terms. The LS estimation for continuous pilots is given as:

$$\hat{H}_{C_i,n} = \frac{Y_{C_i,n}}{X_{C_i,n}} = H_{C_i,n} + W_{C_i,n}, \tag{3.3}$$

where subscripts (C_i, n) denote the position at the i th continuous subcarrier of the n th OFDM symbol. Equation (3.3) also applies to scattered pilot, by only replacing subscripts (C_i, n) with (S_i, n).

3.3.2. Least Squares with Linear Interpolation

Conventional linear interpolation can be used for the DVB-SH system, following the initial LS estimation. Both continuous and scattered pilots in this approach will be interpolated although interpolation over only scattered pilots can also serve the purpose. There are a couple of interpolation strategies available for this approach, one of them being the one-dimensional interpolation over frequency. This approach is performed on a symbol by symbol basis, which will not cause processing delay. On the other hand, two-dimensional interpolation can also be used, in which time interpolation on pilot-occupied subcarriers is performed first, and then followed by frequency interpolation over non-pilot subcarriers. This approach provides improved accuracy over the one-dimensional method, but for increased complexity and longer processing delay. For two-dimensional interpolation, the time interpolation in the first step is given as:

$$H_{S_i,n} = H_{S_i,n-d} + d \times \frac{H_{S_i,n-d+4} - H_{S_i,n-d}}{4}, \tag{3.4}$$

where $H_{S_i,n}$ denote the CFR at the i th scattered pilot subcarrier of the n th symbol, and d is the distance between the subcarrier to be interpolated and its nearest preceding pilot position in the same subcarrier. The subtraction in the latter part of the equation is divided by 4 as it is defined in the standard as the distance of two pilots in the same subcarrier. Similarly, the frequency interpolation on non-pilot subcarriers is given as:

$$H_{m,n} = H_{m-q,n} + q \times \frac{H_{m-q+3,n} - H_{m-q,n}}{3}, \tag{3.5}$$

where m is the subcarrier to be interpolated, q is the distance between m and its nearest preceding pilot subcarrier within the same symbol. The divisor is set as the subcarrier separation between two scattered pilots, which is 3 in this case.

3.3.3. Adaptive Interpolation Method

To optimise the interpolation accuracy and to utilize the different properties of continuous and scattered pilots, European Space Agency (ESA) have presented an adaptive interpolation algorithm, which was used for their performance assessment of DVB-SH [60]. Similar to linear interpolation, the ESA method interpolates over time ahead of over frequency. The main distinctions to conventional linear interpolation are the introduction of a much longer channel filter, as well as an online feedback scheme. In this method, continuous pilots are given a distinguished functionality which is to estimate the time-domain channel transfer function (i.e. interpolation filter coefficients), and it will incur a configurable delay to the interpolator. The method has a procedure which starts with the estimation of the channel transfer function, which is given as:

$$\hat{H}_L(C_i,n) = \sum_{m=-M_1+1}^{M_2} W_L(m,n-1)H(C_i,n-L-4m), \tag{3.6}$$

where $W_L(m,n-1)$ is the m th coefficient of the L th filter, estimated at the $n-1$ th symbol. M_1 and M_2 are the number of symbols exploited by the filter, before and after the targeted symbol respectively. $\hat{H}_L(C_i,n)$ is the estimated CFR using L th filter at the i th continuous pilot of the n th OFDM symbol, where $L=1,2,3$. Since out-dated filter

coefficients are used in the above equation, updating is necessary. This is performed firstly by calculating the estimation error of (3.6), given as:

$$e_L(C_i,n) = H(C_i,n) - \hat{H}_L(C_i,n), \tag{3.7}$$

The filter coefficients are updated by:

$$W_L(m,n) = W_L(m,n-1) + \mu \sum_{i=1}^{P} e_L^*(C_i,n) H(C_i, n-L-4m), \tag{3.8}$$

where μ is the weighing factor for coefficients update. The interpolation at scattered pilot subcarriers is therefore given as:

$$\hat{H}(S_i,n) = \sum_{m=-M_1+1}^{M_2} W_L(m,n) H(S_i, n-L-4m), \tag{3.9}$$

The choice of L is as follows: within one subcarrier, $L=1$ for targeted positions that are right next to their preceding scattered pilots; $L=2$ for targeted positions that are in the middle of two scattered pilots; or $L=3$ for targeted positions that are right before their succeeding scattered pilots,.

After time-domain interpolation, the output is interpolated over frequency for subcarriers without scattered pilots. It also starts with updating the filter coefficients, given as:

$$\hat{H}(k,n) = \sum_{j=-J_1+1}^{J_2} V_I(j,n-1) H(k-I+3j,n), \tag{3.10}$$

where $V_I(j,n-1)$ is the j th filter coefficient of the I th interpolation filter estimated at the $n-1$ th symbol. k is the subcarrier index of the non-pilot subcarriers, equal to

$$k = 3S_i + I, \tag{3.11}$$

Assuming symbol hard decision reliable, the estimation error is given as:

$$\hat{X}(k,n) = H_D\left\{\frac{Y(k,n)}{\hat{H}(k,n)}\right\}, \tag{3.12}$$

$$H(k,n) = \frac{Y(k,n)}{\hat{X}(k,n)}, \tag{3.13}$$

$$D(k,n) = H(k,n) - \hat{H}(k,n), \tag{3.14}$$

where $H_D\{*\}$ represents the complex symbol hard decision, $D(k,n)$ is the estimation error at the k th non-pilot subcarrier of the n th OFDM symbol. The coefficients update can be written as:

$$V_I(j,n) = V_I(j,n-1) + \gamma \sum_{k=3S_i+I} D^*(k,n)H(k-I+3j,n), \tag{3.15}$$

where γ is the weighing factor for coefficients update, and the summation in the above equation is applied to all possible k . The final output of frequency interpolation is given as:

$$\hat{H}(k,n) = \sum_{j=-J_1+1}^{J_2} V_I(j,n)H(k-I+3j,n), \tag{3.16}$$

Simulation results from ESA's DVB-SH assessment show that this adaptive method provides a moderate improvement over the conventional LS method and is not far away from perfect synchronisation. In satellite channels with a Rician K factor of 5dB, the adaptive method is 1.5 dB away from AWGN channel at 50km/h, while it is 1.75dB away at 100km/h. This is a good performance given the relatively low complexity of this method. However, this method involves 12 OFDM symbols over time in their simulated environment, which could potentially lead to long processing delay.

3.3.4. MMSE

MMSE exploits the correlation properties over both time and frequency; therefore it will cause processing delay as well as high computational complexity. A simplified MMSE can be adopted in the DVB-SH system without incurring such delay, in which the data is processed on a symbol basis and only frequency correlation is calculated. Assuming the total number of continuous and scattered pilots within an OFDM symbol is N_P, and the useful pilots are N_{use}, the sizes of the correlation matrices R_{yx} and R_{xx} as in (2.25) are $N_{use} \times N_P$ and $N_P \times N_P$, and their entries are given as:

$$R_{yx}(k,n) = \frac{1}{1 + j2\pi\tau_{rms}\Delta f \cdot (k - P_n)}, \quad 0 \le k \le N_{use} - 1; 0 \le n \le N_P - 1, \tag{3.17}$$

$$R_{xx}(k,n) = \frac{1}{1 + j2\pi\tau_{rms}\Delta f \cdot (P_k - P_n)}, \quad 0 \le k \le N_P - 1; 0 \le n \le N_P - 1, \tag{3.18}$$

where P is the collective subcarrier index of continuous and scattered pilots. The MMSE estimation for the n th OFDM symbol can be carried out as in (2.25). This MMSE approach

avoids the involvement of time correlation and therefore the estimation can start simultaneously at signal reception, but it should also be noted that very often the estimation of SNR, which is required by MMSE, will incur processing delay.

3.3.5. Transform Domain Technique

Transform domain interpolation techniques can be an effective approach for the DVB-SH system, and can be easily implemented in hardware nowadays. The benefits of using transform domain techniques includes lower computational complexity compared to MMSE and smaller processing delay than that caused by 2D interpolation.

The approach is to first apply IFFT on the CFRs of pilots obtained via LS estimation. Given that the number of pilot subcarriers within an OFDM symbol is much larger than the number of channel multipath taps, IFFT processing will transform CFRs into time-domain CIRs, which are a series of samples containing L significant values. Since the noise on pilot subcarriers is AWGN in the frequency-domain, it is also AWGN in the time-domain but has been spread over the whole symbol. These non-significant time-domain samples are regarded as noise in this respect and are eliminated by setting them to 0. The resultant CFRs can be obtained by transforming the L significant time-domain samples back to the frequency-domain using FFT.

3.3.6. Proposed Technique

The pilot allocation structure of DVB-SH enables an alternative method to MMSE to reduce complexity without sacrificing much performance, that is, to use MMSE only for pilot subcarriers of each symbol to improve the estimation accuracy, and interpolate over

frequency by a transform domain technique. Therefore the channel correlation matrix R_{yx} as in (2.25) can be replaced by a smaller sized R_{xx}. By doing so, the noise level is reduced not once, but twice. Also the overall complexity can be reduced significantly due to pilots only occupying 10% of useful subcarriers and a reduction of 90% over the full MMSE. Transform domain interpolation requires additional complexity on top of MMSE but is small compared to the savings.

3.4. Computational Complexity

Computational complexity is an important factor in channel estimation especially in the area of hardware implementation. On one hand, complex algorithms or operations will require more computing resources than simple ones and result in more complicated hardware design, which will ultimately lead to higher manufacturing cost. Also for mobile and handheld devices, where battery power is limited, complicated processes which require higher power consumption, will lead to significantly reduced battery duration. However on the other hand, higher complexity often comes with better performance. Take MMSE as an example: it has been established as the best performing channel estimation method for OFDM systems so far, but at the same time it also has the highest computational complex algorithm, which is largely due to the inclusion of matrix inversion. Therefore the choice of channel estimation method should not be decided on performance or complexity alone, but on a trade-off basis between the two.

It has been established that the number of real multiplications and additions required by MMSE is in the order of N^3, where N is the size of useful subcarriers, and that although the complexity of the FFT process varies, it is generally accepted that its lower bound is in

the order of $N \log_2 N$ [61,62]. Based on these, the computational complexity of each method for DVB-SH channel estimation described above is summarized in Table 3.2, where $O(x)$ means the complexity is decided by the order of x.

Estimation technique	Complexity order
LS with linear interpolation	$O(N_{use})$
LS with ESA adaptive interpolation	$c \cdot O(N_{use})$
MMSE	$O(N_P^3)$
Fourier transform	$O(N_{use} \log_2 N_{use})$
Proposed	$\frac{1}{12} O(N_P^3) + O(N_{use} \log_2 N_{use})$

Table 3.2: Computational complexity of channel estimation techniques for DVB-SH

wherein c is a constant dictated by the time and frequency filter length M_1, M_2, J_1 and J_2. It can be seen that after reducing the size of the matrix R_{yx} the complexity of MMSE combined with Fourier transform is only $1/12$ of the original MMSE with limited additional complexity brought by the Fourier transform. Depending on different transmission mode, the total complexity is reduced by 50.7% to 55.5%.

3.5. Computer Simulations

In order to verify the performance of DVB-SH systems and to test the performance of the combined MMSE and Fourier Transform technique, computer simulations have been carried out for 4 different scenarios. Within each tested scenario, 5 approaches have been simulated and their results compared. These approaches are: Ideal channel estimation as reference; LS with 2D linear interpolation; MMSE on a symbol basis; LS with Fourier Transform interpolation and the proposed method. Details of the DVB-SH specifications

used for simulations are given in Table 3.3 while details of simulation scenarios are given in Table 3.4.

Component	Parameter
Turbo coding	1/3 rate
Time interleaver length	20ms
OFDM mode	2K
FFT size	2048
GI length	1/8
Signal mapping	QPSK

Table 3.3: Simulation specifications of DVB-SH

Scenario	Channel PDP	Velocity (km/h)
1	MAESTRO profile 4	50
2	MAESTRO profile 4	80
3	MAESTRO profile 1	100
4	MAESTRO profile 1	200

Table 3.4: Simulated scenarios

The channel PDPs are taken from real measurements made by the European MAESTRO project [63]. Profile 4 has an outdoor urban propagation characteristic which is similar to street canyon environment. It has 10 multipath taps, one of which is a direct LOS link and 3 intermediate module repeaters (IMR), without any processing delay. IMR was the term used in MAESTRO for a terrestrial gap filler that relays the satellite signal via terrestrial means into urban area. Profile 1 has an outdoor rural propagation characteristic, which is more suitable for receivers at higher speeds. It has a LOS link with 7 multipath taps. Details of the two PDPs are shown in Table 3.5 and Table 3.6.

Tap	Delay (ns)	Relative Power (dB)	K-factor (dB)
1	0	-28.6	7
2	1367.2	0	-inf
3	1627.6	-3.4	-inf
4	1692.7	-4.6	-inf
5	1822.9	-4.7	-inf
6	2148.4	-18.3	-inf
7	2213.5	-18.1	-inf
8	3515.6	-18.8	-inf
9	5078.0	-4.2	-inf
10	6835.8	-19.2	-inf

Table 3.5: Channel PDP for MAESTRO profile 4

Tap	Delay (ns)	Relative Power (dB)	K-factor (dB)
1	0	0	10
2	195.3	-14.4	-inf
3	260.4	-18.2	-inf
4	846.3	-20.6	-inf
5	1171.9	-18.3	-inf
6	1953.1	-20.6	-inf
7	2734.3	-20.6	-inf

Table 3.6: Channel PDP for MAESTRO profile 1

3.5.1. Simulation Case 1 (Profile 4, v=50km/h)

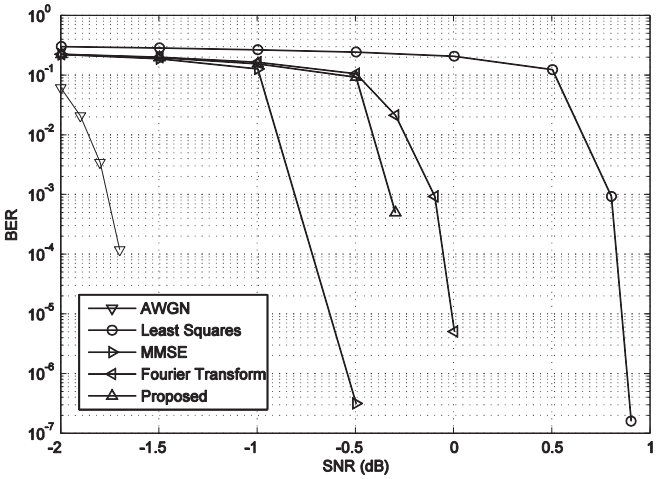

Figure 3.5: BER performance of simulation case 1

Simulation results for Case 1 are shown in Figure 3.5. It can be observed that LS performs the worst among all methods, at around 2.6dB away from ideal estimation. MMSE is around

1dB away from ideal estimation at 10^{-4}, while Fourier Transform method and the proposed method are 1.65dB and 1.4dB away respectively.

3.5.2. Simulation Case 2 (Profile 4, v=80km/h)

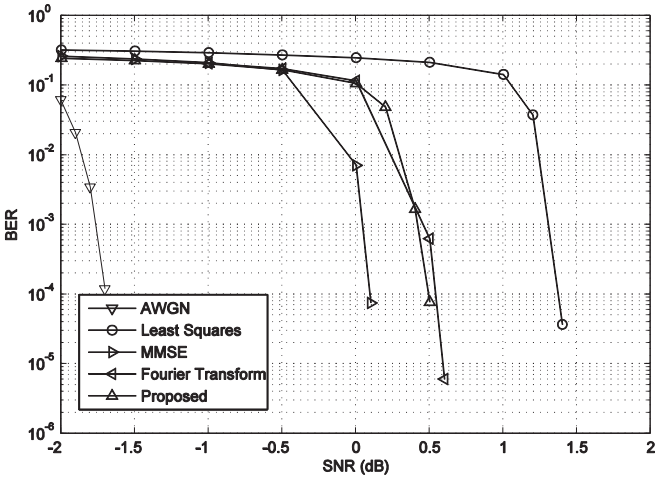

Figure 3.6: BER performance of simulation case 2

Simulation results for Case 2 are shown in Figure 3.6. In this scenario, LS is about 3.1dB away from ideal estimation. MMSE is around 1.8dB away from ideal estimation at 10^{-4}, while Fourier Transform method and proposed method are 2.2dB and 2.1dB away respectively.

3.5.3. Simulation Case 3 (Profile 1, v=100km/h)

Simulation results for Case 3 are shown in Figure 3.7. It can be observed that LS performs the worst among all methods, which is about 1.6dB away from ideal estimation. MMSE is around 0.3dB away from ideal estimation at 10^{-4}, while Fourier Transform method and the proposed method are 0.5dB and 0.4dB away respectively.

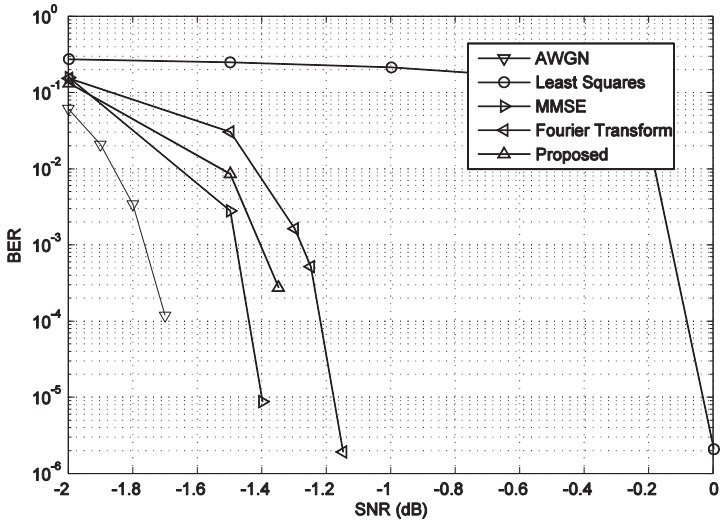

Figure 3.7: BER performance of simulation case 3

3.5.4. Simulation Case 4 (Profile 1, v=200km/h)

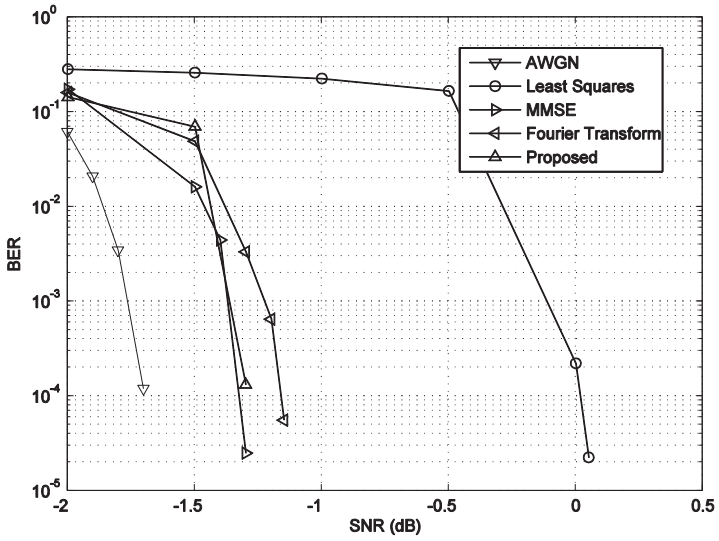

Figure 3.8: BER performance of simulation case 4

Simulation results for Case 4 are shown in Figure 3.8. The performance of LS in this scenario is about 1.8dB away from ideal estimation. MMSE is around 0.4dB away from ideal estimation at 10^{-4}, while Fourier Transform method and the proposed method are 0.6dB and 0.45dB away respectively.

3.5.5. Discussion

A comparison of BER performance at 10^{-4} is shown in Table 3.7.

Case	SNR degradation w.r.t. Ideal (dB)			
	MMSE	Proposed	Fourier Transform	LS
1	1	1.4	1.65	2.6
2	1.8	2.1	2.2	3.1
3	0.3	0.4	0.5	1.6
4	0.4	0.45	0.6	1.8

Table 3.7: BER performance comparison

From the BER results of the 4 scenarios simulated, it is obvious that LS performs the worst in all scenarios, suffering 2-3dB loss compared to ideal channel scenario, and it has a large performance gap compared to other simulated methods. Therefore although simplicity is the main advantage of LS estimation, its performance loss is an issue and may not be the best solution for DVB-SH. On the other hand, MMSE performs best of all methods in all scenarios, but the performance gain is not large compared to Fourier Transform method and the proposed method. In particular, MMSE is around 0.4-0.5dB better off than Fourier Transform and the proposed methods in MAESTRO channel 4, while its superiority is reduced to only 0.1-0.2dB in MAESTRO channel 1. Given its high computational complexity MMSE suffers, especially in the DVB-SH system where the size of the OFDM symbol is large, this performance gain cannot adequately match the cost of additional complexity. Therefore it can be concluded that MMSE is not the optimum method for the DVB-SH system.

Comparison between the Fourier Transform method and the proposed method show that their performance is very close in all scenarios. The proposed method achieves about 0.15dB gain in average. For a small complexity overhead, which is about 8% of the complexity of MMSE, the proposed method achieves better performances than the Fourier

Transform method. Therefore we can conclude that the proposed method can be applied as the optimised channel estimation schemes for DVB-SH.

3.6. Conclusions

In this chapter, we have considered channel estimation techniques for DVB-SH systems, wherein one OFDM symbol has a much larger size than in most OFDM based systems. We have reviewed some state-of-art techniques as applied to the DVB-SH system, including turbo coding, and various estimation methods that could be applicable for the DVB-SH system, namely LS, MMSE, an adaptive method from ESA and the Fourier Transform method. We have then proposed a new combined method which is based on MMSE and Fourier Transform, in order to address the high complexity specific to DVB-SH scenario. Simulation results have been shown in 4 propagation scenarios. Based on these results, we conclude that the optimised channel estimation method proposed for the DVB-SH system achieves close performance to MMSE with a much lower complexity, as well as a superior performance over the Fourier Transform method with a similar complexity. Through our simulation results, we observed large performance degradation when the receiver speed increases, which is due to the large Doppler shift resulting from the receiver velocity, and the small subcarrier spacing. This situation is specific to DVB-SH system, and is not so severe in other systems such as LTE, where subcarrier spacing is much wider. This issue leads to severe inter-carrier interference and is addressed in the next chapter.

4. Inter-Carrier Interference Cancellation for OFDM

4.1. Introduction

In previous chapters, the properties of wireless channels and basic channel estimation techniques have been investigated. In particular, channel estimation for DVB-SH, which is a current application of OFDM, has been studied. The simulation results show that a practical implementation can be established for DVB-SH with similar BER performance but with lower complexity than MMSE. However, it has been observed that there is an increasing performance loss at higher velocity in DVB-SH, which is caused mainly by the loss of orthogonality between subcarriers due to high Doppler shift. This phenomenon is common to many OFDM based systems, which compromise prolonging the symbol duration by dividing a wideband spectrum into narrow subcarriers, each bearing a much smaller data rate. As a result, Doppler shift will have a much larger impact on individual subcarriers than on single carrier systems.

A system with very large number of subcarriers such as DVB-SH is extremely vulnerable to such effects, as a 200Hz Doppler frequency (which is represented by a 100km/h velocity for an S-band carrier) can account for almost 20% of the 1116Hz subcarrier spectrum in DVB-SH 8K mode, and which leads to severe performance degradation. In modern communications, since high-rate and high-speed transmission is becoming an increasingly important feature, the issue with loss of orthogonality in OFDM systems will inevitably need to be addressed.

The remainder of the chapter is organized as follows: firstly the cause of Inter-Carrier Interference is discussed, and then we follow this by the study of existing ICI cancellation

techniques, and finally a new adaptive technique is presented and its performance compared with existing schemes.

4.2. Cause and Impact of Inter-Carrier Interference

Maintaining the orthogonality between subcarriers is a major challenge for detection and equalization in OFDM systems. In much research and publications dedicated to OFDM, the orthogonality between subcarriers is considered by assuming that the time-domain samples have enough CP padding to eliminate ISI and thus the channel remains constant for the duration of an OFDM symbol so as to avoid ICI. The former assumption, can usually be achieved since channel PDPs based on real measurements are available for a large range of propagation scenarios, and thus the length of CP can be configured to be long enough to cover the maximum delay. The latter assumption, however, is much more complicated and difficult to maintain. In fact, temporal variation of the channel can be caused by Doppler shift, oscillator frequency offset as well as frequency drift, all of which will lead to ICI and loss of orthogonality. The impact of ICI can at least partially be compensated by FEC coding or the introduction of null subcarriers. However severe ICI will still lead to the variations of the channel CFR matrix, which will invalidate the classic model as given in (2.21), and thus degrade the accuracy of any subsequent channel estimation or one-tap equalization process. Therefore it is necessary to make modifications to existing schemes to improve the system performance in the presence of ICI. It has been shown that ICI caused by frequency offset and frequency drift can be resolved in [64] and [65], therefore for the remainder of this chapter we will only consider the ICI effect caused by Doppler shift.

Doppler shift is the main source of ICI and is caused by the relative velocity between transmitter and receiver. The magnitude of the shift is proportional to the relative speed between transmitter and receiver and can be calculated as in (2.10). In classic OFDM models, channels are considered time-varying but each multipath tap remains flat for the duration of one symbol. Therefore, although the channels change rapidly between symbols, the orthogonality between subcarriers is retained in each symbol. This facilitates the CFO estimation and subsequent one-tap equalization on a symbol-wise signal processing, and is an important benefit for OFDM transmissions. However, large Doppler shifts (i.e. the quantity of Doppler shift accounts for a relatively large portion of carrier bandwidth) will lead to channel variation within an OFDM symbol, therefore damaging the orthogonality and degrading system performance. The impact of channel ICI on the OFDM subcarriers can be visualized as in Figure 4.1.

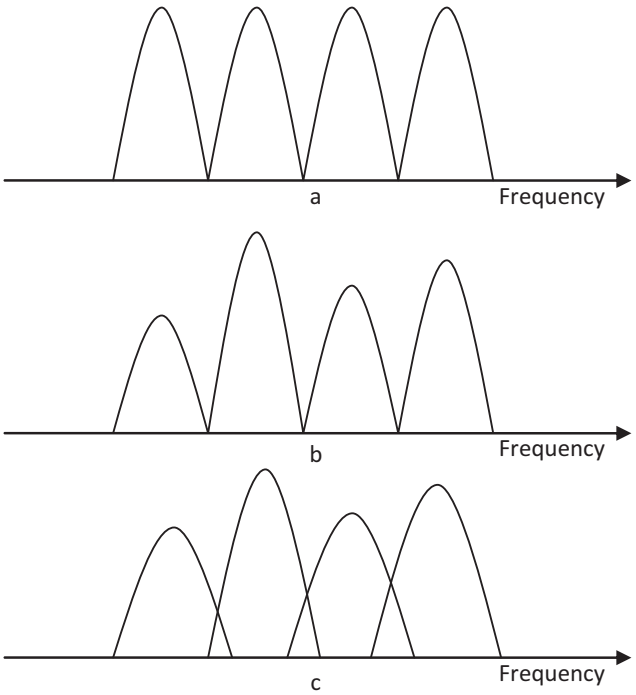

Figure 4.1: Impact of ICI on OFDM subcarriers

Figure 4.1(a) shows the spectrum of subcarriers at the transmitter, i.e. without disturbance from any noise and interference. Figure 4.1(b) shows the power spectrum distorted by fading, wherein each subcarrier suffers individual power attenuations (i.e. channel CFOs). Figure 4.1(c) shows spectrum distorted by fading and ICI, in which it can be clearly observed that each subcarrier not only suffers from power attenuation but also frequency distortion, and as a result, subcarriers interfere with neighbours.

The power of ICI can be further estimated according to [66], in which it was suggested that for the Jakes channel model, the ICI power is dependent on the Doppler frequency and symbol duration. The upper bound of ICI power is given as [66]:

$$P_{ICI} \leq \frac{1}{24}(2\pi f_d T_S)^2, \tag{4.1}$$

where f_d and T_S are maximum Doppler shift and OFDM symbol duration respectively. For system parameters for DVB-SH given in Table 3.1, the ICI power is shown in Figure 4.2.

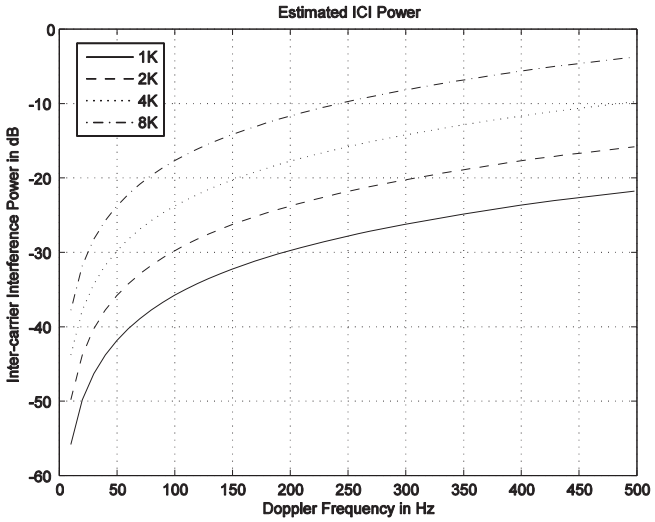

Figure 4.2: Estimated ICI power for DVB-SH modes

For a fixed Doppler frequency, each mode upgrade leads to the symbol duration being doubled, and incurs a 6dB ICI power increase. The interference in the 8K mode will be 64 times more than in the 1K mode, or 18dB higher. At 300Hz Doppler frequency, which represents a velocity of 150km/h for a 2.2GHz carrier frequency, the ICI power will be about 20dB lower than the signal power. At this level the interference will cause degradation and we thus need to consider ICI reduction schemes.

4.3. Estimation of ICI

In conventional OFDM models, it is well established that the received signal can be written in the form of matrix operation as in (2.21), where the channel CFR matrix H is diagonal with all off-diagonal inputs being 0. In this case, each diagonal input represents the channel response on that particular subcarrier, and null off-diagonal entries mean that other subcarriers will have no impact or contribution to the signal on the subcarrier in question. Also, being a diagonal matrix, H can be converted into a vector which only contains the diagonal inputs from the original matrix, and this important feature is fundamental in enabling accurate LS estimation and one-tap equalization. However, when ICI is present, H becomes a dense matrix, where off-diagonal components are the weighting factors indicating the power contribution from neighbouring subcarriers. The signal representation in (2.21) is therefore modified to:

$$Y = \widetilde{H}X + W \ , \tag{4.2}$$

where $\widetilde{H}$ is given as:

$$\widetilde{H} = \begin{bmatrix} h_{1,1} & h_{1,2} & \cdots & h_{1,n} \\ h_{2,1} & h_{2,2} & \cdots & h_{2,n} \\ \vdots & \vdots & \ddots & \vdots \\ h_{n,1} & h_{n,2} & \cdots & h_{n,n} \end{bmatrix}, \tag{4.3}$$

wherein $h_{n,n}$ is the CFR of the n th subcarrier, while $h_{n,m}$ at off-diagonal positions are the ICI components representing the power contribution from the m th subcarrier to the n th subcarrier. It is also possible to separate $\widetilde{H}$ and rewrite (4.2) as:

$$Y = \widetilde{H}X + W = HX + \sum_{\substack{m=0 \\ m \neq n}}^{N} h_{n,m} X_m + W, \tag{4.4}$$

where the second part is the ICI power.

There have been several methods proposed in the literature to estimate the ICI components for OFDM, in particular, constructing the channel matrix $\widetilde{H}$. In [67] and [68] a general method was presented to calculate the off-diagonal components in the presence of both ISI and ICI. However for the ISI-free scenario and ICI due only to Doppler shift, this method is over complicated and may not be the best solution. There are also methods proposed to estimate the matrix $\widetilde{H}$ by a Taylor series expansion [**69**,**70**,**71**,**72**], which differ in the expansion point of the Taylor series within an OFDM symbol and the use of one slope or two slopes for linearisation. The latter method uses actual estimates of the signal and was established particularly for mobility-incurred ICI scenarios with large numbers of subcarriers. It is furthermore shown that the method using one slope approximation with expansion point in the middle of the symbol outperforms other approaches [70], hence we adopt this approach as the method to estimate the ICI-disturbed channel matrix.

The computation of the channel matrix starts with the calculation of the derivatives of the channel CFR, where the CFRs can be obtained using LS with interpolation, to a linear approximation of the varying channel CFR, which is multiplied by a pre-defined matrix to construct the channel matrix. The calculation of derivatives is shown in Figure 4.3 [**72**], wherein $H_n[m]$ is the CFR of the n th subcarrier of the m th OFDM symbol.

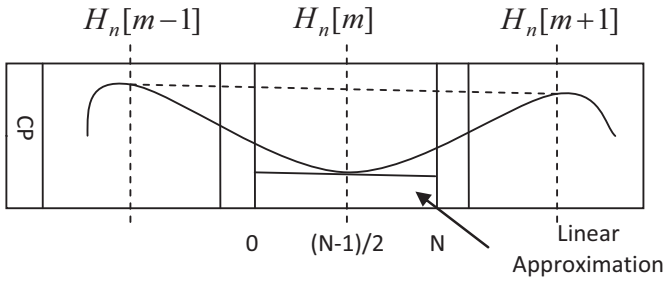

Figure 4.3: Calculation of channel derivatives

As shown in the figure, the derivative is taken as the difference quotient over the preceding and succeeding symbols as:

$$\bar{V}_n'[m] = \frac{H_n[m+1] - H_n[m-1]}{2(N + N_{CP})}, \tag{4.5}$$

where N is the size of NFFT (e.g. 2048 for 2K mode of DVB-SH), and N_{CP} is the size of CP, both in the unit of samples. The linear approximation is then given as:

$$V_n[m,k] \approx H_n[m] + \bar{V}_n'[m]\left(k - \frac{N-1}{2}\right), \tag{4.6}$$

The dense channel matrix can be obtained by taking the Fourier Transformation of $V_n[m]$ directly, or by a matrix operation given as:

$$\widetilde{H}[m] = diag(\overline{V}[m]) + \Xi diag(\overline{V}'[m]), \tag{4.7}$$

where $diag(x)$ denotes a diagonal matrix consisting of the elements of x, and Ξ is a pre-calculated $N \times N$ Toeplitz matrix given as:

$$\Xi = \begin{bmatrix} 0 & \xi_1 & \cdots & \xi_{N-1} \\ \xi_{-1} & 0 & \cdots & \xi_{N-2} \\ \vdots & \vdots & \ddots & \vdots \\ \xi_{1-N} & \xi_{2-N} & \cdots & 0 \end{bmatrix}, \tag{4.8}$$

with the elements defined as:

$$\xi_n = \frac{1}{1 - e^{j\frac{2\pi}{N}n}} = -\frac{1}{2} - j\left[2\tan\left(\frac{\pi}{N}n\right)\right]^{-1}, \tag{4.9}$$

4.4. ICI Cancellation Techniques

After obtaining the channel matrix $\widetilde{H}$, it is possible to apply zero-forcing equalization to cancel the interference, in respect to the channel model given in Equation (4.2), the equalized data is given as:

$$X[m] = \widetilde{H}^{-1}[m] \cdot Y[m], \tag{4.10}$$

wherein the matrix inversion requires $O(N^3)$ operations. It is also possible to equalize the received signal using the MMSE algorithm, which is given as:

$$X = (\widetilde{H} \cdot \widetilde{H}^*) \cdot (\widetilde{H} \cdot \widetilde{H}^* + \frac{I_N}{SNR})^{-1} \cdot Y, \tag{4.11}$$

where x^* denotes the Hermitian conjugate of x, and I_N is an identity matrix of size $N \times N$. It is obvious that this method is even more complicated and involves not only matrix inversion but also matrix-matrix multiplication.

In order to maximally reduce the interference while keeping complexity low, a number of iterative cancellation techniques have been proposed, namely OPT [73], Gauss-Seidel Iteration, PIC [74] and SIC [**75**,**76**]. These techniques have been developed in the last 15 years for other systems, where in particular, OPT was originally used in CDMA systems to eliminate the co-channel interference [77,78]. It was however revealed that ICI in OFDM caused by other subcarriers is mathematically equivalent to co-channel interference [79,80], and thus making the techniques eligible to be re-used in OFDM systems. The idea behind these interference cancellation methods is that the decisions on the subcarriers are improved iteratively [67], and these improvements result from the determination and subtraction of the interference. These techniques all have in common, that a banded or sparse matrix extracted from the original full matrix is inverted instead of the full matrix inversion, and that the cancellation of interference is done iteratively. It is also shown in [67] that all of the above four mentioned techniques, OPT, PIC and SIC have very similar performance and that all significantly reduce the interference level. The differences between the techniques can be categorized into either different ways of forming banded/sparse matrix (e.g. OPT and Gauss-Seidel Iteration) or different application purposes (e.g. PIC and SIC). In the following paragraphs, these techniques are presented in detail.

4.4.1. Operator-Perturbation Technique (OPT)

OPT is an effective way to invert linear or non-linear operators, and is also called the Jacobi iteration. In standard OPT, a banded matrix $\hat{H}$ consists of the diagonal and Q off-diagonals of $\widetilde{H}$ as in (4.3) is extracted and it is given as:

$$\hat{H} = \begin{bmatrix} h_{1,1} & h_{1,2} & h_{1,3} & 0 & \cdots & 0 \\ h_{2,1} & h_{2,2} & h_{2,3} & h_{2,4} & \cdots & 0 \\ h_{3,1} & h_{3,2} & h_{3,3} & h_{3,4} & \cdots & 0 \\ \vdots & \vdots & \vdots & \ddots & \vdots & \vdots \\ 0 & \cdots & h_{n-1,n-3} & h_{n-1,n-2} & h_{n-1,n-1} & h_{n-1,n} \\ 0 & 0 & \cdots & h_{n,n-2} & h_{n,n-1} & h_{n,n} \end{bmatrix}, \tag{4.12}$$

The OPT iteration is therefore written as:

$$X_{(0)} = \hat{H}^{-1} Y, \tag{4.13}$$

$$\varepsilon_{(0)} = (\hat{H} - \widetilde{H}) X_{(0)}, \tag{4.14}$$

$$X_{(i+1)} = \hat{H}^{-1} (\varepsilon_{(i)} + Y), \tag{4.15}$$

$$\varepsilon_{(i+1)} = (\hat{H} - \widetilde{H}) X_{(i+1)}, \tag{4.16}$$

where subscript i denotes i th iteration, and equation (4.13) and (4.14) are initialization steps. The sufficient condition for OPT to converge is that the matrix $\widetilde{H}$ is strictly or irreducibly diagonally dominant, that is within each row the absolute value of the diagonal term is greater than the sum of absolute values of other terms, given as:

$$\left|h_{i,i}\right| > \sum_{j \neq i} \left|h_{i,j}\right|, \tag{4.17}$$

4.4.2. Gauss-Seidel Iteration

A similar method to OPT is called the Gauss-Seidel iteration, which is named after German mathematicians Carl Friedrich Gauss and Philipp Ludwig von Seidel. It is an improved version of OPT in respect of its memory efficiency, as it does not require additional memory to store $X_{(i)}$ [81]. As with the OPT method, although Gauss-Seidel iteration can be applied to matrices with non-zero diagonals, convergence is guaranteed only when the main diagonal is strictly or irreducibly diagonally dominant. The main difference to Jacobi iteration is that when forming the sparse matrix, Gauss-Seidel iteration uses the lower triangle of the matrix $\widetilde{H}$ instead of using a banded matrix as in OPT, which is given as:

$$\hat{H} = \begin{bmatrix} h_{1,1} & 0 & 0 & 0 & \cdots & 0 \\ h_{2,1} & h_{2,2} & 0 & 0 & \cdots & 0 \\ h_{3,1} & h_{3,2} & h_{3,3} & 0 & \cdots & 0 \\ \vdots & \vdots & \vdots & \ddots & \vdots & \vdots \\ h_{n-1,1} & h_{n-1,2} & h_{n-1,3} & \cdots & h_{n-1,n-1} & 0 \\ h_{n,1} & h_{n,2} & h_{n,3} & \cdots & h_{n,n-1} & h_{n,n} \end{bmatrix}, \tag{4.18}$$

The Gauss-Seidel iteration then follows the steps defined in (4.13)-(4.16).

4.4.3. Parallel Interference Cancellation (PIC)

The above described OPT (Jacobi iteration) and Gauss-Seidel iteration use complete linear operations to achieve interference cancellation. It was also shown that non-linear operations can also be incorporated with linear operations to achieve improved accuracy.

Parallel Interference Cancellation (PIC) and Serial Interference Cancellation (SIC) are two of this kind.

PIC uses a similar approach to OPT, where the cancellation process takes place in a symbol-wise way for OFDM based systems. The determination and cancellation of the interference for each iteration are given as:

$$\varepsilon_{(i)} = \widetilde{H}X_{(i-1)} - \hat{H}X_{(i-1)}, \tag{4.19}$$

$$Y_{(i)} = Y_{(i-1)} - \varepsilon_{(i)}, \tag{4.20}$$

where $\widetilde{H}$ is the banded matrix and $\hat{H}$ is the full matrix. A new estimate of X is then given as:

$$\widetilde{X}_{(i)} = \widetilde{H}^{-1}Y_{(i)}, \tag{4.21}$$

In PIC, a non-linear operation is inserted after this step which forces the estimated $\widetilde{X}$ into the used modulation constellation (e.g. BPSK, QPSK). It is suggested in [82] that the hyperbolic tangent function is a good choice for BPSK, as estimates with large amplitudes are forced into {+1, -1} while estimates with small amplitudes are relatively unchanged. This operation can be written as:

$$X_{(i)} = \tanh(c \cdot \widetilde{X}_{(i)}), \tag{4.22}$$

where c is a constant and controls the slope near to zero. Smaller values of c (e.g. $c < 1$) can be chosen at the beginning of the iteration or when the estimates are not reliable, while

larger values (e.g. $c > 10$) can be chosen when the estimates are relatively reliable. It is also shown in [82] that performance can be improved if c is made adaptive, wherein the value of c is chosen according to the channel signal to interference ratio (SIR) and is increased each iteration, as the confidence of the estimates increases after each iteration of cancellation.

4.4.4. Serial Interference Cancellation (SIC)

SIC is an alternative to PIC and cancels the interference in a subcarrier-wise form. The reason for having SIC is to avoid long processing delays as some subcarriers have smaller SIR which requires more iteration while others have larger SIR and convergence may be achieved after only a few iterations. The idea of SIC is to order subcarriers by their respective SIRs, and then process those strong sub-channels with higher SIRs first. By doing so several symbols of one subcarrier can be processed simultaneously and therefore processing delays can be reduced. Using SIC will ensure that high reliability channels (i.e. with high SIR) are processed before the weak channels. In each iteration the subcarriers are processed in the order of their corresponding SIR that was calculated beforehand. The algorithm for SIC is similar to PIC. The main advantage of SIC is that the reduction of long processing delays and that the processing of subcarriers can be distinguished by their channel qualities.

4.5. Proposed Method

PIC and SIC have provided an effective way to cancel the ICI. However, PIC disregards the difference of qualities in subcarriers and uses a banded matrix to carry out the cancellation, whilst SIC processes several symbols on one subcarrier together which requires memories to

store the symbols on the remaining subcarriers pending processing. In practice, SIRs on subcarriers are independently distributed and it results in SIRs on each subcarrier differ from one to another, effectively making subcarriers with a relatively high SIR being considered more reliable while others are considered less reliable. Figure 4.4 illustrates an example of SIR distribution for 256 subcarriers where the Doppler shift accounts for approx 20% of subcarrier spacing.

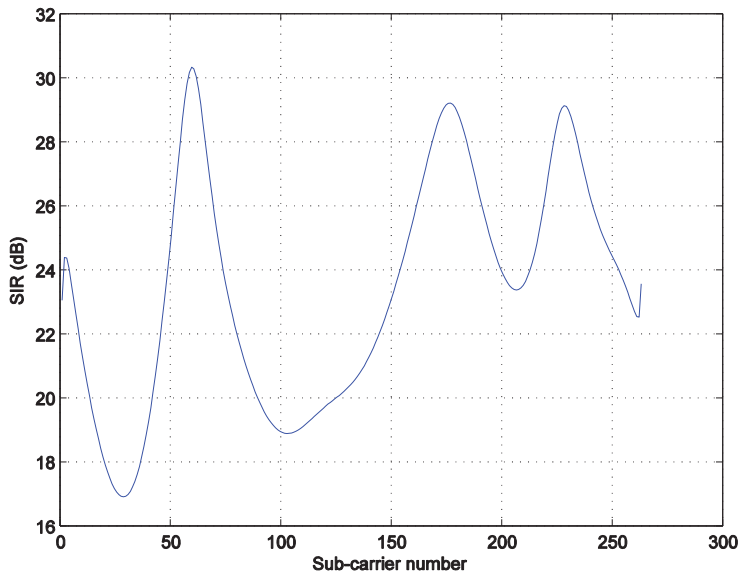

Figure 4.4: Distribution of SIR

Due to the fact that PIC treats all subcarriers equally when constructing the matrix $\hat{H}$, it is not an efficient process. This is illustrated by the rows in $\hat{H}$ which represent reliable subcarriers consisting of a large number of off-diagonals which exceeds requirement, while on the other hand, the value of Q may be insufficient for certain weak subcarriers to achieve a reasonable accuracy and thus degrades the overall system performance. This kind of arrangement will inevitably reduce the system efficiency and performance.

In order to optimise the system performance and maximize the resource efficiency, we propose an adaptive method based on PIC that adaptively allocates matrix components in the sparse matrix $\hat{H}$. The idea of this method is to consider the independent channel SIR as a weighting factor, and use this information to determine the number of off-diagonals to be allocated for each row. For more reliable subcarriers which have high SIR, fewer matrices will be allocated, whilst for less reliable subcarriers with low SIR, more matrices will be allocated. Therefore, balanced cancellation can be achieved across subcarriers and thus the risk of one weak subcarrier affecting others will be reduced. Firstly, the SIR of a given subcarrier is defined as:

$$SIR_k = \frac{\left|h_{k,k}\right|^2}{\sum_{\substack{n=0 \\ n\neq k}}^{n=N-1} \left|h_{k,n}\right|^2}, \tag{4.23}$$

where SIR_k is the SIR of the k th subcarrier, $h_{k,k}$ and $h_{k,n}$ are respectively the diagonal and off-diagonals of matrix $\widetilde{H}$. The sufficient condition that the channel matrix being strictly or irreducibly diagonally dominant as set in (4.17) which guarantees methods like OPT or PIC to converge can also be interpreted in terms of SIR, given as:

$$SIR_k > 1, \tag{4.24}$$

The SIR information is then used to determine the allocation of off-diagonal matrices, and here it is done by a hyperbolic tangent function, given as:

$$a_k = round(\frac{1}{\tanh(SIR)}), \tag{4.25}$$

where a_k is the number of off-diagonals on one side allocated to row k, and is effectively an adaptive Q. In order to maintain the complexity at a similar level to PIC, the total number of off-diagonals should be similar to a banded matrix with Q off-diagonals. A simple normalization step can therefore be taken as:

$$\widetilde{a}_k = round(\frac{a_k \cdot N \cdot Q}{\sum_k a_k}), \tag{4.26}$$

where N is the total number of subcarriers. Hence based on SIR information on each subcarrier, a vector of a_k can be calculated and a new sparse matrix $\hat{H}$ constructed, which can be illustrated as:

$$\hat{H} = \begin{bmatrix} h_{1,1} & 0 & 0 & 0 & \cdots & 0 \\ h_{2,1} & h_{2,2} & h_{2,3} & 0 & \cdots & 0 \\ h_{3,1} & h_{3,2} & h_{3,3} & h_{3,4} & \cdots & 0 \\ \vdots & \vdots & \vdots & \ddots & \vdots & \vdots \\ h_{n-1,1} & \cdots & h_{n-1,n-3} & h_{n-1,n-2} & h_{n-1,n-1} & h_{n-1,n} \\ 0 & 0 & \cdots & h_{n,n-2} & h_{n,n-1} & h_{n,n} \end{bmatrix}, \tag{4.27}$$

where it is easy to distinguish that the first subcarrier (first row) is a strong one, with no off-diagonals, while the subsequent subcarrier (row $n-1$) being a weak one, with all off-diagonals remaining. The subsequent cancellation process follows that of PIC as defined in (4.19) and (4.20).

4.6. Computer Simulations

Computer simulations were carried out to validate and demonstrate the performance of some of the above mentioned methods as well as to prove the superiority of the adaptive

cancellation method. Since the level of ICI is proportional to the receiver velocity and fast moving receivers are more likely to occur in rural areas rather than urban areas, the simulated propagation channel is chosen as MAESTRO profile 1 [63] in order to best reflect the propagation environment likely to be experienced in practice. The chosen channel PDP was shown in Table 3.6 and has an outdoor rural characteristic with a LOS satellite link and 6 other NLOS multipath links.

The OFDM simulation test scenario is a simple system without coding or interleaving. In each transmission, a group of symbols is QPSK mapped and inserted with scattered pilot tones and modulated via IFFT. Five methods were simulated and are listed as: Ideal channel state information as reference; LS with 2D linear interpolation; based on LS estimates, we estimate dense ICI matrix from which Zero-forcing equalization (i.e. full channel matrix inversion), PIC and the proposed adaptive method are also simulated. The details of the OFDM simulation parameters are shown in Table 4.1, and the details of simulated scenarios are shown in Table 4.2.

Parameter	Value
NFFT	256
GI length	16
Subcarrier spacing	4464Hz
OFDM symbol per transmission	10
Useful symbol per transmission	8
Carrier frequency	2.2GHz
Scattered pilot spacing	8 subcarriers
Signal mapping	QPSK
Number of off-diagonals on each side (Q)	4
Number of iterations for PIC	4

Table 4.1: Simulation parameters of OFDM test bench

Scenario	Channel PDP	Velocity (km/h)
1	MAESTRO profile 1	100
2	MAESTRO profile 1	200
3	MAESTRO profile 1	300

Table 4.2: Simulated scenarios

4.6.1. Simulation Case 1 (100km/h)

The results for simulation scenario 1 are shown in Figure 4.5, wherein the receiver is moving at 100km/h. The Doppler shift under this case accounts for approx 5% of the subcarrier spacing.

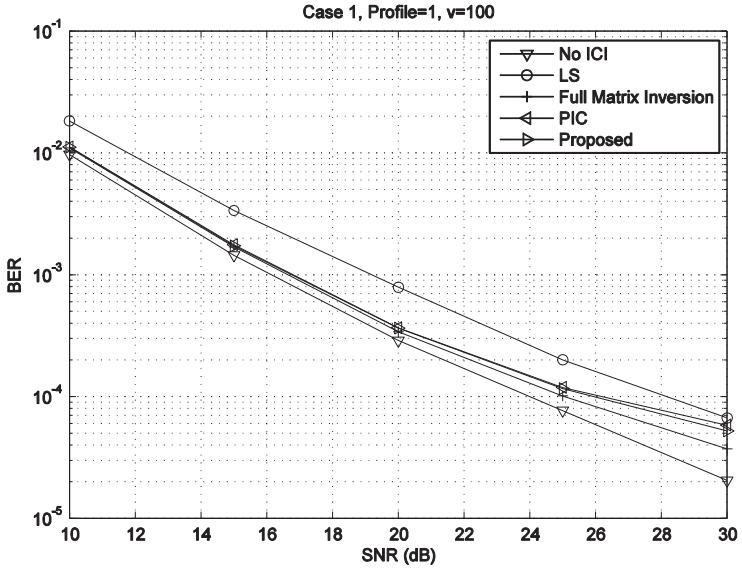

Figure 4.5: Simulation results for scenario 1

Simulation results show that at BER=10^{-4}, full matrix inversion method achieves 1dB better than PIC and adaptive cancellation and is 1dB away from ideal estimation, while adaptive cancellation performs slightly better than PIC, and LS is 2dB away from PIC.

4.6.2. Simulation Case 2 (200km/h)

The results for simulation scenario 2 are shown in Figure 4.6, wherein the receiver is moving at 200km/h. The Doppler shift under this case accounts for approx 10% of the subcarrier spacing.

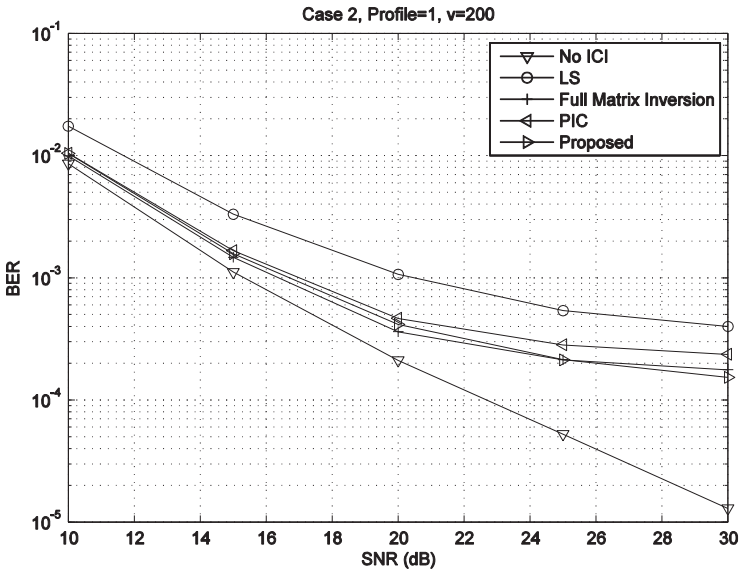

Figure 4.6: Simulation results for scenario 2

Simulation results show that all methods suffer from a performance gap from ideal estimation and LS performs much worse than the three other cancellation methods. It can be seen that the adaptive method performs almost identically to the full matrix inversion method, but performs much better than PIC.

4.6.3. Simulation Case 3 (300km/h)

The results for simulation scenario 3 are shown in Figure 4.7, wherein the receiver is moving at 300km/h. The Doppler shift under this case accounts for approx 15% of the subcarrier spacing.

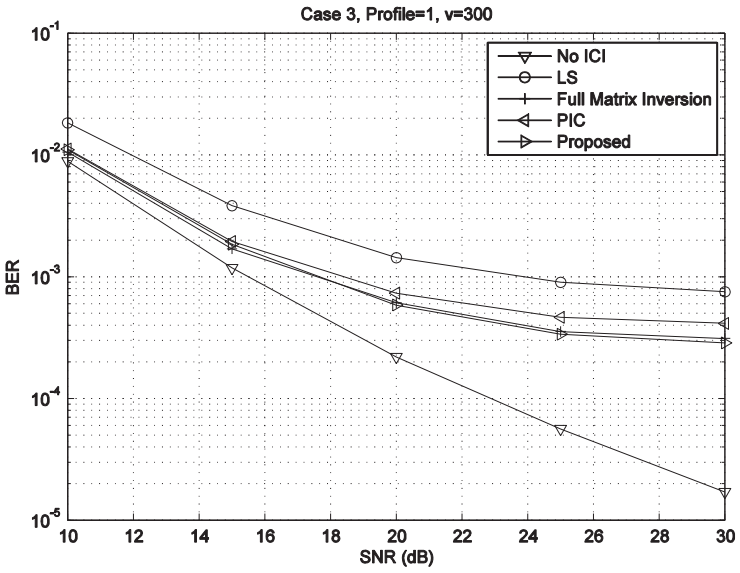

Figure 4.7: Simulation results for scenario 3

Simulation results show that all methods suffer from a performance gap from ideal estimation and LS performs much worse than the other cancellation methods. Within the three cancellation methods, adaptive cancellation performs very similar to full matrix inversion, while its performance is much better than that of PIC.

4.6.4. Discussion

A comparison of BER performance at 10^{-3} is shown in Table 4.3.

Case	Velocity (km/h)	SNR degradation w.r.t. Ideal (dB)			
		Full Matrix inversion	Proposed	PIC	LS
1	100	1	1	1.2	2.5
2	200	1.5	1.7	2	5
3	300	2	2	3	10

Table 4.3: BER performance comparison

From the BER results of the 3 scenarios simulated, it is obvious that LS performs the worst of them all in all scenarios, and is some way off compared to other simulated methods. On the

other hand, Full matrix inversion performs best of all methods in all scenarios, but the performance gain is not significant compared to the proposed method and PIC. To be specific, the proposed method performs almost the same as full matrix inversion in all cases. PIC performs similar to the proposed adaptive method, however with an average loss at around 0.5dB for each case. Therefore it is verified that the proposed adaptive method optimises the PIC method by achieving a performance gain without imposing any significant computational complexity, while in some cases it performs very well to achieve an indistinguishable performance compared to full matrix inversion.

4.7. Conclusions

In this chapter, we have considered OFDM systems suffering from ICI, due to the large Doppler shift associated with high velocity of the receiver. The main impact of ICI in an OFDM system is to destroy the orthogonality between subcarriers. Loss of orthogonality between subcarriers leads to the introduction of off-diagonal elements in the channel matrix, making the traditionally considered diagonal channel matrix inaccurate and increasing the complexity of channel estimation and equalization. All of these effects will in the end degrade the system performance in terms of BER.

In order to compensate the impacts of ICI, we estimated ICI as a separate term and mitigated it using cancellation methods. We have shown that the ICI terms can be represented as off-diagonal elements in a dense channel CFR matrix, and these off-diagonal terms can be estimated by Taylor series expansion and using linear operations. It is however computationally intensive to cancel these terms using a direct approach as this involves the inversion of a potentially very large matrix. As a result, iterative cancellation methods have

been studied as they require the inversion of only a small portion of the original full matrix and thus the complexity is reduced. These iterative methods, namely OPT, Gauss-Seidel iteration, PIC and SIC, all have similar iterative algorithms but their method of constructing the sparse matrix to be inverted are different. It is however noticed that as they treat all subcarriers equally, their method of constructing the matrix is not optimised and will thus limit the accuracy of the cancellation performance. Therefore we have proposed an adaptive method to construct the sparse matrix which uses signal to interference ratio (SIR) as an indication of subcarrier quality and to determine the number of off-diagonals to be allocated to each row. This proposed adaptive method treats subcarriers unequally in terms of forming the matrix but will guarantee a relatively equal cancellation performance from each subcarrier and thus reduce the risk of domination by the weakest.

The proposed adaptive method has been simulated to verify its performance. The simulated propagation environment is that of outdoor rural environment where severe ICI is more likely to occur due to higher speeds. Computer simulations have shown that the adaptive method outperforms PIC in all cases for a similar level of complexity and in some cases it achieves performances very close to the direct interference cancellation method which has a much higher complexity. Therefore these results verify the superiority of the proposed adaptive method over the PIC in terms of BER performance at a similar level of computational complexity. It is also noteworthy that the performance of the proposed adaptive method may be further improved if the algorithms set in (4.25) and (4.26) can be optimised.

5. Low-Complexity OFDM Channel Estimation in the Time-Domain

5.1. Introduction

In previous chapters, a number of popular channel estimation techniques for OFDM have been reviewed, such as LS, MMSE and several widely used interpolation methods. We have also presented several ICI cancellation techniques, such as OPT and PIC, which can be incorporated with existing channel estimation methods. It is noteworthy that a majority of these methods are based in the frequency-domain, and that an efficient time-domain channel estimation technique with similar accuracy or complexity is lacking. In fact, time-domain channel estimation methods for OFDM have not attracted as much interest as frequency-domain techniques. This is mainly due to the difference in modelling the multipath channels in the two domains, wherein the multipath channel is represented as a complex valued power gain in the frequency-domain while in time-domain it is an FIR-filter. Therefore frequency-domain channel estimation techniques have an advantage over their time-domain counterparts in respect of low complexity and implementation simplicity. An issue with frequency-domain estimation is the use of scattered pilots, which facilitate 2D interpolation and is common in OFDM systems. However, these scattered pilots may not adequately serve other purposes such as synchronisation. Although in scattered pilot based systems, synchronisation can be achieved by exploiting the correlation properties between pilots and the received signal, this comes at the cost of higher complexity and larger processing delay since the pilots are generally sparse. It has been shown that the best synchronisation accuracy is achieved in the time-domain using preamble or training symbols, and in [83] near-ideal synchronisation can be achieved under such conditions. Therefore in

systems where a preamble is already in place, time-domain channel estimation becomes attractive in the form of an integrated synchronisation and channel estimation scheme and could optimise the spectral efficiency by re-using the data and the training symbols that were designated for synchronisation and could thus reduce the overall complexity and increase spectral efficiency. Thus in this chapter, we review channel estimation techniques in the time-domain. The challenges with time-domain techniques such as issues in complexity and imperfect synchronisation are first presented. Then an integrated scheme of synchronisation and channel estimation with imperfect synchronisation scenario which is applicable to WiFi and Fixed WiMAX is developed. The performance of this new scheme is then verified by simulation results.

5.2. Channel Estimation in the Time-Domain

Time-domain channel estimation aims to accurately approximate the channel PDP, whose coefficients form the FIR-filter as in (2.15). The channel PDP is helpful in removing the channel effects from the received signal in the time-domain, and it can also be transformed into frequency-domain CFRs by FFT processing to enable one-tap equalization.

Time-domain channel estimation techniques are essential in single-carrier systems and have been extensively studied for these systems. However they became less favourable in multi-carrier systems as they suffer from a number of drawbacks, most notably higher complexity and higher vulnerability to imperfect timing synchronisation. These drawbacks, which will lead to performance degradation or even reception breakdown, need to be compensated in order to maintain the system performance. In subsequent paragraphs these drawbacks will be reviewed.

5.2.1. Complexity

Complexity is an important factor in communication systems, as complex methods are often more difficult in practical implementation which adds cost to both manufacturers and consumers. The popularity for time-domain channel estimation is hugely affected by complexity issues, as most time-domain methods are more complicated than similar approaches in the frequency-domain. Since pilots for channel estimation purposes are usually allocated either continuously over frequency (training symbol) or scattered as in section 2.3.5. , a complexity comparison between time-domain and frequency-domain channel estimation techniques can be performed for these two pilot allocation schemes.

In a training symbol scheme, the simplest channel estimation method in the frequency domain is LS, wherein full CFRs can be obtained by time interpolation. If additional complexity is affordable, the estimation accuracy of training symbols can be further improved by FFT processing, which was reviewed in section 2.3.6. Since complete time-domain samples of the training symbol can be obtained by IFFT processing, CIR estimation can be carried out by a filtering process. In section 5.2 it was shown that ML estimation can also be applied in this case. However, all of these time-domain methods will necessitate complexity that is higher than that of the frequency-domain LS with interpolation, and will be unable to guarantee an improved performance.

In the scattered pilot mode, LS in the frequency-domain enjoys maximum flexibility, and techniques in this field have been reviewed thoroughly in section 2.3. In the time-domain, since scattered pilots only appear non-continuously within one OFDM symbol, the time-domain samples have several identical parts depending on the pilot subcarrier spacing.

Therefore, directly estimating CIRs or channel PDP in the time-domain requires more data and achieves less accuracy. In addition, since time-domain approaches usually involve threshold setting to identify tap positions and explore the correlation properties, the overall complexity is much higher than similar methods in the frequency-domain.

5.2.2. Timing Synchronisation Error

Timing synchronisation seeks to establish the SoF point in order to facilitate subsequent processes such as the positioning of the FFT window. Therefore it is important that an effective system employs an accurate synchroniser. Literature in the field of OFDM channel estimation usually assumes perfect synchronisation to simplify the estimation process. However, due to the channel variance and the randomness of noise, perfect synchronisation is not achievable and will have to be addressed in the interest of practical implementation.

In OFDM systems, the use of CP can provide some tolerance to timing synchronisation error. This tolerance is achieved as long as the detected SoF falls within the ISI-free region (i.e. orthogonality of the subcarriers are not affected), in which case the timing errors are reflected as a linear phase shift of the data subcarriers and can be compensated by frequency-domain based channel estimation techniques. In the worse case, where the detected SoF falls outside the ISI-free zone, severe performance degradation is expected in both domains due to the damage to orthogonality. This effect is illustrated in Figure 5.1. It is obvious from this that the received signal within the ISI-free zone is formed entirely from data of the current symbol, and thus the orthogonality will not be affected.

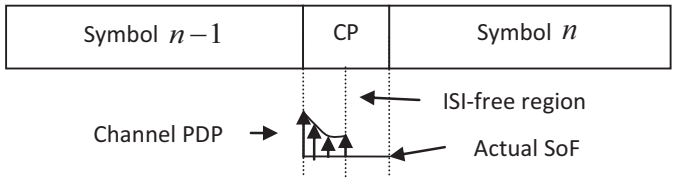

Figure 5.1: ISI-free zone

5.2.3. Existing Time-Domain Channel Estimation Techniques

Assuming perfect synchronisation, there are several techniques that have been established for time-domain OFDM channel estimation. Among these is a straightforward approach that is based on training symbols. The training symbol in this method is set to all '1's in the frequency-domain, which results in impulse-shaped time-domain samples after IFFT processing. CIR coefficients can be estimated by detecting the multiple replicas of such impulses. Alternatively, a PN sequence can also be used as the training symbol. Using a PN sequence in this approach will not affect the estimation performance, however it will facilitate the synchronisation process since the correlation of PN sequence in the time-domain will result in a sharp peak. The drawback of this approach is the complexity of threshold setting during detection when noise is severe.

Without using training symbols, ML estimation offers an alternative with good accuracy. It considers the CIR as a vector with deterministic but unknown parameters, and thus does not require a large volume of channel statistics, resulting in lower complexity and smaller processing delay compared to techniques such as MMSE, which require more channel information. Given the frequency-domain signal representation as in (2.21), the time-domain ML estimation is [57,84,85,86]:

$$\hat{h}_{ML} = (F^* F)^{-1} F^* diag(X)^* Y, \tag{5.1}$$

where F is the unitary Fourier matrix. A few variants have been developed from this approach, which either assume the length of the multipath channel to reduce complexity or consider the arrangement of pilots to optimise performance. The complexity of this method is always higher than that of the frequency-domain LS regardless of the approach taken.

In addition some more complex methods have also been proposed. The authors of [87] proposed a method called TPTCTE (Time domain Pilot Time Cross-correlation and Time varying Estimation), wherein the channel fading process is divided into long-term and short-term fading. Long-term fading is modelled as a log-normal distribution and the rate of such fading can be obtained on a symbol basis. The short-term fading aims to compensate in the time-domain the variations of phase and amplitude caused by Doppler shift, which is similar to the ideas of ICI cancellation. The method divides one OFDM symbol into several sub-blocks and iteratively estimates the CIR of each sub-block. The final CIR is obtained by averaging the CIRs among all sub-blocks within one symbol, and simulation results show that moderate improvement in terms of uncoded BER can be achieved. However, the additional complexity required by this method can be high for OFDM systems with large FFT window sizes, and the efficiency of ICI cancellation by averaging CIR will not outperform those methods that consider ICI as part of a dense channel matrix.

In [88] the authors consider the cyclic correlation error caused by spectral leakage as a result of null subcarriers. They proposed a method to effectively remove such error in fast multipath fading channels. The proposed method estimates the CIR via the Fourier transformation of the frequency-domain CFRs, and then applies an iterative cancellation algorithm to eliminate unwanted noise terms, without exploiting large-sized correlation

properties. The simulation results show that this method achieves reasonable accuracy. However its improvement over conventional methods is limited while the complexity of such iterative methods can be a drawback.

In most time-domain channel estimation methods, CIR can usually be obtained in one of two ways: via ML estimation (or its variation) or via DFT-based frequency pilot estimation. Either method results in a time-domain vector which contains estimates of CIR at tap positions and noise terms at non-tap positions. In order to improve the accuracy, these noise terms should be eliminated, usually by setting up a threshold. Several methods have been presented to optimise the threshold setting, most notably the most significant sample (MSS) approach as reviewed in section 2.3.6. Although this approach is the simplest, it requires in general knowledge of the number of channel taps which is not easy to obtain and requires additional processing. In scenarios where channel knowledge is not available, the threshold is usually set according to statistics, or according to a maximum likelihood function. In [89] the authors proposed an efficient threshold setting algorithm based on wavelet decomposition, wherein the received signal in the frequency-domain is divided into two groups: approximation coefficients which are important, and detail coefficients which are relatively unimportant. The threshold is obtained by calculating the median of these unimportant coefficients. Simulation results show that this method achieves an improvement over conventional methods, while the additional complexity is affordable.

Apart from pilot-based estimation methods, blind estimation has also been studied in the time-domain, where it is usually carried out by exploring the special properties of CP. In [90] the authors propose a method to estimate the noise variance (or SNR) as well as the CIRs

based on the correlation between CP and the rest of the symbol. This method achieves reasonable accuracy when sufficient data are processed and increases the spectral efficiency by avoiding the use of pilots. However the procedures in estimating the required parameters are complex, and that the method requires up to 3000 symbols to achieve good performance. This level of complexity and processing delay is unrealistic in many OFDM systems, where high data-rate real-time reception is essential.

5.3. Proposed Low-Complexity Technique

From the above reviews, it is obvious that in the time-domain a low complexity, implementable channel estimation scheme with good accuracy is necessary. Ideally, this scheme should be able to compensate the performance degradation caused by imperfect synchronisation, as well as a feedback function which enables the estimator to utilize parameters obtained from previous estimations to ease future processing. In this section, we present a low complexity time-domain channel estimation method. The scheme uses a simplified ML approach to estimate CIR information under imperfect timing synchronisation, which can be compensated by a CIR optimisation algorithm. Furthermore, delay spread can be estimated and noise terms reduced as part of the process, which helps to further reduce complexity and improve system performance. The scheme re-uses the existing training symbol used for synchronisation, for channel estimation with a significantly lower complexity than the popular MMSE technique.

5.3.1. Scheme Overview

The scheme comprises of several modules and a block diagram representation is shown in Figure 5.2. The processes in this scheme can be summarized as follows: Firstly, the received

time-domain signal samples are processed for timing and frequency synchronisation as defined in [83]. The synchronisation process uses a preamble consisting of one training symbol with two identical parts in the time domain which is generated in the frequency-domain using PN sequences. The preamble is then re-used with the estimated SoF to obtain CIR estimates via a simplified ML approach, whose output is in the form of a matrix containing up to $G \times G$ elements, which represents CIR estimates at various timing points up to $G-1$ samples preceding the estimated SoF. This is followed by a decision mechanism wherein the optimised CIR estimate is chosen and converted via FFT processing to obtain the CFR estimate. Frequency-domain equalization is then performed in a similar fashion to conventional techniques. The optimised CIR information can also be used for the channel delay spread estimation, which can then be used to further reduce the complexity of this scheme in subsequent CIR estimations.

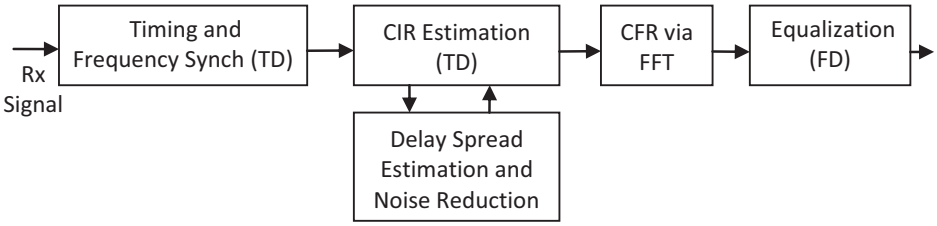

Figure 5.2: Block diagram of the low complexity estimation method

5.3.2. System Model

The samples of an OFDM symbol at the output of the IFFT in the transmitter are given by:

$$x(k) = \frac{1}{N}\sum_{n=0}^{N-1} X(n) e^{j\frac{2\pi}{N}nk} \qquad 0 \le k \le N, \tag{5.2}$$

where N is the FFT size and N_{used} is the number of subcarriers used. $X(n)$ represents the data modulated on the n th subcarrier while $x(k)$ represents the symbol samples after IFFT processing. Each transmitted OFDM symbol is usually preceded by a guard interval or CP of length G in order to eliminate the ISI arising from the wideband channel. Assuming sampling precision, since the channel delay profile is unknown, we hence consider a pseudo channel delay profile wherein the multipath channel has G taps with uniformly distributed delays of one sample and unknown power gains. This assumption is made on the basis that it is common to assume that the channel delay spread is less than the length of the CP. The complex samples of the received signal from an ISI (wideband) channel can be represented as:

$$r(k) = y(k-\theta)e^{j2\pi\varepsilon k/N} + \omega(k), \tag{5.3}$$

where $r(k)$ is the k th received signal sample, θ is the integer symbol timing offset measured in samples, ε is carrier frequency offset normalized to the subcarrier spacing, $\omega(k)$ represents the zero-mean complex AWGN and

$$y(k) = \sum_{l=0}^{L-1} h_l x(k-l), \tag{5.4}$$

where h_l is the impulse response of the wideband channel whose memory order is $L-1$ samples.

5.3.3. Simplified ML Estimation

In the simplified ML estimation, we consider imperfect timing synchronisation wherein the received signal still has a residual timing error i_d whose value represents its distance to the actual SoF $i_d = 0$ (i.e. positive value of i_d means the detected SoF succeeds the actual SoF in time, and vice versa). The channel PDP is considered as a uniformly delayed G tap ISI channel, wherein the first tap has zero delay. It has been observed in [83] that the actual SoF may be missed due to severe fading of the first arriving channel tap. In this case, the strongest received channel tap (such as the 2nd or 3rd) is detected as SoF, resulting in a positive residual timing error. This effect is not desirable from a CIR estimation point of view since the estimation process will miss the first arriving tap, thereby causing large performance degradation. Therefore, we propose to compensate the effect of imperfect timing synchronisation by making a variation to the conventional ML technique, the goal of which is to be able to capture all arriving channel taps while maintaining a low computational complexity. We do this by scanning for the CIR estimate within G timing points preceding the detected SoF, and subsequently choosing the optimised CIR estimate through a decision mechanism.

Taking i_d into account and assuming perfect frequency synchronisation, the received signal can be rewritten as:

$$r(k) = \sum_{l=0}^{G-1} h(l)x(k-l+i_d) + \omega(k), \tag{5.5}$$

The cross-correlation of the received signal and the transmitted training symbol with m samples delay, wherein m varies from 0 to $G-1$ is given as:

$$\gamma_m = \sum_{k=0}^{N-1} r(k) \cdot x^*(k-m), \tag{5.6}$$

where x^* is the conjugate of x. Substituting (5.5) into (5.6), γ_m can be rewritten as:

$$\begin{aligned} \gamma_m &= \sum_{k=0}^{N-1} \sum_{l=0}^{G-1} h_l \cdot x(k-l+i_d) \cdot x^*(k-m) + \beta(w) \\ &= \sum_{l=0}^{G-1} h_l \cdot \alpha_{m-l+i_d} + \beta(w) \end{aligned}, \tag{5.7}$$

where α_{m-l+i_d} is the auto-correlation of the transmitted preamble and its circular shift of $m-l+i_d$ samples. $\beta(w)$ is the correlation between preamble and the noise terms and will be neglected subsequently. α_{m-l+i_d} is given as:

$$\alpha_{m-l+i_d} = \sum_{k=0}^{N-1} x(k+i_d) \cdot x^*(k-m+l), \tag{5.8}$$

It is important to note at this stage that Equation (5.7) covers a G sample long CIR h_0 to h_{G-1}, which is defined as a CIR estimation window. When i_d exceeds the ISI-free region ($L-G \le i_d \le 0$), it is obvious that α_{m-l+i_d} is not accurate as $x(k+i_d)$ will extend into either preceding or succeeding symbols. Therefore, since the values of α_{m-l+i_d} is pre-stored in a memory and thus not flexible for change, their accuracy in (5.7) should be guaranteed. It is

thus possible to transfer the error term i_d from α_{m-l+i_d} to h_l, by shifting CIR estimation window for i_d samples that covers h_{i_d} to h_{i_d+G-1}. Therefore, (5.7) can be re-written as

$$\gamma_m = \sum_{l=0}^{L-1} h_{l+i_d} \cdot \alpha_s \,, \tag{5.9}$$

with

$$\alpha_s = \sum_{k=0}^{N-1} x(k) \cdot x^*(k-s)\,, \tag{5.10}$$

At this stage, the channel impulse response covered under the CIR estimation window may miss some of the arriving taps due to synchronisation error. Since near-ideal synchronisation in [83] can always locate the strongest tap, which is no further away than G samples from the actual SoF, the missed tap can be compensated by estimating CIRs for up to G timing points preceding and including the detected SoF, and it is assumed that the actual SoF is among these timing points.

Given these timing points, (5.9) can be represented in the form of matrix operation:

$$\Gamma = \mathrm{A} \cdot \mathrm{H}\,, \tag{5.11}$$

where

$$\Gamma = \begin{bmatrix} \gamma_0 & \gamma_{-1} & \gamma_{-2} & \cdots & \gamma_{2-G} & \gamma_{1-G} \\ \gamma_1 & \gamma_0 & \gamma_{-1} & \cdots & \gamma_{3-G} & \gamma_{2-G} \\ \gamma_2 & \gamma_1 & \gamma_0 & \cdots & \gamma_{4-G} & \gamma_{3-G} \\ \vdots & \vdots & \vdots & \ddots & \vdots & \vdots \\ \gamma_{G-2} & \gamma_{G-3} & \gamma_{G-4} & \cdots & \gamma_0 & \gamma_{-1} \\ \gamma_{G-1} & \gamma_{G-2} & \gamma_{G-3} & \cdots & \gamma_1 & \gamma_0 \end{bmatrix}, \tag{5.12}$$

$$\mathrm{H} = \begin{bmatrix} h_{i_d} & h_{i_d-1} & h_{i_d-2} & \cdots & h_{i_d+2-G} & h_{i_d+1-G} \\ h_{i_d+1} & h_{i_d} & h_{i_d-1} & \cdots & h_{i_d+3-G} & h_{i_d+2-G} \\ h_{i_d+2} & h_{i_d+1} & h_{i_d} & \cdots & h_{i_d+4-G} & h_{i_d+3-G} \\ \vdots & \vdots & \vdots & \ddots & \vdots & \vdots \\ h_{i_d+G-2} & h_{i_d+G-3} & h_{i_d+G-4} & \cdots & h_{i_d} & h_{i_d-1} \\ h_{i_d+G-1} & h_{i_d+G-2} & h_{i_d+G-3} & \cdots & h_{i_d+1} & h_{i_d} \end{bmatrix}, \tag{5.13}$$

$$\mathrm{A} = \begin{bmatrix} \alpha_0 & \alpha_1 & \alpha_2 & \cdots & \alpha_{G-2} & \alpha_{G-1} \\ \alpha_{-1} & \alpha_0 & \alpha_1 & \cdots & \alpha_{G-3} & \alpha_{G-2} \\ \alpha_{-2} & \alpha_{-1} & \alpha_0 & \cdots & \alpha_{G-4} & \alpha_{G-3} \\ \vdots & \vdots & \vdots & \ddots & \vdots & \vdots \\ \alpha_{2-G} & \alpha_{3-G} & \alpha_{4-G} & \cdots & \alpha_0 & \alpha_1 \\ \alpha_{1-G} & \alpha_{2-G} & \alpha_{3-G} & \cdots & \alpha_{-1} & \alpha_0 \end{bmatrix}, \tag{5.14}$$

where Γ is comprised of the cross-correlation between received signal samples and the stored training symbol, with a correlation lag that spans both sides of the detected SoF. Each column of H contains a set of CIR that starts at a different timing point that precedes the detected SoF. It has also been noted that $\alpha_s = \alpha_{-s}$ for BPSK or QPSK modulated preambles as well as FFT generated training symbol. So that in (5.14) matrix A is a Toeplitz matrix which is given as:

$$\mathrm{A}=\begin{bmatrix} \alpha_0 & \alpha_1 & \alpha_2 & \cdots & \alpha_{G-2} & \alpha_{G-1} \\ \alpha_1 & \alpha_0 & \alpha_1 & \cdots & \alpha_{G-3} & \alpha_{G-2} \\ \alpha_2 & \alpha_1 & \alpha_0 & \cdots & \alpha_{G-4} & \alpha_{G-3} \\ \vdots & \vdots & \vdots & \ddots & \vdots & \vdots \\ \alpha_{G-2} & \alpha_{G-3} & \alpha_{G-4} & \cdots & \alpha_0 & \alpha_1 \\ \alpha_{G-1} & \alpha_{G-2} & \alpha_{G-3} & \cdots & \alpha_1 & \alpha_0 \end{bmatrix}, \tag{5.15}$$

The CIR for different timing points can therefore be obtained by:

$$\mathrm{H}=\mathrm{A}^{-1}\cdot\Gamma, \tag{5.16}$$

The resultant H comprises G sets of CIRs, each of which starts from a different timing point. The next task here is to choose the best CIR estimates, or in other words, to choose the best timing point. It has already been shown that if the selected timing point falls within the ISI-free region, the capturing of all arriving channel taps is guaranteed. It has been observed that when all arriving channel taps are covered by the CIR estimation window the total PDP power at that timing point is at its maximum. Therefore the optimised timing point can be chosen at such a point as to achieve maximum PDP power. Although this process may not necessarily locate the actual SoF due to the variance of noise, it is sufficient to always find the best CIR as long as timing synchronisation yields the detected SoF no further than G samples from the actual SoF. A vector P is thereby defined as the PDP power for each set of estimated CIR, given as:

$$P=\begin{bmatrix} p_0 & p_1 & \cdots & p_{G-2} & p_{G-1} \end{bmatrix}, \tag{5.17}$$

where

$$p_n = \sum_{m=0}^{G-1} |h(m,n)|^2 , \tag{5.18}$$

where $h(m,n)$ is the element in the m th row and n th column of H. The optimised CIR estimates is therefore the column of H which corresponds to the maximum value of p_n, where

$$p_n = \arg\max_n \{P\} , \tag{5.19}$$

According to the corrected SoF, the optimised CIR can therefore be recovered from H, as well as the time-shifted received signal. After the optimised CIR estimates are padded with zeros, both OFDM data r and padded CIR H_{pad} are transformed to the frequency-domain by FFT, enabling one-tap equalization as:

$$X_{eq} = \frac{FFT(r)}{FFT(\mathrm{H}_{pad})} , \tag{5.20}$$

The idea of this CIR estimation and optimisation scheme is also illustrated in Figure 5.3, which shows the case of a 4-tap multipath channel PDP. In this case, the first tap is severely faded (mark 1 in the figure), which results in the second tap being detected as the SoF (mark 2). CIR estimation as defined in (5.16), estimates CIR information for extended timing points up to G samples preceding and including the detected SoF (mark 4), and the optimised CIR can be chosen accordingly.

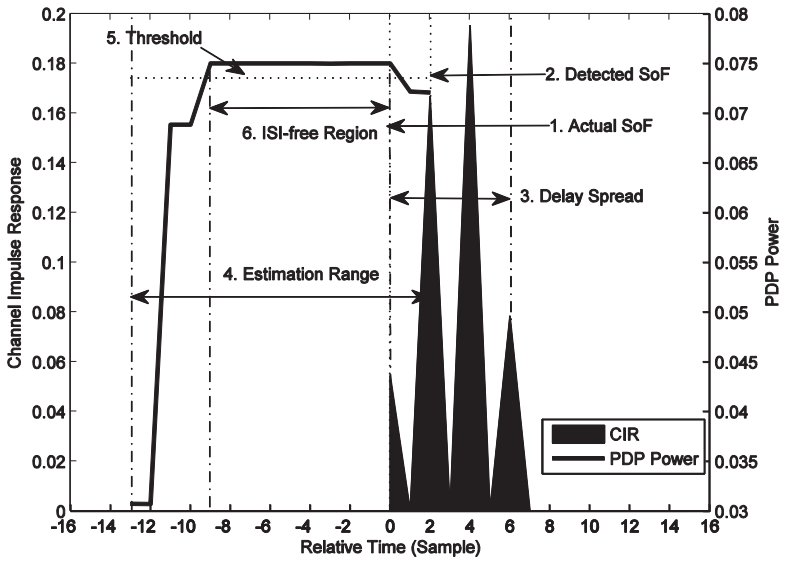

Figure 5.3: Concept of CIR optimisation

Figure 5.3 clearly shows that the PDP power is maximized in the ISI-free region (mark 6), and that all arriving taps can be estimated as long as the corrected SoF is in this region.

5.3.4. Delay Spread Estimation

The CIR information obtained from the above described procedures can be used for delay spread estimation and noise reduction, which may further reduce the system complexity and increase efficiency. Noise reduction is part of the procedure for delay spread estimation, so that the processes can be performed simultaneously. Delay spread is an important factor in many wireless communication systems, and it is particularly crucial for OFDM systems, as it is a vital indicator of the channel length which affects the length of CP in system design. In the proposed scheme, delay spread estimation can be very useful in helping reduce the estimation complexity, as well as optimising the synchronisation output in terms of the corrected SoF. Given an estimated delay spread D, the length of the pseudo channel delay profile can therefore be reduced accordingly, allowing all matrix sizes in (5.11) to reduce to

$D \times D$. On the other hand, the CIR optimisation search range can also be reduced to D, in which case the timing point that maximizes PDP power will be the actual SoF where $i_d = 0$, and thus a perfect correction to the timing synchronisation will be guaranteed. Therefore, delay spread estimation is an important aspect of our proposed scheme.

Delay spread estimation usually involves threshold setting, which is also known as MSS in FFT based channel estimation algorithms. These methods tend to consider the more significant terms in CIR samples as channel taps, while the less significant ones as noise. Noise reduction is achieved by discarding these noise terms and setting them to zero, whereas delay spread estimation is acquired by calculating the maximum distance between these significant terms. Ideally, given that noise terms between channel taps are relatively small, complete channel PDP can also be acquired. In [91] the authors proposed a delay spread estimation technique using correlations of subblocks with threshold setting. Their simulation results show that improved accuracy can be achieved and complexity reduced compared to Beek's classical method [92], although no detailed algorithm on setting the threshold has been presented. This proposed technique is limited since the algorithm will only work in systems with large numbers of subcarriers to allow sufficient samples in the subblock, and its usage is further restricted as it requires the delay spread to be a multiple integer of the subblock size.

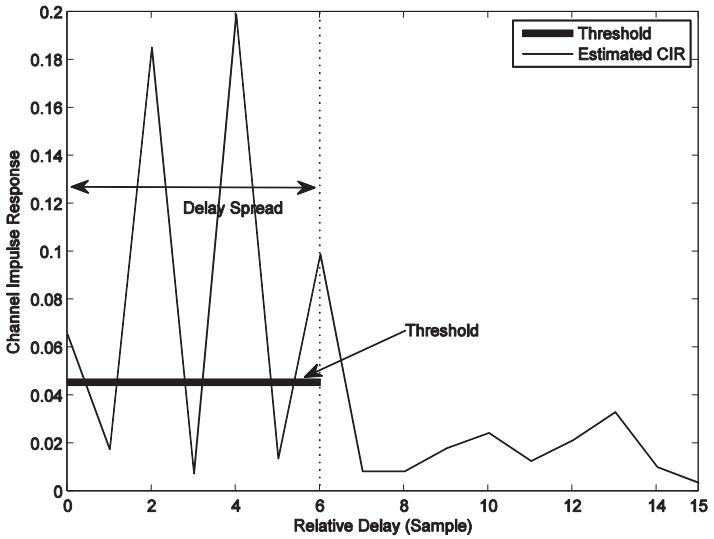

Figure 5.4: Delay spread estimation using optimised CIR

In our proposed scheme, the delay spread can be estimated using the optimised CIR and threshold setting via a MSS method, which is shown in Figure 5.4. The estimated samples can be considered as consisting of two parts: the channel tap power at arriving tap positions and AWGN at all timing positions. By setting a threshold similar to that shown in Figure 5.4, unwanted noise terms can be eliminated via a high-pass filter, while the delay spread can be estimated according to the remaining taps.

The threshold setting has been extensively studied and generally there exists two groups of solutions. The first group tends to utilize the channel statistics and knowledge, especially the estimation or assumption of the number of channel taps. The selection is simple and straightforward once this information is available; however obtaining such channel tap information usually requires much more complexity than the selection itself. The second group does not require channel information but considers the estimated CIR to have followed the central limit theorem. In this case, assuming sufficient samples, CIRs at non-tap

positions are considered as complex Gaussian variables having a Rayleigh distributed amplitude. The PDF and the expected value of Rayleigh distribution is written as:

$$p(x) = \frac{x}{\sigma^2} e^{-\frac{x^2}{2\sigma^2}}, \tag{5.21}$$

$$E(x) = \sigma\sqrt{\frac{\pi}{2}}, \tag{5.22}$$

where $p(x)$ is the PDF of x, $E(x)$ is the expected value of x and σ is the variance of either the real or imaginary part of x. The variance of the Gaussian variable can thereby be obtained by calculating their mean. However since the CIR output is only G samples long, it is not sufficient for the algorithm to calculate an accurate variance. Hence, all CIR information obtained from (5.16) is taken into account instead, which provides a sample space of G^2. Considering all samples that fall below the average amplitude are noise, σ can be estimated as:

$$\sigma = \sqrt{\frac{2}{\pi}} \times \overline{CIR}_{ls}, \tag{5.23}$$

where $\overline{CIR}_{ls}$ is the amplitude average of all samples that fall below the average amplitude of all G^2 samples. Given the Rayleigh cumulative distribution function (CDF) in (5.24), the threshold can be set as in (5.25):

$$p(x > \delta) = P_e = e^{-\delta^2/2\sigma^2}, \tag{5.24}$$

$$\delta = \sqrt{-ln(P_e) \times 2\sigma^2}\,, \tag{5.25}$$

The delay spread is hence obtained by applying the threshold to the optimised CIR and calculating the distance between the first and last value exceeding the threshold, which ideally will be the 1st and the last arriving taps. Since the delay spread relies solely on the detection of these two taps, the estimation accuracy will be affected when either or both of the taps are severely faded, and thus an error floor is expected.

Delay spread information can also be acquired using the total PDP power information as in Figure 5.3. Two approaches can be taken: firstly via setting a threshold according to mark 5, where all inputs that exceed the threshold fall in the ISI-free region; and secondly by detecting the sharp rise and fall of the total PDP power. Regardless of the approach taken, the delay spread is obtained by:

$$D = G - I_{ISI} + 1\,, \tag{5.26}$$

where I_{ISI} is the estimated length of ISI-free region, in samples.

5.3.5. Computational Complexity

The overall complexity of the proposed scheme is low compared to other techniques such as MMSE. As the estimation proceeds, the complexity can be further reduced at different stages. A complexity comparison of different approaches is given in Table 5.1.

Simulated Technique	Order of Complexity
Least Squares	N
MMSE	N^3
Time-Domain Scheme	G^3
Time-Domain Scheme & Delay Spread Estimation	D^3
Time-Domain Scheme & Delay Profile Estimation	$D \times M^2$

Table 5.1: Comparison of computational complexity

The time-domain scheme involves two $G \times G$ sized matrix multiplication, whose maximum complexity is in the order of G^3. After obtaining the channel delay spread, the complexity of this scheme in the succeeding transmissions can be reduced to the order of D^3 by only considering D taps of the pseudo channel delay profile. If the channel delay profile is also correctly estimated via threshold, the complexity can be further reduced to the order of $D \times M^2$, where M is the number of multipath taps. For slow varying channels where channel delay profile and synchronisation are unlikely to change in a short duration, it may be feasible to reduce the size of H to a vector that only estimates CIR starting from the corrected SoF, and full estimation of H is performed only periodically to regain synchronisation and to update channel information. Therefore for the majority period of the transmission the complexity will remain of the order of M^2.

5.4. Practical Implementation

The proposed time-domain scheme can benefit from seamless integration between modules, and since many parameters can be re-used for different modules, the complexity of practical implementation is low. A process diagram is shown in Figure 5.5 for demonstration.

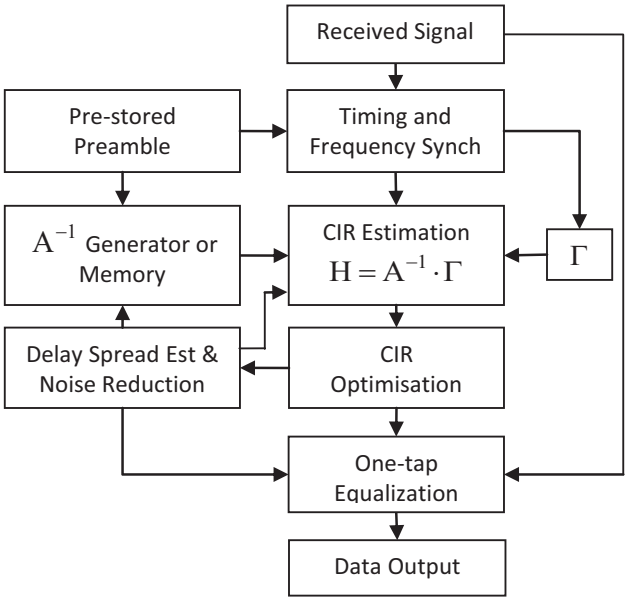

Figure 5.5: Practical implementation of the time-domain scheme

The received signal is first sent to the timing and frequency synchroniser, where cross-correlation Γ is calculated using pre-stored preamble information. After synchronisation is completed, part of Γ is stored in a $2G-1$ sized memory for re-use. The signal is then passed through the CIR estimation module, where Γ is recovered from memory and A^{-1} is either generated or recovered from the second memory. This is followed by the CIR optimisation, the output of which is then equalized using one-tap equalization. Also, the output of CIR can be used for delay spread estimation, whose information can thus be fed back to adjust the size of A^{-1} as well as the size of Γ. This scheme requires three memories in total: the first one is N samples long where preamble is held; the second one is $2G-1$ samples long for Γ; while the third one can be either G samples long for information of A or a $G \times G$ sized for A^{-1}.

5.5. Computer Simulations

Simulations have been carried out using two test wideband channels. The first channel is with 10 fading taps, having a channel PDP measured by the EU project MAESTRO (Case 5) [63] for satellite digital multimedia broadcasting as shown in Table 2.1, where channel profile follows an outdoor urban characteristic with a direct satellite path and the use of 3 terrestrial repeaters. The second channel is ITU-R pedestrian B channel PDP which has 6 fading taps, representing an outdoor pedestrian environment shown in Table 5.2. This channel profile is more close to the propagation environment associated with WiFi and WiMAX. Simulation parameters are chosen as follows: FFT size $N = 256$, $N_{used} = 200$, CP length $G = 32$, carrier frequency $F_c = 3.5GHz$, subcarrier spacing $\Delta f = 15.625KHz$, sampling rate $F_S = 4MHz$ and QPSK subcarrier modulation is implemented. Repetitive training symbols (with two identical parts, generated in the frequency domain) are transmitted in every 8 OFDM symbols (i.e. 1 training symbol followed by 7 data symbols) for MMSE and the proposed scheme, while 1 in 8 subcarriers are used as scattered pilots for LS, therefore giving the same overhead to all cases.

Tap	Delay (ns)	Relative Power (dB)	K-factor (dB)
1	0	0	-inf
2	200	-0.9	-inf
3	800	-4.9	-inf
4	1200	-8	-inf
5	2300	-7.8	-inf
6	3700	-23.9	-inf

Table 5.2: Power delay profile of ITU-R Pedestrian B

Scenario	Channel PDP	Velocity (km/h)
1	MAESTRO profile 5	0
2	MAESTRO profile 5	50
3	ITU-R pedestrian B	0
4	ITU-R pedestrian B	3

Table 5.3: Simulated scenarios

Four channel estimation methods were simulated: Ideal, LS on scattered pilots with cubic-spline frequency interpolation, MMSE on training symbols and the proposed method. All methods (apart from the ideal) employ linear interpolation over time. These techniques are simulated under 4 scenarios, which are given in Table 5.3.

Figure 5.6 shows the performance of the delay spread estimation, where increasingly close performance to the ideal estimation is observed as SNR increases. It is also observed that as expected, the performance will experience an error floor, which is due to severe fading of the first or last arriving channel taps.

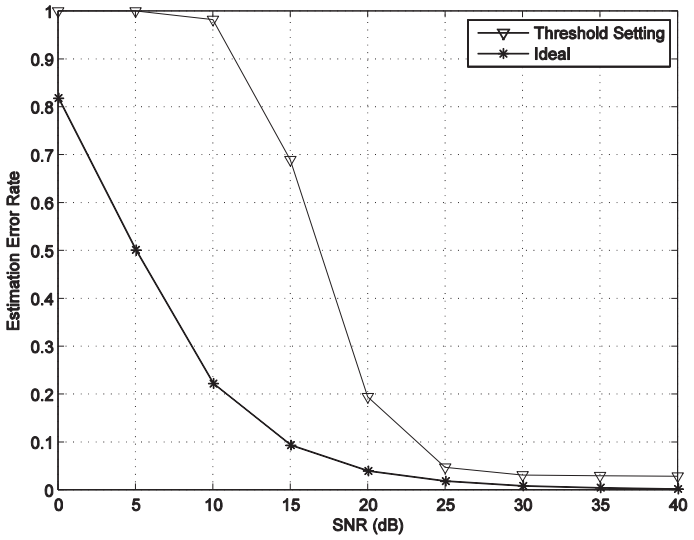

Figure 5.6: Delay spread estimation performance

5.5.1. Simulation Case 1 (Profile 5, 0km/h)

Simulation result for case 1 is shown in Figure 5.7. It can be seen that in the static channel (v=0km/h) scenario the proposed methods achieve comparable performance to the ideal channel estimation and MMSE, while performs much better than the LS technique.

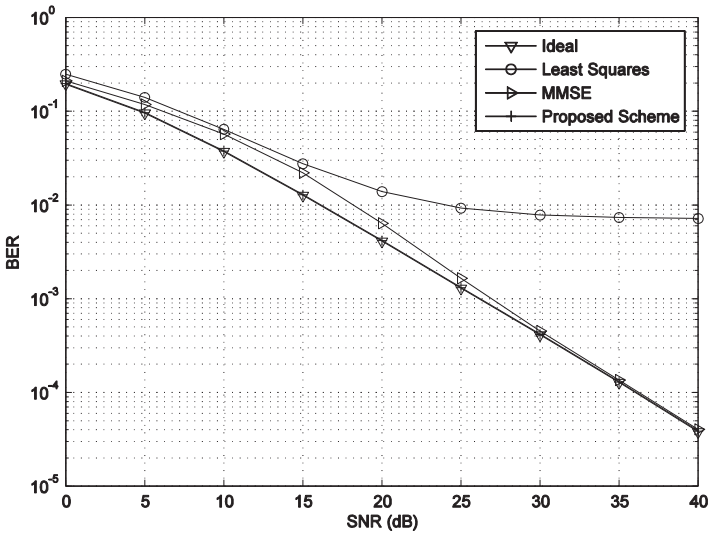

Figure 5.7: Uncoded BER performance at 0km/h for MAESTRO profile 5

5.5.2. Simulation Case 2 (Profile 5, 50km/h)

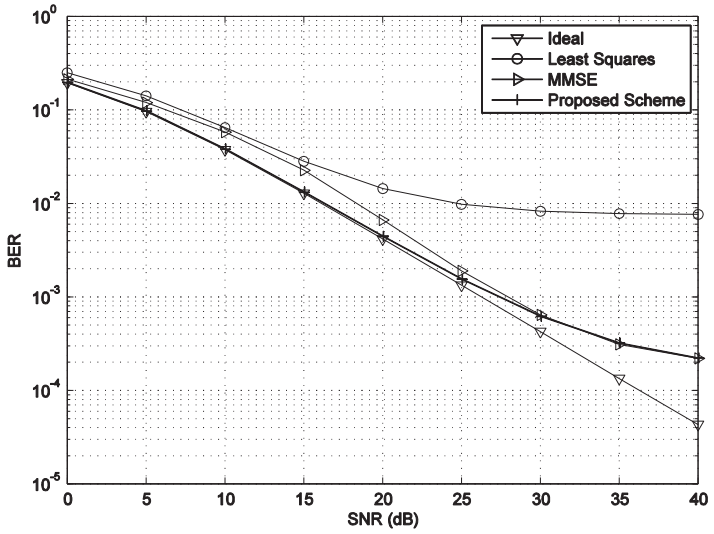

Figure 5.8: Uncoded BER performance at 50km/h for MAESTRO profile 5

Figure 5.8 shows the BER performance when the receiver is moving at 50km/h, where linear interpolation is applied over time between two training symbols. It can be seen that although the performance of the proposed method degrades due to mobility, it is still similar to that of MMSE and much better than LS.

5.5.3. Simulation Case 3 (Pedestrian B, 0km/h)

Figure 5.9 shows the performances of the simulated methods in a pedestrian transmission environment. It can be clearly seen that in static channels (v=0km/h), the proposed method achieves close performance to the ideal estimation and almost identical performance to MMSE, while performing much better than the LS technique.

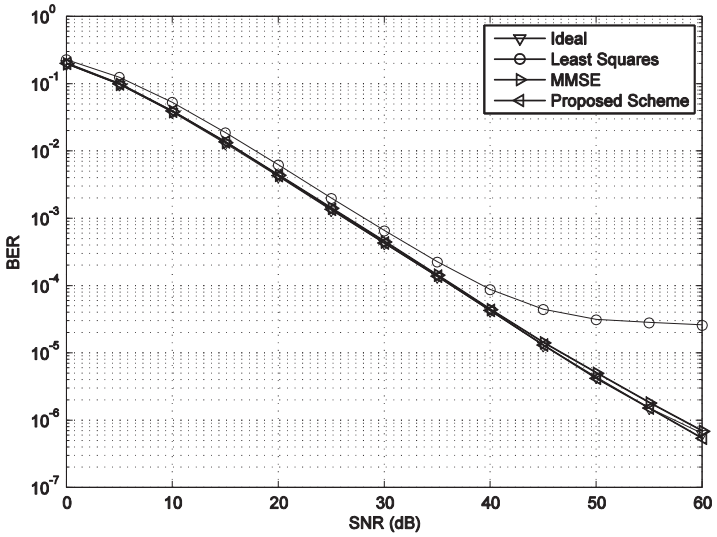

Figure 5.9: Uncoded BER performance in static channel for ITU-R pedestrian B

5.5.4. Simulation Case 4 (Pedestrian B, 3km/h)

Figure 5.10 shows the performances of the simulated methods in pedestrian scenario at pedestrian speed (3km/h). Although the performance of the proposed scheme degrades slightly due to mobility, it is still almost identical to that of MMSE and close to the ideal estimation while much better than the LS technique.

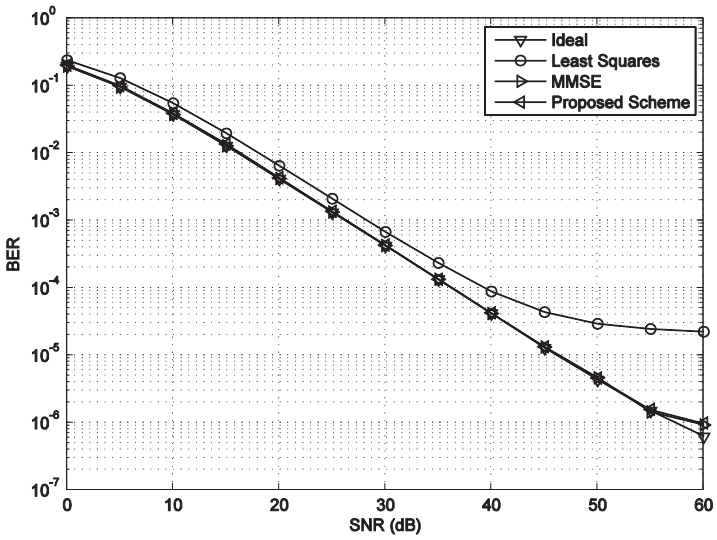

Figure 5.10: Uncoded BER performance in pedestrian speed for ITU-R pedestrian B

5.5.5. Discussion

From the results shown, LS performs worst in all cases and is some way off other simulated techniques. Meanwhile it can be clearly seen that the proposed method achieves near-ideal accuracy when the velocity is small, while almost identical – if not the same – accuracy as MMSE is observed in all cases. It is also noteworthy that the proposed method has a significantly lower complexity level than MMSE and does not require any additional channel information. Therefore it is verified that the proposed method achieves similar performance to MMSE at a much lower computational complexity, whilst it is more feasible for implementation.

5.6. Conclusions

In this chapter we have considered time-domain channel estimation in the presence of timing synchronisation errors. Conventionally most channel estimation methods for OFDM have been based on scattered frequency-domain pilots, such as LS and MMSE, while

preamble or training symbols are used for synchronisation. This mechanism is however not efficient in terms of bandwidth due to the use of both training symbol and scattered pilots. Ideally a combined synchronisation / channel estimation scheme using only training symbols or scattered pilots is desirable, thus saving the bandwidth. Since near-ideal timing synchronisation is achieved via preamble/training symbols [83], thus the proposal of an efficient time-domain channel estimation based on preamble/training symbols is desired.

In order to propose an efficient method we have reviewed established methods in the field of time-domain estimation. These methods take different approaches to carry out estimation and they all assume perfect synchronisation which is acceptable if the synchronisation is in the ISI-free region. However, we have observed that in some cases synchronisation will fall out of the ISI-free region due to severe fading of the first arriving tap, leading to performance degradation.

To mitigate such adverse effects, we have proposed a low-complexity time-domain channel estimation scheme using preamble or training symbols. This scheme considers an imperfect synchronisation scenario where missed multipath taps can cause severe performance degradation. Firstly it assumes a pseudo channel delay profile in which the channel length is equal to that of the CP. Then it uses a simplified ML estimation mechanism to simultaneously estimate CIRs at multiple timing points and the degradation caused by synchronisation error can be compensated by a CIR optimisation mechanism which searches for the best CIR. The optimisation mechanism chooses the CIR estimates at whose timing synchronisation point maximum CIR power is achieved. It may not adjust the synchronisation to the exact timing point but always brings the synchronisation back into

the ISI-free region. The proposed method can also utilize the estimated CIR to estimate the channel delay spread, and also to reduce the CIR noise level via threshold setting. The performance of the proposed method is verified by computer simulations, whose results for delay spread estimation show that the algorithm achieves good accuracy which is close to the ideal scenario. Uncoded BER results show that the proposed method achieves comparable performance to established pilot-based techniques such as MMSE with a much lower complexity. The proposed time-domain channel estimation scheme can easily be implemented in many OFDM systems such as mobile telephony, WiFi, WiMAX and digital television, thus providing a feasible alternative to existing techniques.

6. Conclusions and Future Work

6.1. Conclusions

In this thesis, low complexity channel estimation algorithms for OFDM based satellite systems have been investigated, in order to achieve the optimised performance in terms of both complexity and performance, and to facilitate practical implementation.

Firstly, channel estimation algorithms for DVB-SH have been investigated. Computational complexity is a vital factor in channel estimation for DVB-SH whose symbol has very large number of subcarriers. We have reviewed several existing methods that could be applicable to DVB-SH, namely LS, MMSE, adaptive interpolation and FFT based method. LS is computationally efficient but with low estimation accuracy, whilst MMSE achieves the best accuracy at the cost of very high complexity. We have proposed the combined MMSE and FFT method as an optimised channel estimation algorithm for DVB-SH with respect to both estimation accuracy and complexity. Computer simulations show that the proposed scheme achieves much better accuracy than LS whilst being close to the MMSE performance. However it reduces the complexity by more than 50% in comparison to MMSE and is easily implementable in practical DVB-SH terminal. Therefore the proposed combined scheme is very suitable for development of lower cost DVB-SH terminals.

Secondly, we have considered OFDM systems suffering from inter-carrier interference, due to the large Doppler shift associated with high velocity of the receiver. We have reviewed existing techniques for ICI cancellation, namely OPT, PIC, SIC, and proposed an optimised method based on PIC. It utilizes signal to interference ratio (SIR) information to adaptively

construct the channel matrix, rather than constructing a banded matrix as was the case in PIC. This adaptive method treats subcarriers unequally in terms of forming the matrix but will guarantee a relatively equal cancellation performance from each subcarrier, thus reducing the risk of performance degradation caused by the weakest link. Computer simulations show that the adaptive method achieves improved BER performance over PIC for a similar complexity. In addition, its BER performance is almost identical to the conventional full-matrix inversion in our simulated scenarios up to 300km/h while its complexity is much lower. This proves that the proposed method is not only an optimised method for PIC but also can be a feasible alternative to the full-matrix inversion method. The proposed adaptive scheme is therefore verified as an improved ICI cancellation technique in terms of accuracy and complexity. It could be incorporated into DVB-SH terminals for use in high speed passenger vehicles such as trains and aircrafts.

Lastly, time-domain channel estimation techniques have been investigated in the presence of timing synchronisation error. Perfect synchronisation is not achievable in practice and errors in the ISI-free region are acceptable since they can easily be compensated by frequency-domain channel estimation. However synchronisation errors beyond the ISI-free region will cause large performance degradation and they have been observed when the first channel multipath tap is severely faded. We have proposed and demonstrated a low-complexity time-domain channel estimation scheme using preamble or training symbols to address this issue. The degradation is compensated in this scheme by a CIR optimisation mechanism which searches for the best CIR estimate. The scheme can also estimate the channel delay spread as well as reduce the CIR noise level by threshold setting. The estimated delay spread information can be fed back to the estimation mechanism to further

reduce its complexity. Computer simulation results show that the proposed scheme achieves near-ideal accuracy at low speeds or quasi-static channels. Its performance is comparable to established pilot-based techniques such as MMSE at higher speeds. Apart from the promising results in performance, the proposed scheme enjoys much lower complexity compared to MMSE, and is capable of carrying out other estimations simultaneously. The proposed time-domain channel estimation scheme is widely applicable and can be easily implemented in many OFDM systems such as mobile telephony, WiFi, WiMAX and digital television, and further lower terminal costs to those currently produced.

6.2. Future Work

Based on the achievements of this thesis, some future research work can be proposed:

- Parallel sub-block MMSE estimation for DVB-SH or other OFDM systems with large-sized symbol structure: This proposal is feasible since the correlation impact of two distant subcarriers is very limited due to their frequency separation. By dividing the whole symbol into small sub-blocks (e.g. 16 sub-blocks each contains 64 subcarriers in 1K mode) MMSE is performed on each sub-block in parallel. As a result, the overall computational complexity is in the linear order of one sub-block rather than in exponential order as is applied to full MMSE. Performance degradation caused by this approach is expected to be minimal.
- Optimisation of the adaptive ICI cancellation method: The proposed method in this thesis uses a hyperbolic tangent function to decide the allocation of off-diagonal elements for each row. This allocation can be optimised if the impact of interference at difference SIR levels can be explored and hence utilized.

- Combined schemes of interference cancellation and turbo decoding: Turbo decoding is an iterative process and is well known as an advanced coding system. Improvement may be achieved if an integrated channel estimation / ICI cancellation and turbo decoding scheme can be realized.
- Optimisation of threshold setting for delay spread estimation: As predicted from theory and observed through simulation results, the proposed delay spread estimation algorithm through CIR estimates suffer from an error floor as the amplitude variances of the first and last channel multipath are unknown. The estimation accuracy may be improved if these properties can be explored.

Bibliography

[1] ETSI, "Radio Broadcasting Systems: Digital Audio Broadcasting to Mobile, Portable and Fixed Receivers," ETSI EN 300 744, 1995.

[2] ETSI, "Digital Video Broadcasting (DVB); Framing Structure, Channel Coding and Modulation for Digital Terrestrial Television," ETSI, ETSI EN 300 744 v.1.5.1, November 2004.

[3] ETSI, "Digital Video Broadcsting (DVB); DVB-H Implementation Guidelines," ETSI, ETSI TR 102 377 v1.3.1, March 2009.

[4] ETSI, "Digital Video Broadcasting (DVB); Framing Structure, Channel Coding and Modulation for Satellite Services to Handheld Devices (SH) below 3 GHz," ETSI, ETSI EN 302 583 v1.1.0, January 2008.

[5] IEEE, "Part 11: Wireless LAN Medium Access Control (MAC) and Physical Layer (PHY) Specifications," IEEE, New York, IEEE Std 802.11-2007, 2007.

[6] IEEE, "Air Interface for Fixed Broadband Wireless Access Systems," IEEE, New York, IEEE Std 802.16-2004, 2004.

[7] 3GPP, "3rd Generation Partnership Project; Technical Specification Group Radio Access Network; Evolved Universal Terrestrial Radio Access (E-UTRA); Multiplexing and channel coding (Release 8)," 3GPP TS 36.212 v8.7.0, 2009.

[8] Claude Shannon, "A Mathematical Theory of Communication," *Bell System Technical Journal*, vol. 27, pp. 379-423 and 623-656, July and October 1948.

[9] S. Saunders, *Antennas and Propagation for Wireless Communication Systems*. Chichester: John Wiley & Sons, 1999.

[10] J.D. Parsons, *The Mobile Radio Propagation Channel*, 2nd ed.: John Wiley, 2002.

[11] J.D. Parsons, *The Mobile Radio Propagation Channel*. Chichester: John Wiley & Sons, 2000.

[12] C. Chrysanthou and H.L. Bertoni, "Variability of Sector Averaged Signals for UHF Propagation in Cities," *IEEE Transactions on Vehicular Technology*, vol. 39, no. 4, pp. 352-58, 1990.

[13] S.R. Saunders and F.R. Bonar, "Mobile Radio Propagation in Built-up Areas: A Numerical Model of Slow Fading," in *IEEE Vehicular Technology Society Conference*, St. Louis, 1991, pp. 295-300.

[14] [Online]. http://en.wikipedia.org/wiki/Fading

[15] R.H. Clarke, "A Statistical Theory of Mobile Radio Reception," *Bell Systems Technical Journal*, vol. 47, no. 6, pp. 957-1000, 1968.

[16] T. Himsoon, S. Weifeng, and K.J.R. Liu, "Single-Block Differential Transmit Scheme for Broadband Wireless MIMO-OFDM Systems," *IEEE Transactions on Signal Processing*, vol. 54, no. 9, pp. 3305-14, September 2006.

[17] W. Hashim, F. Said, B. Allen, A.H. Aghvami, and A.F. Ismail, "Performance Comparison of Differential Space-Time Signalling Schemes for OFDM Systems," in *IEEE Malaysia International Conference on Communications and International Conference on Networks*, Kuala Lumpur, Malaysia, 2005.

[18] A.I. El-Arabawy and S.C. Gupta, "Reduced Mobile Complexity Scheme for Fast Fading Channel Estimation in OFDM-FDD Mobile Communication Systems," in *IEEE International Conference on Universal Personal Communications*, San Diego, October 1997, pp. 274-78.

[19] H. Arslan and G.E. Bottomley, "Channel Estimation in Narrowband Wireless Communication Systems," *Wireless Communications and Mobile Computing*, vol. 1, no. 2, pp. 201-19, April 2001.

[20] S. Wu and Y. Bar-Ness, "OFDM Channel Estimation in the Presence of Frequency Offset and Phase Noise," in *IEEE International Conference on Communications*, Anchorage, May 2003, pp. 3366-70.

[21] B. Han, X. Gao, X. You, J. Wang, and E. Costa, "An Iterative Joint Channel Estimation and Symbol Detection Algorithm Applied in OFDM System with High Data To Pilot Power Ratio," in *IEEE International Conference on Communications*, Anchorage, May 2003, pp. 2076-80.

[22] M. Bossert, A. Donder, and A. Trushkin, "Channel Estimation and Equalization in Orthogonal Frequency Division Multiplexing Systems," in *ITG-Fachberitcht, Mobile Kommunikation*, Neu-Ulm, Germany, September 1995, pp. 485-92.

[23] V. Mignone, A. Morello, and M. Visintin, "Cd3-OFDM: A New Channel Estimation Method to Improve the Spectrum Efficiency in Digital Terrestrial Television Systems," in *International Broadcasting Convention*, Amsterdam, the Netherlands, September 1995, pp. 122-28.

[24] R.W. Chang, "Synthesis of Band-Limited Orthogonal Signals for Multi-Channel Data Transmission," *Bell System Technical Journal*, vol. 45, pp. 1775-96, December 1966.

[25] L. Cimini, "Analysis and Simulation of a Digital Mobile Channel Using Orthogonal Frequency Division Multiplexing," *IEEE Transactions on Communications*, vol. 33, no. 7, pp. 665-75, July 1985.

[26] [Online]. http://mobilewireless.wordpress.com/2008/03/01/an-overview-of-ofdm/

[27] M.K. Ozdemir and H. Arslan, "Channel Estimation for Wireless OFDM Systems," *IEEE Communications Surveys*, vol. 9, no. 2, pp. 18-48, 2007.

[28] A. Dowler, A. Doufexi, and A. Nix, "Performance Evaluation of Channel Estimation Techniques for a Mobile Fourth Generation Wide Area OFDM System," in *IEEE Vehicular Technology Conference*, Vancouver, September 2002, pp. 2036-40.

[29] S. Coleri, M. Ergen, A. Puri, and A. Bahai, "A Study of Channel Estimation in OFDM Systems," in *IEEE Vehicular Technology Conference*, Vancouver, September 2002, pp. 894-98.

[30] J. Rinne and M. Renfors, "Pilot Spacing in Orthogonal Frequency Division Multiplexing Systems on Practical Channels," *IEEE Transactions on Consumer Electronics*, vol. 42, no. 3, pp. 959-62, November 1996.

[31] X. Wang and K.J.R. Liu, "OFDM Channel Estimation Based on Time-Frequency Polynomial Model of Fading Multipath Channel," in *IEEE Vehicular Technology Conference*, Atlantic City, October 2001, pp. 460-64.

[32] S.G. Kang, Y.M. Ha, and E.K. Joo, "A Comparative Investigation on Channel Estimation Algorithms for OFDM in Mobile Communications," *IEEE Transactions on Broadcasting*, vol. 49, no. 2, pp. 142-49, June 2003.

[33] A. Dowler and A. Nix, "Performance Evaluation of Channel Estimation Techniques in a Multiple Antenna OFDM System," in *IEEE Vehicular Technology Conference*, Orlando, October 2003, pp. 1214-18.

[34] M.X. Chang and Y.T. Su, "Model-Based Channel Estimation for OFDM Signals in Rayleigh Fading," *IEEE Transactions on Communications*, vol. 50, no. 4, pp. 540-44, April 2002.

[35] A. Huang and Y. Zhao, "Estimating Channel Response From Pilot Subcarrier Pairs for OFDM Systems," in *Midwest Symposium on Circuits and Systems*, Sacramento, August 1997, pp. 774-77.

[36] X. Ma, H. Kobayashi, and S.C. Schwartz, "An Enhanced Channel Estimation Algorithm for OFDM: Combined EM Algorithm and Polynomial Fitting," in *IEEE International Conference on Acoustic, Speech and Signal Processing*, Hong Kong, April 2003, pp. IV - 680-3.

[37] M.X. Chang and Y.T. Su, "2D Regression Channel Estimation for Equalizing OFDM Signals," in *IEEE Vehicular Technology Conference*, Tokyo, May 2000, pp. 240-44.

[38] J.S. Chow, J.M.Cioffi, and J.A.C. Bingham, "Equalizer Training Algorithms for Multicarrier Modulation Systems," in *IEEE International Conference on Communications*, Geneva, May 1993, pp. 761-65.

[39] A.V. Oppenheim, R.W. Schafer, and J.R. Buck, *Discrete-Time Signal Processing*, 2nd ed.: Prentice Hall, 1999.

[40] S Sun, I. Wiemer, C.K. Ho, and T.T. Tjhung, "Training Sequence Assisted Channel Estimation for MIMO OFDM," in *IEEE Wireless Communications and Networking Conference*, New Orleans, March 2003, pp. 38-43.

[41] S. Coleri, M. Ergen, A. Puri, and A. Bahai, "Channel Estimation Techniques Based on Pilot Arrangement in OFDM Systems," *IEEE Transactions on Broadcasting*, vol. 48, no. 3, pp. 223-29, September 2002.

[42] M.J.F.G. Garcia, J.M. Paez-Borrallo, and S. Zazo, "DFT-Based Channel Estimation in 2D-Pilot-Symbol-Aided OFDM Wireless Systems," in *IEEE Vehicular Technology Conference*, Rhodes, May 2001, pp. 810-14.

[43] Y. Zhao, W. Li, and W. Wu, "An Efficient Channel Estimation Method for OFDM Systems with Multiple Transmit Antennas," in *International Conference on Info-Tech and Info-Net*, Beijing, November 2001, pp. 335-39.

[44] A.A. Tahat and D.R. Ucci, "An Extrapolated Matched-Filter Approach to Multi-User Channel Estimation for OFDM in SDMA," in *IEEE Antennas and Propagation Society*

Conference, San Antonio, June 2002, pp. 636-39.

[45] Y. L and N.R. Sollenberger, "Clustered OFDM with Channel Estimation for High Rate Wireless Data," *IEEE Transactions on Communications*, vol. 49, no. 12, pp. 43-50, December 2001.

[46] Y.H. Yeh and S.G. Chen, "Efficient Channel Estimation Based on Discrete Cosine Transform," in *IEEE International Conference on Acoustic, Speech and Signal Processing*, Hong Kong, April 2000, pp. 676-79.

[47] Y.H. Yeh and S.G. Chen, "Dct-Based Channel Estimation for OFDM Systems," in *IEEE International Conference on Communications*, Paris, June 2004, pp. 2442-46.

[48] M. Stege, P. Zillmann, and G. Fettweis, "MIMO Channel Estimation with Dimension Reduction," in *International Symposium on Wireless Personal Multimedia Communications*, Honolulu, October 2002, pp. 417-21.

[49] Y. Li, "Pilot-Symbol-Assisted Channel Estimation for OFDM in Wireless Systems," in *IEEE Vehicular Technology Conference*, Houston, May 1999, pp. 1131-35.

[50] M Sandell and O Edfors, "A Comparative Study of Pilot-Based Channel Estimators for Wireless OFDM," Lulea University of Technology, Research Report TULEA September 1996.

[51] O. Edfors, M. Sandell, J.J. van de Beek, S.K. Wilson, and P.O. Borjesson, "OFDM Channel Estimation by Singular Value Decomposition," in *IEEE Vehicular Technology Conference*, April 1996, pp. 923-927.

[52] M. Sandell, S.K. Wilson, and P.O. Borjesson, "Performance Analysis of Coded OFDM on Fading Channels with Non-Ideal Interleaving and Channel Knowledge," Lulea University of Technology, Research Report TULEA September 1996.

[53] J.J. van de Beek, O. Edfors, M. Sandell, S.K. Wilson, and P.O. Borjesson, "On Channel Estimation in OFDM Systems," in *IEEE Vehicular Technology Conference*, July 1995, pp. 715-19.

[54] R. van Nee and R. Prasad, *OFDM for Wireless Multimedia Communications*.: Artech House, 2000.

[55] E.G. Larsson, G Liu, J Li, and G.B. Giannakis, "Joint Symbol Timing and Channel Estimation for OFDM Based WLans," *IEEE Communications Letters*, vol. 5, no. 8, pp.

325-27, 2001.

[56] S.M. Kay, *Fundamentals of Statistical Signal Processing: Estimation Theory*. Englewood Cliffs: Prentice-Hall, 1993.

[57] M. Morelli and U. Mengali, "A Comparison of Pilot-Aided Channel Estimation Methods for OFDM Systems," *IEEE Transactions on Signal Processing*, vol. 49, no. 12, pp. 3065-73, December 2001.

[58] 3GPP2, "Physical Layer Standard for cdma2000 Spread Spectrum Systems, Revision D," 3GPP2 C.S0002-D September 2005.

[59] DVB Project, "DVB-SH Fact Sheet," July 2009.

[60] ESA, "ESA Assessment of DVB-SH Performance," June 2007.

[61] V. Pan, "The trade-off between the additive complexity and the asyncronicity of linear and bilinear algorithms," *Information Processing Letters*, vol. 22, pp. 11-14, 1986.

[62] J. Morgenstern, "Note on a Lower Bound on the Linear Complexity of the Fast Fourier Transform," *Journal of the ACM*, vol. 22, no. 2, pp. 305-6, April 1973.

[63] ETSI. (March 2010) Satellite Earth Stations and Systems (SES); Advanced Satellite Based Scenarios and Architectures for Beyond 3G Systems.

[64] P.H. Moose, "A Technique for Orthogonal Frequency Division Multiplexing Frequency Offset Correction," *IEEE Transactions on Communications*, vol. 42, no. 10, pp. 2908-14, October 1994.

[65] M.J. Fernandez-Getino-Garcia, O. Edfors, and J.M. Paez-Borollo, "Frequency Offset Correction for Coherent OFDM in Wireless Systems," *IEEE Transactions on Consumer Electronics*, vol. 47, no. 1, pp. 187-93, February 2001.

[66] Y. Li, L.J. Cimini, and N.R. Sollenberger, "Bounds on the Interchannel Interference of OFDM in Time-Varying Impairments," *IEEE Transaction onCommunications* , vol. 49, no. 3, pp. 401-4, March 2001.

[67] A.F. Molisch, M. Toeltsch, and S. Vermani, "Iterative Methods for Cancellation of Intercarrier Interference in OFDM Systems," *IEEE Transactions on Vehicular Technology*, vol. 56, no. 4, pp. 2158-67, July 2007.

[68] D. Kim and G.L. Stuber, "Residual ISI Cancellation for OFDM with Applications to HDTV

Broadcasting," *IEEE Journal on Selected Areas in Communications*, vol. 16, no. 8, pp. 1590-99, October 1998.

[69] J.P.M.G. Linnartz and A. Gorokhov, "Doppler-Resistant Receivers for Mobile Multimedia Communications," in *2nd International Symposium on Mobile Multimedia Systems and Applications*, Delft, November 2000, pp. 87-92.

[70] V. Fischer, A. Kurpiers, and D. Karsunke, "ICI Reduction Method for OFDM Systems," in *8th International OFDM Workshop 2003*, Hamburg, September 2003.

[71] Y. Mostofi, D.C. Cox, and A. Bahai, "ICI Mitigation for OFDM Mobile Sstems," in *38th IEEE International Conference on Communications*, Anchorage, May 2003, pp. 3351-55.

[72] K. Schmidt, C. Gunter, and A. Rothermel, "Improving the Mobility of DVB Handheld Devices with Inter-carrier Interference Compensation," in *2004 IEEE International Symposium on Consumer Electronics*, Reading, September 2004, pp. 182-87.

[73] J. Cannon, "Non-local Perturbation Techniques," in *Methods in Radiative Transfer*, W. Kalkofen, Ed. Cambridge, UK: Cambridge University Press, 1984.

[74] S. Verdu, *Multiuser Detection*. Cambridge, UK: Cambridge University Press, 1998.

[75] M. Toeltsch and A.F. Molisch, "Equalization of OFDM-systems by Interference Cancellation Techniques," in *IEEE International Conference on Communications*, Helsinki, 2001, pp. 1950-54.

[76] J. Cai, J.W. Mark, and X. Shen, "ICI Cancellation in OFDM Wireless Communication Systems," in *IEEE Globecom*, Taipei, 2002, pp. 656-60.

[77] H. Elders-Boll, H.D. Schotten, and A. Busboom, "Efficient Implementation of Linear Multiuser Detectors for Asynchronous CDMA Systems by Linear Interference Cancellation," *European Transactions on Telecommunications*, vol. 9, no. 5, pp. 427-437, September 1998.

[78] L.K. Rasmussen, T.J. Lim, and A.L. Johansson, "A Matrix-Algebraic Approach to Successive Interference Cancellation in CDMA," *IEEE Transactions on Communications*, vol. 48, no. 1, pp. 145-151, January 2000.

[79] B. O'Hara and A. Petrick, *The IEEE 802.11 Handbook: A Designer's Companion*, 2nd ed. Piscataway, US: IEEE Standard Publications, 2005.

[80] F. Ohrtmann, *WiMax Handbook*. New York, US: McGraw-Hill, 2005.

[81] R. Barrett et al., *Templates for the Solution of Linear Systems: Building Blocks for Iterative Methods*, 2nd ed. Philadelphia, US: SIAM, 1994.

[82] D. Raphaeli, "Iterative Cochannel Interference Cancellation in Synchronous CDMA on a Frequency Selective Channel," in *5th IEEE International Conference on Universal Personal Communications*, Cambridge, MA, 1996, pp. 336-40.

[83] A.B. Awoseyila, C. Kasparis, and B.G. Evans, "Robust Time-Domain Timing and Frequency Synchronisation for OFDM Systems," *IEEE Transactions on Consumer Electronics*, vol. 55, no. 2, pp. 391-99, May 2009.

[84] E.G Larsson, G. Liu, J. Li, and G.B Giannakis, "Joint Symbol Timing and Channel Estimation for OFDM Based WLANs," *IEEE Communications Letters*, vol. 5, no. 8, pp. 325-27, August 2001.

[85] F.D. Nunes and J.M.N. Leitao, "Nonlinear Channel Estimation in Fading OFDM Systems," in *IEEE Globecom Conference*, Rio De Janeireo, Brazil, 1999, pp. 2157-61.

[86] E.G. Larsson, G. Liu, J. Li, and G.B. Giannakis, "An Algorithm for Joint Symbol Timing and Channel Estimation for OFDM Systems," in *IEEE Statistical Signal Processing Workshop*, Singapore, 2001, pp. 393-96.

[87] C. Yeh, Y. Lin, and Y. Wu, "OFDM System Channel Estimation Using Time-Domain Training Sequence for Mobile Reception of Digital Terrestrial Broadcasting," *IEEE Transactions on Broadcasting*, vol. 46, no. 3, pp. 215-20, September 2000.

[88] M. Li, J. Tan, and W. Zhang, "A Channel Estimation Method Based on Frequency-Domain Pilots and Time-Domain Processing for OFDM Systems," *IEEE Transactions on Consumer Electronics*, vol. 50, no. 4, pp. 1049-57, November 2004.

[89] Y.S. Lee, H.C. Shin, and H.N. Kim, "Channel Estimation Based on a Time-Domain Threshold for OFDM Systems," *IEEE Transactions on Broadcasting*, vol. 55, no. 3, pp. 656-62, September 2009.

[90] T. Cui and C. Tellambura, "Power Delay Profile and Noise Variance Estimation for OFDM," *IEEE Communications Letters*, vol. 10, no. 1, pp. 25-27, January 2006.

[91] J.H. Wen, S.H. Lee, and G.R. Lee, "Timing and Delay Spread Estimation Scheme in OFDM Systems," *IEEE Transactions on Consumer Electronics*, vol. 54, no. 2, pp. 316-20, May

2008.

[92] J.J. Van de Beek, M. Sandell, and P.O. Borjesson, "ML Estimation of Time and Frequency Offset in OFDM Systems," *IEEE Transactions on Signal Processing*, vol. 45, no. 7, pp. 1800-05, July 1997.

[93] T.S. Rappaport, *Wireless Communications: Principles and Practice*. Englewood Cliffs: Prentice Hall, 1996.

Appendix: DVB-SH Simulation Test Bed

This appendix gives a description of the DVB-SH simulation test bench which was used to verify the performances of the schemes given in Chapter 3. A simplified version of this test bench is used as the foundation of simulation platforms adapted in Chapter 4 and 5. The simulation test bench is executable under MatLab 7.8.0 (R2009a) version.

List of Files

The lists of files contained in the Module Description section below form the DVB-SH simulator. In most cases one file equals to one function module as shown below in the Architecture section, but in some cases one module may involve more than one file.

Module Description

Module	Relative Files	Description
Main file	DVBSH.m; ModeSel.m;	This is the main file of the test bench, where parameters are set and other modules are called from. This module also calculates and plots BER error information.
Load stored data	Data\PRBSseq; Data\Tab; Data\MM	This module loads the parameters that can be pre-calculated and stored.
Turbo Encoder	TC.m RSC.m Rsc_trellis.m	This module performs Turbo encoding, in which turbo interleaving uses the data loaded from previous module.
Bit Interleaving	BitIntrlv.m	This module carries out bit interleaving, in which about 1.6% puncturing is performed.
Time Interleaving	TmIntrlv.m	This module performs time interleaving, also known as convolution interleaving.
Symbol Interleaving	SymIntrlv.m	This module performs symbol interleaving, the table for which was loaded from previous module.
Mapper / Pilot & TPS Insertion	Map.m PIn.m	This module maps bit data into modulated symbols such as QPSK and pilots & TPS settings are inserted.
IFFT & CP Insertion	OFDMIFFT.m	This module performs IFFT to the signal and inserts CP afterwards.
Channels & AWGN Noise	Modified_IMR_Channel_power_delay.m	This module applies multipath channel to the transmitted noise and adds additive AWGN to it.
FFT & CP	OFDMFFT.m	This module removes CP from received signal and

Removal		performs IFFT.
LS Pilot Estimation	PEst.m	This module extracts signal from pilot subcarriers and carry out LS estimation on those subcarriers.
Interpolation & Equalization	ESAInt.m FTInt.m LinInt.m MMSEInt.m	This module performs interpolation and equalization on pilot estimates. One or more of the methods described can be performed simultaneously.
Demapper & LLR Calculation	DeMap.m	This module splits the mapped signal into bit signal and calculates their LLR information.
Symbol Deinterleaving	SymDeIntrlv.m	This module performs the reverse operation of symbol interleaving
Time Deinterleaving	TmDeIntrlv.m	This module performs the reverse operation of time interleaving.
Bit Deinterleaving	BitDeIntrlv.m	This module performs the reverse operation of bit interleaving, the punctured bits are padded with 0.
Turbo Decoder	TDeC.m Logmap_c.dll	This module performs Turbo decoding, in which turbo interleaving uses the data loaded from previous module.
Error Calculation	DVBSH.m	This module compares the output of Turbo decoder with the generated data and calculates the error
Plot BER Data	DVBSH.m	This module plots the data error rate into visual representation.

Architecture

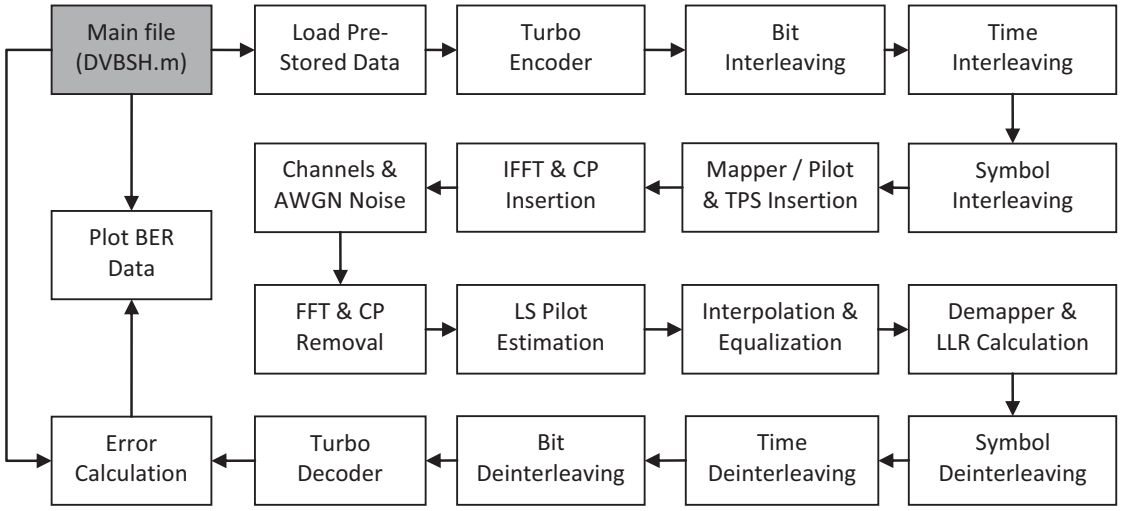

Parameter Settings

The parameter settings are included at the start of the main file (DVBSH.m). It contains the setting of critical parameters required for simulation, as well as the enabling or disenabling

of a specific module or estimation method within the system. Since some of the tables involved in interleaving (such as bit, symbol and turbo) can be pre-calculated, they are stored in a file and loaded at the beginning of the simulation in order to save time and resources.

The details of the parameters defined in the main file are as follows:

Profile	The MAESTRO or ITU-R channel PDF profile index to be simulated
Mode	DVB-SH Mode (1K, 2K, 4K or 8K)
v	The speed of the receiver, in km/h (e.g. 50, 100)
MaxFrames	The total number of transmissions to be simulated (e.g. 10000)
InL=12282	DVB-SH frame length, this has been defined in the standard
GIR	The ratio of CP (e.g. 1/4, 1/8, 1/16, 1/32)
Prm	A collection of frame parameters depending on 'GIR' and 'Mode', including OFDM frame sizes, length of CP and OFDM symbol and bit duration
CR	Turbo encoder rate (e.g. 1/3, 2/5)
MR	Mapping mode, (e.g. 'QPSK')
Fc	Carrier frequency in MHz (e.g. 2200 for S band)
Fm	Maximum Doppler shift (calculated from Fc and v)
PDP	The collection of simulated channel PDP parameters according to the 'Profile'